Remedial Action Scheme for Transmission System Instability Mitigation using Generator Terminal Phasor Measurement Unit Signals

Avishek Paul

Department of Electrical & Computer Engineering
McGill University
Montréal, Canada

August 2020

A thesis submitted to McGill University in partial fulfillment of the requirements for the degree of Doctorate of Philosophy in Electrical Engineering.

Abstract

Currently deployed Remedial Action Scheme (RAS) implementations are event based and parameter based and rely on comparison with offline studies or violation of pre-determined thresholds before initiating the control action. With the changing dynamics of the grid, its operating nature becomes unpredictable and it becomes difficult to determine critical contingencies for all possible operating conditions. Additionally, identification of a suitable control action to address an identified contingency involves multiple iterations through offline studies. Hence it is apparent that the conventional method of RAS is computationally demanding and with an increasing number of scenarios the process becomes intensive and requirements of computational resources also increase.

The thesis proposes to address this issue by establishing a response based multi-shot RAS action that identifies an impending critical contingency and determines the appropriate online response to stabilize the network. Execution of the proposed scheme involves an aggregated knowledge of network wide generator dynamic states as well as the controller's states (Governor Torque and Exciter Field Voltage). An improved dynamic state estimator (DSE) is presented that tacks the dynamic states with greater precision and also deals with issues of communication interruption typically observed while transferring Phasor Measurement Unit (PMU) data over in transmission network covers a vast geographic expanse. The utility of applying the dynamic state information of the generators is that, unlike PMU, it provides a more accurate representation of network dynamics.

Effective realization of the proposed RAS first involves identifying network instability from indices evaluated from a combination of generator electro-mechanical states and the rates of generator energy change. The second part of RAS is an energy function based critical generator identification block that comes into effect when an impending instability has been detected. The availability of dynamic state information makes it possible to compute the individual generator energies. Also the proposed algorithm continuously monitors the network and takes further actions if required. The proposed methodology is entirely based on generator terminal phasor measurements and overcomes the stated problem of conventional schemes.

Performance evaluation has been made on the IEEE 39 bus network and it has been demonstrated that the proposed RAS is robust with regards to instability prediction and can effectively identify critical generators and stabilize the network by tripping the same.

Résumé

Les implémentations RAS (Remedial Action Scheme) actuellement déployées reposent sur des événements et des paramètres et dépendent de la comparaison avec des études hors ligne ou de la violation de seuils prédéterminés avant le lancement des actions de contrôle. Avec la dynamique changeante du réseau, sa nature opérationnelle devient imprévisible et il devient difficile de déterminer une contingence critique dans toutes les conditions d'exploitation possibles. En outre, l'identification des mesures de contrôle appropriées pour faire face à l'éventualité identifiée implique plusieurs itérations via des études hors ligne. Il est donc évident que la méthode conventionnelle de RAS est très exigeante en calcul et que, avec un nombre croissant de scénarios, le processus devient intensif et les besoins en ressources de calcul augmentent également.

La thèse propose de résoudre ce problème en établissant une action RAS multi-plans basée sur une réponse qui identifie une éventualité critique imminente et détermine la réponse en ligne appropriée pour stabiliser le réseau. L'exécution du schéma proposé implique une connaissance agrégée des états dynamiques du générateur sur l'ensemble du réseau ainsi que des états du contrôleur (couple du régulateur et tension du champ de l'excitateur). On présente un estimateur d'état dynamique amélioré (DSE) qui s'attaque aux états dynamiques avec une plus grande précision et traite également les problèmes d'interruption de communication généralement observés lors du transfert de données d'unité de mesure de phasor (PMU) dans un réseau de transmission couvrant de vastes étendues géographiques. L'utilité d'appliquer l'information d'état dynamique des générateurs est qu'elle fournit une représentation plus précise de la dynamique du réseau que juste la PMU.

La réalisation efficace de RAS proposé implique d'abord de déterminer l'instabilité du réseau à partir d'indices évalués d'une combinaison d'états électromécaniques et de taux de changement d'énergie des générateurs. La deuxième partie de RAS est un bloc d'identification critique de générateur basé sur une fonction d'énergie qui prend effet lorsqu'une instabilité imminente a été détectée. La disponibilité d'information d'état dynamique permet de calculer les énergies individuelles du générateur. De plus, l'algorithme proposé surveille en permanence le réseau et prend d'autres mesures si nécessaire. La méthodologie proposée est entièrement basée sur les mesures de phase du terminal du générateur et résout le problème posé par les systèmes conventionnels.

Les performances ont été évaluées sur le réseau de bus IEEE 39 et il a été démontré que le RAS proposé est robuste en ce qui concerne la prévision de l'instabilité et qu'il peut identifier efficacement les générateurs critiques et stabiliser le réseau en le déclenchant.

Acknowledgments

First and foremost I would like to thank Prof. Geza Joos for his sincere guidance and support throughout my work. His pragmatic comments along with insightful suggestion and constatnt feedback kept me on track. In addition his guidance helped me realize how to be an independent researcher and always challenged to improve further and it resulted in unforseen opportunities.

My gratitude goes towards Prof. Innocent Kamwa not only for his guidance and supervision but also being a mentor. His expert opinion and plethora of ideas that he shared with me expedited the progress of my research. I am also grateful to him for being encouraging and optimistic at crucial stages of my doctoral studies.

The following sources of financial support are acknowledged: the NSERC/Hydro-Quebec Industrial Research Chair on the Integration of Renewable Energies and Distributed Generation into the Electric Distribution Grid, held by Prof Joos, NSERC Canada Research Chair in Powering Information Technologies, held by Prof Joos, and the McGill Engineering Doctoral Award (MEDA).

I am also thankful to my supervisory committee consisting of Prof. Geza Joos, Prof. Innocent Kamwa, Prof. Francois Bouffard and Prof. James Richard Forbes for their comments and advise in various stages of research.

I am grateful to Prof. Jon Sakata who recruited me as a research assistant for performing data analysis on his computational biology project through work study program. Apart from being an amazing person, he encouraged to explore and try out new techniques in his domain of research which broadened my knowledge of machine learning that I applied in my research as well.

I would also like to thank my supervisor from M.Tech professor at Indian Institute of Technology Delhi, Prof. Nilanjan Senory for motivating me to pursue research and my supervisors. Mr. B.N.De Bhowmick and Mr. Shankar Rao. at Power Grid Corporation of India Ltd. for creating the opportunity to take study leave and start my doctoral studies.

I would also like to appreciate the assistance provided by my lab colleagues Dr. Syed Qaseem Ali, Dr. Dmitry Rimorov, Dr. Subhadeep Bhattacharya for providing counseling, direction and ideas. Also I would like to acknowledge Dr. Quishi Cui, Mr. Sourabh Sharma, Mr. Debi Prasad Mishra Mr. Chu Sun, Mr. Hugo Antoine, Miss Urbbi Paik, Miss Navdeep Dhaliwal for being there as friend and for the enjoyable moments that we shared. The list would not be complete with mentioning my current room-mate Mr. Arun Taneja who made my time in Montreal an exciting experience and my previous room-mate Mr. Soumyasundar Pal who provided good suggestion on addressing technical problems.

Lastly but not the least I would like to express my gratitude towards my parents Mr. Indranath Paul and Mrs. Srilekha Paul for their constant love, patience and encouragement and it would not have been possible without their support.

Preface

In the interest of full disclosure, four publications resulted from this thesis consisting of two conference papers and two journal articles (as listed below). Main contributions by candidate involves identifying problem definition, proposing solution, executing software simulations and compiling results and composing thesis article. The contributions of co-authors are also listed below.

Journals

(A) A. Paul, I. Kamwa and G. Jóos, "Centralized Dynamic State Estimation Using a Federation of Extended Kalman Filters With Intermittent PMU Data From Generator Terminals," IEEE Transactions on Power Systems, vol. 33, no. 6, pp. 6109-6119, Nov. 2018.

Dr. Innocent Kamwa provided suggestions in the formation of solution process, assessed the performance of final model and assisted in addressing and rewriting some of the reviewer's queries. Prof. Geza Jóos is responsible for supervisory guidance to the candidate and providing necessary computing resources and financial assistance in completion of project and publication.

(B) A. Paul, I. Kamwa and G. Jóos, "PMU Signals Responses-Based RAS for Instability Mitigation through on-the Fly Identification and Shedding of the Run-Away Generators," IEEE Transactions on Power Systems.

Dr. Innocent Kamwa assisted the candidate in defining the problem statement, providing reference to relevant literature and guidance in development of the solution. He also helped in composing most of the reviewer's comments. Prof. Geza Jóos provided supervisory comments, necessary computing resources for performing simulations and financial assistance in completion of project and publication.

Conference

(C) A.Paul,I.Kamwa,G.Jóos, "Parameter Validation for Kalman Filter Based Dynamic State Estimation of Power Plant Dynamics", Proceeding of IEEE Electrical Power and Energy Conference, Oct 2017, Saskatoon, Canada.

Dr. Innocent Kamwa evaluated the methodology used and the final results of the study. Prof. Geza Jóos provided supervisory comments, necessary computing resources for performing simulations and financial assistance in completion of project and attending the conference.

(D) A.Paul, I.Kamwa, G.Jóos, "Dynamic State Estimation of Full Power Plant Model From terminal Phasor Measurements", Proceeding of IEEE Power and Energy Society Transmission and Distribution 2018, Denver Colorado.

Dr. Innocent Kamwa proposed the problem statement, evaluated the solution method used and the final results of the study. Prof. Geza Jóos provided supervisory comments, necessary computing resources for performing simulations and financial assistance in completion of project and attending the conference.

Contents

List of Figures

List of Tables

List of Acronyms

AVR	Automatic Voltage Regulator
BA	Balancing Authority
CDSE	Centralized Dynamic State Estimator
COI	Center-Of-Inertia
COP	Center of Power
DAE	Differential-Algebraic Equations
DSE	Dynamic State Estimator
DT	Decision Tree
EKF	Extended Kalman Filter
HIL	Hardware-In-the-Loop
HQ	Hydro-Québec
MC	Monte Carlo
MLSTM	Multi-Variate Long Short Term Memory Network
PDC	Phasor Data Concentrator
POD	Power Oscillation Damping
POW	Point on Wave
PSS	Power System Stabilizer
RAS	Remedial Action Scheme
RES	Renewable Energy Source
RTS	Real-Time Simulator
SPS	Special Protection Schemes
SIPS	System Integrity Protection Schemes
SG	Synchronous Generation, Synchronous Generator
UKF	Unscented Kalman Filter
WAMS	Wide Area Monitoring Systems

List of Symbols

$\mathbf{x}$	Vector of state variables
$\mathbf{y}$	Vector of algebraic variables
$\mathbf{u}$	Vector of inputs
ω	Machine rotor speed, p.u.
$\Delta\omega$	Rotor speed deviation, p.u.
δ	Rotor Angle, rad
e'_d, e'_q	d and q axis transient emf, p.u.
P_m	Mechanical power, p.u.
T_m	Mechanical torque, p.u.
P_e	Electrical power, p.u.
P_t	Bus Terminal Active power, p.u.
Q_t	Bus Terminal Reactive power, p.u.
V_t	Bus Terminal Voltage, p.u.
I_t	Bus Terminal Current, p.u.
f_r	Bus Terminal Frequency, p.u.
E_{fd}	Exciter Field Voltage, p.u.
T_m	Governor Torque p.u.
x_d, x_q	d and q axis steady state reactance, p.u.
x'_d, x'_q	d and q axis transient reactance, p.u.
J	Inertia constant, s
T'_{d0}, T'_{q0}	d and q transient open circuit time constant, p.u.
i_d, i_q	d and q axis current, p.u.
V_{ref}, P_{ref}	Voltage and Power reference, p.u.
K_a, T_a	Exciter gain and Overall time constant, p.u.

R_p	Governor droop rate, p.u.
T_g	Governor overall time constant, p.u.
λ_k	Successful data transmission probability at k^{th} instant
γ_k	Binary random variable for data transmission status at k^{th} instant
w, v	Process and measurement noise
'+','-'	aposteriori and apriori estimates
C_k	Covaraince matrix for Kalman filter
S_k, R_k	Process noise and measurement noise matrix
$\gamma_{COP}, \kappa_{COP}$	Centre of Power instatbility index
W_{di}	Rate of transient energy change index for i^{th} generator, p.u.
W_i^T	Total energy of i^{th} generator, p.u.
W_i^{KE}	Kinetic energy of i^{th} generator, p.u.
W_i^{PE}	Potential energy of i^{th} generator, p.u.

Chapter 1

Introduction

1.1 Background

Traditional power systems, built on large-scale remote generation models are subjected to increased stress as demand and supply technologies are continually evolving. Even though the basic principle of power transmission remains the same, more constraints are imposed by policies and regulations that aim to reduce carbon footprint [2].

The addition of renewable energy sources is changing the nature of the grid and its operation. There is the rapid integration of new renewable resources to U.S. power grid, e.g., in California to meet mandates in renewable energy portfolio [3] and also similar trends can be witnessed in European networks, e.g., Denmark government strategy to ensure that 50% of the consumption is supplied by wind power in 2020 [4]. In a detailed congestion study [5] on the U.S. grid, it has been found that the changes in demand pattern and proliferation of renewable energy sources, particularly wind, have resulted in the operation of lines at reduced constraint limits despite considerable investment and construction of transmission lines [6].

Hence the existing grid operation and infrastructure need to be restructured to be more flexible, agile, yet more robust and resilient to accommodate low-inertia generation sources and volatile demands. Thus the first step would be to improve the monitoring of the grid condition and then establish local and wide area control strategies [7–9]. Conventionally power system network monitoring was performed by estimating voltage magnitudes and angles, which were considered as states, at the buses of the network. Because of measurement error and communication problems (delay, missing data), the state estimates have

uncertainties, and a robust monitoring mechanism was needed. This requirement became more apparent following the 2003 Northeast U.S. blackout, which occurred as a result of limited understanding of the system, lack of visualization tools, and availability of real-time data [10]. The United States-Canada Task Force recommended all utilities to use "time-synchronized data recorders" for better situational awareness. With the improvement in technology, computational power, and data transmission rates increased, which resulted in synchrophasor devices capable of providing discretized voltage and current phasor information (phase and magnitude) at 60 Hz with a timing accuracy of 0.2 μsec [11]. These synchrophasor devices or PMUs (Phasor Measurement Units) have been deployed across the entire North American grid, as shown in Fig. 1.1

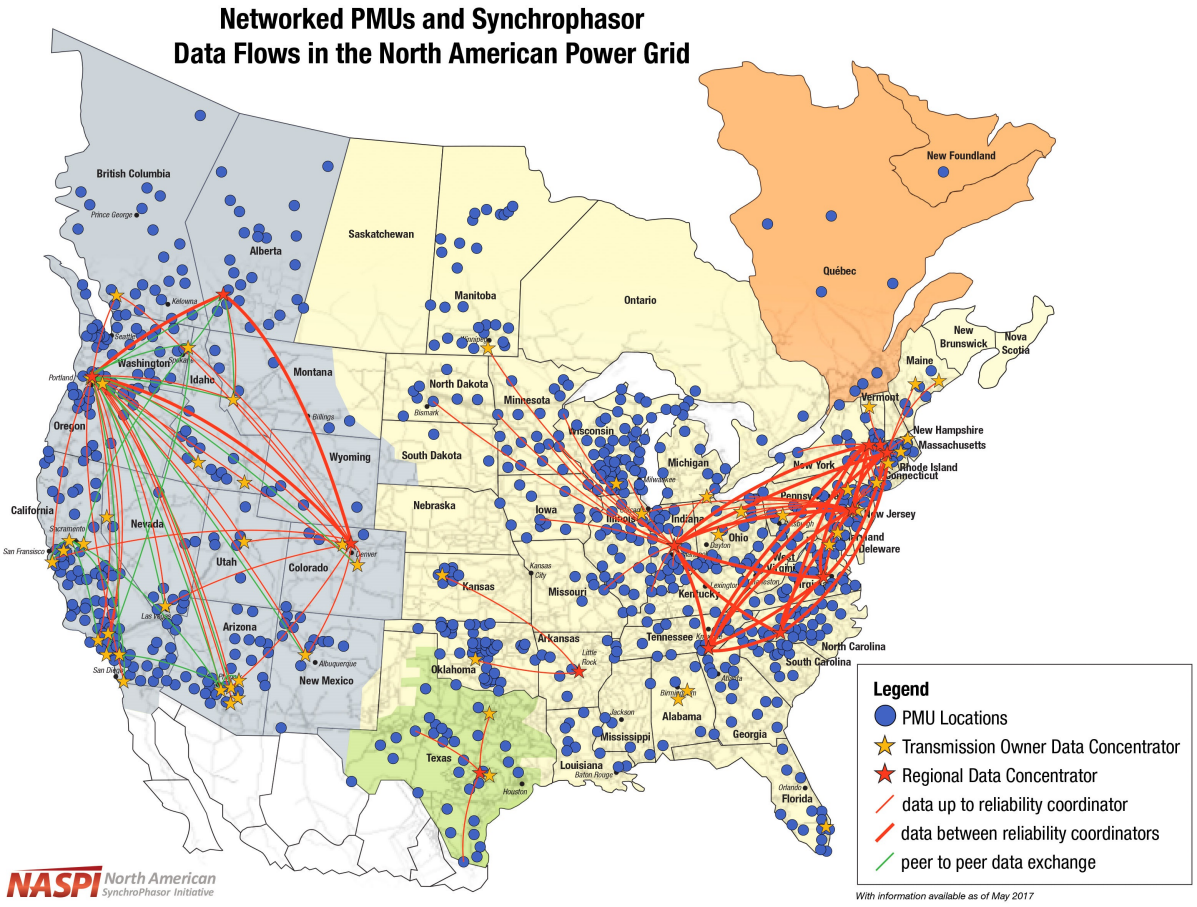

Fig. 1.1 PMU location and data transmission in the North American Grid [1]

High resolution data from PMU makes it feasible to observe dynamics that were missed out by the SCADA (Supervisory Control and Data Acquisition) system. which has led to a network of PMUs spatially distributed across the grid. Data from these spatially distributed PMU devices are sent to a central location, which is termed as Phasor Data Concentrators (PDC). Real time monitoring of network conditions has now become possible with a fast communication network with reasonable bandwidth, which is termed as Wide Area Monitoring Systems (WAMS).

With an established improved monitoring system, the next step is to create a mechanism to detect an outage event that can escalate into a significant system wide disturbance and prevent it. Utilization of wide area information in designing a potential innovative specialized protection scheme has been envisaged in [12]. The societal and financial implications of a blackout are enormous for utilities, as is evident from the analysis of two severe blackout cases in the U.S. [13] and India [14]. Hence efforts have been made to utilize the spatiotemporal information provided by PMUs and develop instability detectors, which would predict an impending instability before its onset. An initial concept of using generator terminal phasor data and applying a decision tree for prediction is presented in [15]. This is improved further by taking into consideration generator angle, speed, rate of change of speed, and indices that combine the same and thereby applying decision trees for instability detection in [16]. Subsequently there have been numerous publications on the application of decision trees and other machine learning techniques in instability detection or transient stability assessment of power systems [17–22]. A comparative analysis of the decision tree with other variants of classifiers is presented in [23]. Application of state of the art time adaptive Long Short Term Memory Network (LSTM) classifier used for real time instability detection can be found in [24].

Once an impending instability has been detected following a contingency, an automatic system wide mitigation action, without operator intervention, is used to maintain system stability. This functionality is incorporated through Remedial Action Scheme (RAS) which is defined by North American Electric Reliability Corporation (NERC) [25] as “an automatic protection scheme that detects “abnormal or predetermined system conditions and takes corrective actions other than and in addition to faulted component isolation in the form of changes in generation and/or demand, system configuration to maintain system reliability”. Conventionally RAS is designed through offline simulation studies and executing the pre-planned actions to prevent system collapse.

1.2 Literature Review

One of the earliest formal works on RAS [26] presents an algorithm for automatically identifying constraint violations and deploying mitigation actions while addressing computational constraints. In conventional RAS design, critical contingencies and control actions for similar cases are identified through offline studies and stored in a database. The actions are executed when an abnormal condition similar to that observed in studies is detected in the system [27]. The RAS Control principles are categorized as:

- Event-based: It is an open-loop type of control action which detects outages and/or fault events and executes generator/load trip as necessary to mitigate event impact.
- Parameter based: It performs an indirect event detection by measuring system variables, i.e., power, angles, and their derivatives as an occurrence of critical events result in a significant change in them.
- Response based: This is a closed-loop process and, the control actions are implemented in an incremental manner by monitoring the system conditions and response.

The literature reports several innovations as implemented by utilities in various grids. In [28], a pattern matching technique to relate real time system conditions to existing ones in the database before executing the predetermined control action is implemented in BC Hydro. Also, a load shedding based RAS scheme in BC hydro that operates on sensitivity analysis of load impact on voltage profile is reported in [29], and Bonneville Power Administration's experience of implementing a RAS in power flow that operates on the initial condition and topology change is cited in [30]. A detailed design overview of implementing RAS in the PG&E grid is depicted in [31] while in [32] PacificCorp's Jim Bridger RAS experience on implementing and coordinating a dual, triple modular redundant Programmable logic controller is presented. [33] provides a summary of worldwide industry experience and design guidelines for the system integrity protection scheme, which includes RAS as well. Simulation results demonstrating an increase of resiliency through RAS in a radially configured and vulnerable Central American Power Grid is reported in [34]. Motivated by a blackout incident in an ultra-mega-power project, Special Protection Scheme (SPS) as a proposed solution has been explored in [35]. The design and development process of

a unique protection scheme through a global and local control of compensator to maintain stability and security of the Hydro-Québec network is presented in [36]. Industrial experience of the methodology adopted for solving an issue of coordination between under frequency relay and implemented SPS in Kinmean Island, Taiwan, is reported in [37].

An analytical corrective control selection of an online remedial action scheme is described in [38] that takes into consideration the possibility of cyber-attack. Even though most of the mentioned RAS schmess are not optimized, a few work have been done that attempts to implement optimized schemes, e.g. [39] minimize generation-shedding cost while wind curtailment minimization is done in [40]. Also in [41], the optimal operation of RAS considering wind farm grid code and unified power flow is tested on a benchmark system. The performance of a robust special protection scheme considering the effects of the communication network has been studied in a hybrid simulation setup by interfacing a power system simulator with a network simulator in [42]. An innovative method of SPS in which Transient Stability Emergency Control is modeled as a mixed-integer nonlinear optimization problem and tested on an electric grid in China can be found in [43]. A study considering centralized and decentralized system integrity protection depending on the application and tested on a grid consisting of wind generation is presented in [44]. In a recent publication [45], an adaptable system integrity protection scheme is presented to deal with the challenging effects of intermittent renewable generation while the industrial experience of RAS deployment in Southern California, while addressing this challenge is described in [46]. [47] explores new capabilities of SPS to maximize the cost-effective integration of solar power while addressing technical challenges of mitigation congestion and maintaining appropriate dynamic response.

1.3 Problem Definition

The major problem with currently deployed RAS schemes mentioned in the previous section is that the implementations are mostly event-based and parameter-based, which relies on comparison with offline studies or violation of certain predetermined threshold of network variables before initiating control action. However, it is evident that because of the unpredictable nature of the modern grid, it is tough to determine impending critical contingency at all possible operating conditions and identify possible control actions from a previously stored lookup table created from offline studies for its mitigation.

The implication of the operating scenario increase is that a system operator will need to invest considerably in computational resources and extensive data management for the conventional RAS scheme. Insufficiency of existing offline and computationally demanding approaches and a need for real-time approaches has also been acknowledged in [38, 48]. Moreover, the control actions are typically determined by iterating over multiple post-contingency scenarios, which is not ideal for real-time implementation as the execution speed of control action is crucial [38, 40] for mitigating instability. Also, utilities face the problem of the limited applicability of RAS due to lack of inter-communication amongst different RAS as faced by Southern California Edison [46], resulting in a need for a centralized network-wide RAS.

Interestingly the authors in [46] accentuate that the problem of the rapid interconnection of renewable energy sources without siting new transmission lines can be mitigated through the implementation of an effective RAS scheme as it allows the network to operate at reduced stress conditions. Thus, the problems associated with RAS in regards to renewable energy source integration are interrelated and can be solved using a centralized RAS architecture that detects and identifies control actions extemporaneously.

A centralized online RAS would evidently be based on the high fidelity spatio-temporal information provided by PMUs, as has been proposed in [48, 49]. However, it has been shown in [50], that the terminal phasor measurement units are not able to capture the generator terminal dynamics accurately and it may affect the performance of a RAS that utilize this data.

Finally even though RAS consists of two parts: –i) instability detection and ii) mitigation, most of the existing literature focuses on the latter while makes the assumption of successful detection.

1.3.1 Thesis Statement

In order to address the problems stated in the previous subsection, the thesis primarily focuses on establishing a response based RAS action that identifies and formulates control actions online and stabilizes the network by its execution. The concept and its contrast to the conventional RAS scheme are explained through block diagrams in Fig. 1.2,

In conventional RAS, as shown in Fig.1.2a if a predetermined topology change of the post-disturbance power system occurs, then a predefined set of control action is selected

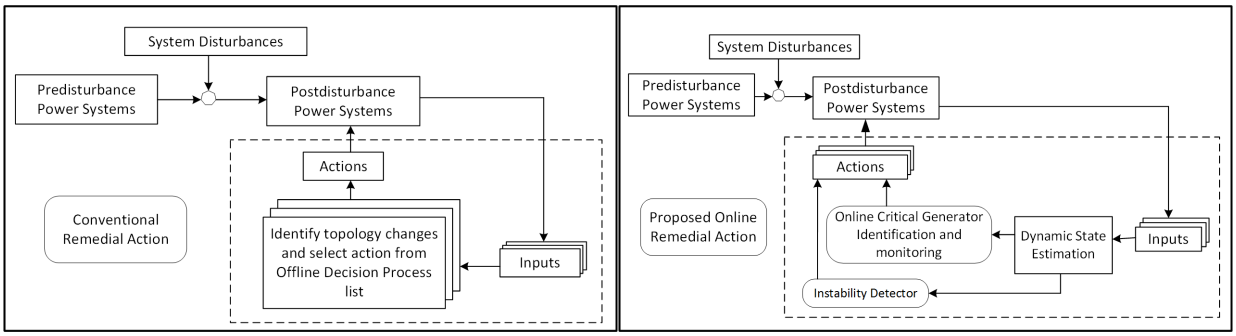

(a) Block Diagram of Conventional RAS (b) Block Diagram of Proposed RAS

Fig. 1.2 Block Diagram Comparison

from Offline Decision Process List and executed. The proposed RAS shown in Fig.1.2b first estimates the dynamic states of generators in the network using the PMU-based inputs of the post-disturbance power system. Thereby an Instability Detector is proposed, which operates on indices derived from dynamic state information rather than on raw PMU data and predicts an imminent instability. Also, a methodology is presented to identify critical generators in real-time, take corrective action in incremental steps, and monitor the system for further actions if necessary. It is to be noted that although the initial training of Instability Detector requires offline simulation for training a classifier, however, the remedial action scheme does not require any offline analysis for its operation and take decisions in real-time.

1.4 Research Objective and Methodology

1.4.1 Objectives

The objectives to address the research gaps mentioned in the previous section have been divided into the following tasks:

1. Establish a decentralized dynamic state estimator (DSE) for full power plants while keeping the model order low for ensuring scalability and minimizing the computational requirement for an extensive network.

2. Perform parametric variations and understand the effect of variations and dependency of individual parameters on the state estimates.

3. Implement a Centralized Dynamic State Estimator (CDSE) from the individual DSEs while taking into consideration communication network problems of interruption and delays and resulting synchronization issues.

4. Compute instability indices and develop an instability detector by training a classifier.

5. Develop a mutli-shot response based RAS that can detect critical generators and stabilize the network.

1.4.2 Tools and Methodology

List of software tools used for research

1. Simulations : Time-domain Simulation and modelling of the test power system network has been done using SimPowerSystems (MATLAB/Simulink). Dynamic State Estimator has been coded in Matlab user-defined embedded function block. Testing the performance of the proposed RAS has been done on Simulink as well.

2. Instability Detector : Training of instability detector has been done using the Classification Learner toolbox and also using Keras(Tensorflow), a python-based package with the ability to run on GPU resulting in faster execution time.

3. HyperSim: For real-time hardware validation of the proposed methodology

1.4.3 Benchmark

The popular benchmark network IEEE 39 bus system [51] is used for demonstration and validation of the effectiveness of the proposed RAS. It is based on the New England Power System in the United States and consists of 10 generators and 46 lines and exhibits complex dynamics that are typically observed in modern power systems. Each of the generators is equipped with Automatic Voltage Regulator (AVR) and Governor. The system and controller parameters are as specified in [51]. IEEE Taskforce on Benchmark Systems for Stability Control [52] has also cited this network as a benchmark model for stability analysis.

1.5 Claims of Originality

The contributions of the work are outlined below :

1. An improved DSE model is proposed, which estimates the exciter field voltage and governor torque along with internal generator states. The estimator uses a reduced-order model and an improved variant of the Extended Kalman Filter (EKF), which deals with communication interruption and delays that may happen during data transmission.

2. An energy function based RAS is proposed, which is significantly different from any active RAS in the existing research literature or industry practice. The proposed algorithm consists of two parts an Instability Detector and a Critical Generator Identification block. The instability detector predicts an impending instability from the aggregated network-wide generator states provided by DSEs while critical generator identification block identifies the critical (run-away) generators from computed individual generator energies and subsequently stabilizes the network through corrective actions. The proposed formulation is a multi-shot scheme as once an action has been instantiated, network stability is monitored continuously, and further actions are taken if required.

1.6 Thesis Outline

1.6.1 Chapter 2: Centralized Dynamic State Estimation Using a Federation of Extended Kalman Filters

In this chapter, the individual generator dynamic state estimator is modified to be able to deal with probabilistic communication interruption and delays. Also the state estimation accuracy of the DSE is improved compared to a previous implementation while keeping the model order low compared to the actual system model. The performance of this new DSE model is demonstrated on two generators of the IEEE 39 bus system under varying levels of noise and communication interruption values.

1.6.2 Chapter 3: Parameter Validation of Dynamic State Estimator

The effect of variation of generator parameters on the DSE model mentioned in Chapter 2 is studied by individually varying the parameters and observing the effect on dynamic states. Additionally it has also been investigated if a selection of Kalman filter affects parametric variation.

1.6.3 Chapter 4: Application Instability Detection

The availability of dynamic state information from DSE established in Chapter 2, offers the possibility of computing the time derivative values of individual generator energy which is used as an instability index for an instability predictor. The new instability indices, along with conventional ones based on generator speed and angle, are used to train classifiers to predict instability. The intricacy of the classification problem is demonstrated, and the performance of two different types of classifiers are compared and contrasted here.

1.6.4 Chapter 5: Automated Remedial Action Scheme

An online remedial action scheme is proposed in this chapter that identifies by developing on the ideas of Chapter 4 the critical generator in the network following a disturbance that would lead to instability, takes appropriate action,and continues monitoring the network for further action if required. The proposed algorithm is tested on an IEEE 39 bus network, and multiple examples of network stabilization have been demonstrated.

1.6.5 Chapter 6: Summary and Conclusions

In this last chapter, the contributions of the thesis are summarized, the discussion provided on the applicability of the algorithm, and prospective directions for this work is mentioned.

Chapter 2

Centralized Dynamic State Estimation Using a Federation of Extended Kalman Filters

2.1 Introduction

In conventional static state estimation, the network states are estimated from present measurement only without any due regard for past information and need to be recomputed at every sample interval. Also, as the nature of the load is dynamic, the inherent assumption that the network is always at steady state is not always valid. It is to be noted that fast estimation of static states, namely, bus voltage magnitude and phase angle, at high PMU sampling rate does not imply that these are dynamic states. As highlighted in many other papers, synchronous generators rotor angle and speed are the relevant dynamic states for all practical matters in wide-area control and stability monitoring [53].

A preferable alternative would be to monitor the network state variables indicating the transient nature of the power system. This technique is termed a dynamic state estimation (DSE). It has the advantage of making apriori estimate of the states from measured data, which results in an accurate aposteriori estimate by appropriate gain computation from the non-linear dynamical equation of model and measurement functions.

A considerable amount of work has been done on DSE with multiple variants of Kalman Filtering and varying degree of dynamical model detail. Most of the early work used Kalman

filtering either for bad data processing [54, 55], tracking dynamic nature of load buses [54] , addressing non-linearity of measurement function [56] or anomaly detection [57]. All these works consider bus voltage magnitude and angle as state estimates but do not consider the dynamic model of synchronous generators. The first paper to consider a non-linear dynamical model of a generator in a Single Machine Infinite Bus system appears in [58].

The model order of DSE is important as it is related to the computational complexity, and availability of the input signals in practical scenarios will dictate the feasibility of implementation of the proposed model. Although [59–62] present reduced-order DSE, their consideration of the availability of exciter voltage, rotor angle, and input torque limits its applicability. As stated in [63] availability of rotor speed and acceleration is difficult to acquire with enough accuracy and so the installation of sensors around the rotor is difficult and often rendered useless because of improper gapping of speed measurement probes or failure of physical and electrical connections.

To address these challenges, the authors in [64] demonstrated a technique for estimating the states as well as exciter field voltage(E_{fd}) as an unknown input and using generator terminal data from PMU and fourth-order model only. Proper estimation of E_{fd} is crucial as steep variations may occur with grid condition change, and it provides a generic way for state estimation where E_{fd} is not readily available as in brushless excitation [64]. The work is further extended in [63] by considering mechanical input (T_m) as an unknown input and thereby estimating it.

Although EKF is the most commonly used formulation for well-defined models, there are other variants of Kalman filter, which has been found promising [65]. Since the Unscented Kalman filter (UKF) does not need an explicit model, there is no need for Jacobian computation, and linearization becomes redundant. Some of the earliest work on using UKF for DSE are presented in [66] and [67]. A decentralized UKF DSE considering a 6^{th} order model for synchronous generator and detailed controller models (governors and exciters) is presented in [68], making the assumptions that all parameters, as well as controller models, are known. A comparative analysis of EKF with UKF based Kalman filter on a single machine infinite bus model is presented in [69]. Another UKF based DSE formulation is performed in [67]. In [70], UKF with Unknown Input (UKF-UI) formulation has been proposed, and the paper also provides a comparison with other Unknown Input based KF formulations.

Recently, the superiority of particle filter (PF) over UKF is shown in [71] by considering

a detailed synchronous machine and parametric model of governor and exciter. However, because a large number of particles were required for satisfactory accuracy, the computational burden was high compared to UKF and EKF. Besides, the PF appeared sensitive to initial conditions, parametric variations and prone to divergence as well [71]. Several other papers either proposing various modifications of the EKF algorithm [56, 72] or considering a different order model by assuming E_{fd} and/or T_m as measurable or constant are the following: [61, 73, 74]. The authors in [74] perform a comparison of different types of Kalman Filter based DSE of synchronous machines. Joint parameter and state estimation has been studied in [75] while a practical case of model validation and parameter calibration is presented in [76]. Almost all of the mentioned papers assume uninterrupted data transmission and no delays.

An improved DSE scheme is presented in this chapter that estimates the states of the generator, as well as exciter field voltage and output mechanical torque from the governor, using signals of PMUs connected to the nearest bus from generator, state variables of generators and controllers are estimated using EKF formulation. A Centralized Dynamic State Estimator is established in subsequent sections by federating EKF of individual generators in the network and also addressing the problem of communication channel interruption and delays.

2.2 Modelling

The full system (generator with exciter and governor) is developed expanding on the model specified in [63]. A fourth-order generator model is used to estimate the generator states rotor angle ($\hat{\delta}$), rotor seed deviation ($\hat{\Delta\omega}$) and d-q axis transient EMFS ($\hat{e'_q}$ $\hat{e'_q}$) while the controller states E_{fd} and T_m are estimated as unknown inputs using EKF-UI (EKF with Unknown Input). The generator terminal PMU device takes in the instantaneous voltage and current measurement of three phases (V_{abc} I_{abc}) and provides as output the phasor values of voltage V_t, current I_t, frequency f_r, active power P_t reactive power Q_t.

In contrast, the proposed methodology estimates $\hat{E_{fd}}$ and $\hat{T_m}$ as states by relating to measured outputs using explicit relation in contrast to [63] alongwith the four generator states. This is a significant improvement as most of the papers have assumed E_{fd} and T_m to be available or tried to estimate them as unknown inputs . As a result of this modification, DSE requires an additional input Power Reference (P_{ref}) and Voltage Reference (V_{ref})

which are decided by the control system operator and can be easily acquired. The estimation results in subsequent sections will demonstrate the improvement in the estimation accuracy of generator states and especially for E_{fd} and T_m. The state estimator operates based on PMU located on the generator terminal only and thus can be implemented in a decentralized manner. An overview of the implementation is depicted in Fig. 2.1

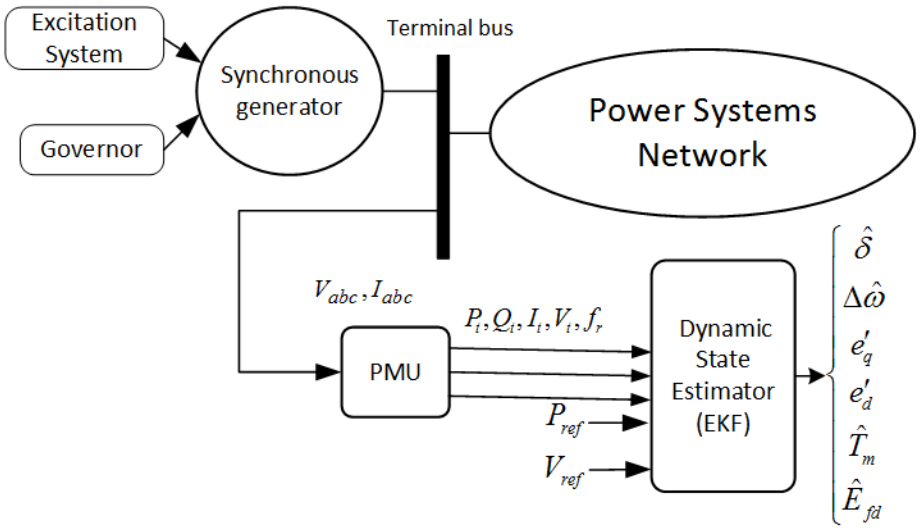

Fig. 2.1 Overview of dynamic state estimator of a synchronous machine

2.2.1 Choice of Kalman Filter

Popularly used EKF has been used for estimation. Since our power system state estimation model and measurement equations are non-linear, they need to be linearized about operating point to make it applicable for state estimation using EKF. It is well known that the linearization assumption is valid only when the operating point of the linearization process is the mean of the state variable [77]. Furthermore some techniques that do not require linearization and use a non-linear transformation to approximate the probability density function [78, 79].

Despite these limitations, it has been established that because of implicit integration, each sample for UKF and PF has the same computational complexity as that of full EKF. The same has been validated by the computational requirement comparison in [80] which makes EKF the obvious choice. For a 30-Bus network, EKF takes about 7 times less time and for 118-Bus it is 34 times less when compared with Unscented Kalman Filter (UKF). Besides, it has been observed in [77] that the nonlinearity of the equations affects EKF

and UKF almost identically, and an increase in error with an increase in sampling time is almost identical.

The computational requirement of the EKF algorithm is $O(n^3)$ where n is the number of states [81]. Apart from this, due consideration have been given to keep the model complexity of the full estimator as minimal as possible without sacrificing estimation accuracy to alleviate the computational burden for large networks.

2.2.2 Simplified Exciter and Governor Model

A generic block diagram of the exciter model is shown in Fig. 2.2 which consists of regulator and exciter that are usually of first-order transfer function each with derivative feedback. Three differential equations would be needed for representing this model in full detail.

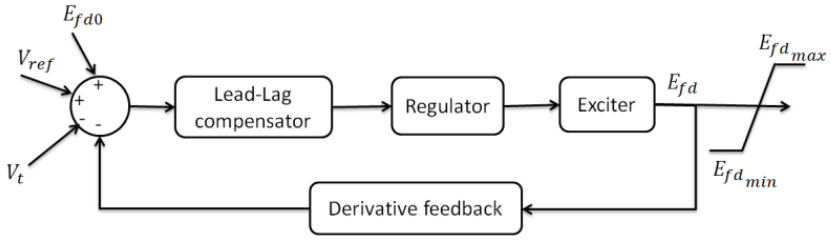

Fig. 2.2 Generic block diagram of an exciter

A simplified exciter model which has concatenated the second order dynamics of regulator and exciter into a single first order model and the effect of derivative feedback is ignored is shown in Fig. 2.3.

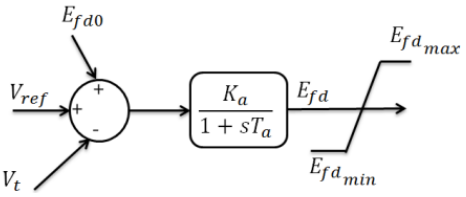

Fig. 2.3 Block diagram of simplified exciter model considered in-state estimator

The exciter equation for this simplified model can be represented by following first order equation (2.1)

$$\frac{dE_{fd}}{dt} = \frac{1}{T_a}\left(K_a\left(V_{ref} - V_t\right) - E_{fd}\right) \tag{2.1}$$

where K_a and T_a are combined gain and overall time constant of exciter and voltage regulator.

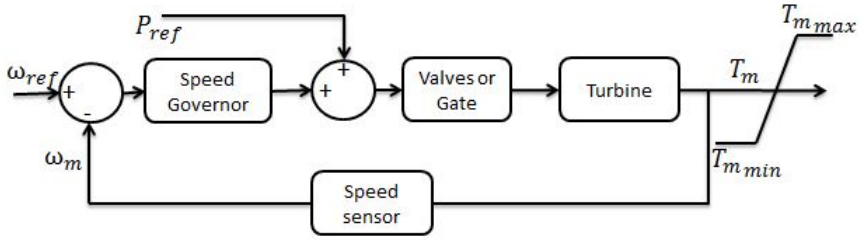

Fig. 2.4 Generic block diagram of the governor

Similarly a model order reduction is performed for the governor and turbine as well. A generic model of governor and turbine is shown in Fig. 2.4 consisting of a speed governor, valve, and turbine. The model of a speed sensor is usually a first-order transfer function with a very small time constant which does not have too much implication and can be ignored. Gates and valves being mechanical units may have considerably higher time constants while turbines are multi-staged consisting of several cascaded units of the first-order transfer function.

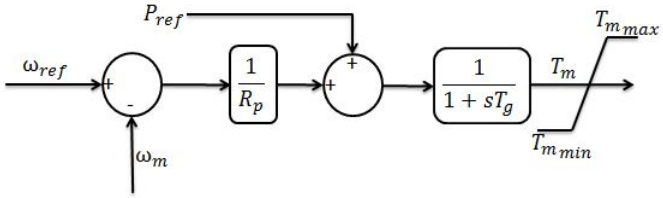

Fig. 2.5 Block diagram of the simplified governor and turbine model in state estimator

In the simplified model as shown in Fig. 2.5, all these units are represented by a single first-order transfer function while the speed governor has a droop gain R_p. Hence the simplified turbine governor model equation considered in the state estimator is given by eq. (2.2)

$$\frac{dT_m}{dt} = \frac{1}{T_g}\left(\frac{\Delta\omega}{R_p} + P_{ref} - T_m\right) \tag{2.2}$$

where T_m is governor output torque, R_p is permanent droop, P_{ref} is mechanical power reference, $\Delta\omega$ is rotor speed deviation in per unit. Because of these two simplifications, it

is expected that the state estimates may show some divergence from the actual response. However, it will be shown in the simulation section that the extent of variation is acceptable. Physical limits on excitation and prime-mover as shown in Fig. 2.4 is incorporated.

$$E_{fdmin} \leq E_{fd} \leq E_{fdmax} \tag{2.3}$$

$$T_{mmin} \leq T_m \leq T_{mmax} \tag{2.4}$$

2.2.3 Generator Modelling

Separating the rotor angle evaluation from the set of dynamical equations in the Kalman filter decreases the computational requirement as the number of states to be estimated reduces. δ_o is the initial value of the rotor angle and can be obtained from the load flow of the network.

$$\delta = \omega_0 \int_{\delta_0}^{t} \Delta\omega dt \tag{2.5}$$

Combining eqs. (2.1) and (2.2) with the fourth order transient model of generator, the state-space model of the entire plant with generator and controllers is as shown below

$$\text{state:} \quad x = \begin{bmatrix} \Delta\omega & e'_q & e'_d & E_{fd} & E_{fd0} & T_m \end{bmatrix}^T = \begin{bmatrix} x_1 & x_2 & x_3 & x_4 & x_5 & x_6 \end{bmatrix}^T \tag{2.6}$$

$$\text{output:} \quad y = \begin{bmatrix} P_t & Q_t & f_r & I_t \end{bmatrix}^T = \begin{bmatrix} y_1 & y_2 & y_3 & y_4 \end{bmatrix}^T \tag{2.7}$$

$$\text{input:} \quad u = \begin{bmatrix} V_{ref} & P_{ref} & V_t \end{bmatrix}^T = \begin{bmatrix} u_1 & u_2 & u_3 \end{bmatrix}^T \tag{2.8}$$

$$\dot{x_1} = \frac{dx_1}{dt} = \frac{1}{J}\left[x_6 - P_t - Dx_1\right] \tag{2.9}$$

$$\dot{x_2} = \frac{dx_2}{dt} = \frac{1}{T'_{d0}}\left[x_5 - x_2 - (x_d - x'_d)\, i_d\right] = \frac{1}{T'_{d0}}\left[x_5 - x_2 - (x_d - x'_d)\, I_t \sin(\phi + \delta_i)\right] \tag{2.10}$$

$$\dot{x_3} = \frac{dx_3}{dt} = \frac{1}{T'_{q0}}\left[-x_3 + \left(x_q - x'_q\right) i_q\right] = \frac{1}{T'_{q0}}\left[-x_3 + \left(x_q - x'_q\right) I_t \cos(\phi + \delta_i)\right] \tag{2.11}$$

$$\dot{x_4} = \frac{dx_4}{dt} = \frac{1}{T_a}\left[K_a\left(V_{ref} - V_t\right) - x_4\right] \tag{2.12}$$

$$\dot{x_5} = \frac{dx_5}{dt} = 0 \tag{2.13}$$

$$\dot{x_6} = \frac{dx_6}{dt} = \frac{1}{T_g}\left[\frac{\Delta\omega}{R_p} + P_{ref} - T_m\right] \tag{2.14}$$

Active Power (P_t), Reactive Power(Q_t), rotor frequency (f_r) and Current (I_t) are four measurable output signals given by

$$y_1 = P_t = V_t \sin(\delta_i)\left(\frac{e'_q - V_t\cos(\delta_i)}{x'_d}\right) + V_t\cos(\delta_i)\left(\frac{V_t\sin(\delta_i) - e'_d}{x'_q}\right) \tag{2.15}$$

$$y_2 = Q_t = V_t \cos(\delta_i)\left(\frac{e'_q - V_t\cos(\delta_i)}{x'_d}\right) + V_t\sin(\delta_i)\left(\frac{V_t\sin(\delta_i) - e'_d}{x'_q}\right) \tag{2.16}$$

$$y_3 = f_r = f_0\left(\Delta\omega + 1\right) \tag{2.17}$$

$$y_4 = I_t = \sqrt{\left(\frac{E_{fd} - e'_q}{x_d - x'_d}\right)^2 + \left(\frac{V_t\sin(\delta_i) - e'_d}{x'_q}\right)^2} \tag{2.18}$$

where f_r is not a directly measured PMU signal but derived frequency of effective internal voltage E_i as explained in [63]. It should be noted here that (2.18) is valid only in steady state and has been incorporated to relate the state representing exciter field voltage to stator current. Also equation (2.1) does not relate to the initial value of exciter E_{fd0}. Hence to obtain the initial value of E_{fd} and separate the unwanted dynamics an extra state variable x_5 is considered. The resultant estimation of E_{fd} will be thus a combination of (2.12),(2.13) and E_{fd0} obtained for new state variables. While it may be argued that E_{fd0} can be computed by equating $\dot{x_5} = 0$, proper indicators for identifying the steady state value of system have to be defined which is particularly difficult in case of noisy data. Instead, x_5 is computed through Kalman filter formulation through equation (2.13) where the current state variable at every time instant will be the sum of the state variable at previous instant plus a random value sampled from a gaussian distribution. So x_5 will

take a path consisting of a succession of random steps before converging to its actual value making it a random walk model. Moreover, as V_{ref} is changed, the steady state value of E_{fd} varies and this is tracked automatically by estimator through E_{fd0}.

In the model (2.9)-(2.14) generator parameters, (transient and steady state reactances, time constants and inertia values) and controller parameters are required to be known to a reasonable degree of accuracy. The resiliency of this model to parametric variation is studied in detail in the next chapter. The novelty of the proposed estimator is that the EKF input signal consists of exogenous variables P_{ref} and V_{ref} which are determined by system operators and can be safely considered as known and the remaining signals V_t and I_t obtained directly from PMU. It is also worthwhile mentioning that in sharp contrast to [63], the excitation system and governors are explicitly modeled and their states incorporated into the EKF dynamic state estimation. Of particular importance is (2.18) which relates E_{fd} to the output measurement I_t and this leads to better estimation as compared to [63] as can be seen in the results section. Additionally because of the changes is modeling it is possible to use the standard EKF formulation rather than the Extended Kalman Filter with Unknown Input Formulation which involves more computational steps [82].

2.3 Centralized State Estimator Formulation

The concept of state estimator for a single generator elucidated in the previous section is extended to that for a centralized one by considering that PMU devices are placed on terminal buses of all generators in the networks under consideration. The Centralized State Estimator can be implemented in two possible configurations and block diagram comparing the two architectures is shown in Fig. 2.6

1. Case 1: State estimator is assumed to be at the location of the generator and transmitted to a centralized location

2. Case 2: PMU data aggregated at a centralized location or at Phasor Data Concentrator (PDC) and state estimation is performed.

Since the state estimates from all generators ultimately need to be aggregated for performing improved monitoring and control, so in case 1 state estimates have to be transferred over a communication channel to a centralized location. Depending on the distance of the generator from the centralized location, there will be varying delays involved because of

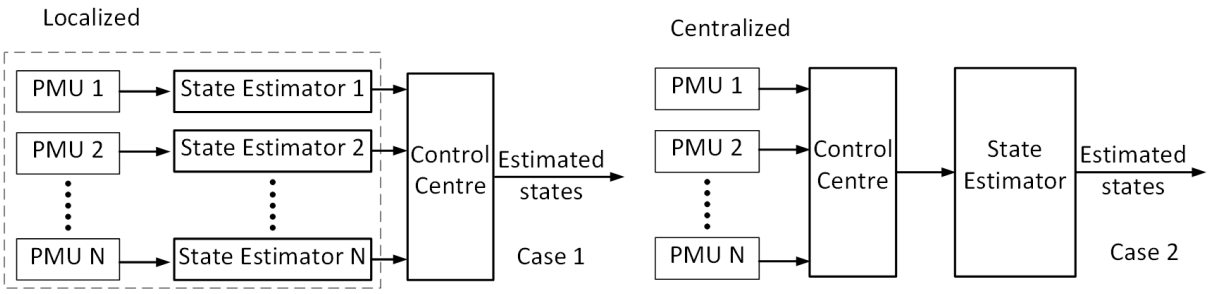

Fig. 2.6 Centralized and Distributed Dynamic State Estimator Architecture

communication channel length and state estimates of all generators will not be received at the same time. Thus for the methodology described in case 1, there is a need to timestamp the state estimates before transmission. This becomes a repetition of the time-stamping process already done by PMU. On the contrary for case 2, as PMU data is already time-stamped, so once it arrives at PDC it is easier to synchronize them despite the delays. Once the PMU data has been received and synchronized, state estimation can be performed without any additional requirement for synchronization. Thus in this paper, we consider case 2 where PMU data is transferred to a centralized location to perform state estimation. In addition to delays, communication channels are subjected to failure resulting in interruption of data transmission which is addressed in the next subsection.

2.3.1 EKF Formulation for Intermittent Observation

A Standard formulation for EKF operates in discrete time but the system equations are in generic continuous form as:

$$\dot{x} = f(x, u, w) \tag{2.19}$$

$$y = g(x, u, w) \tag{2.20}$$

The PMU sends data at discrete time instants kT_s (k = 0,1....n, T_s being sampling time). Hence the continuous-time equations need to be discretized using the following formulation

$$\dot{x} = \frac{x(k) - x(k-1)}{\Delta t} \implies x(k) = \dot{x}\Delta t + x(k-1) \tag{2.21}$$

where Δt is step time, k and $k-1$ correspond to the time at $t = k\Delta t$ and $t = (k-1)\Delta t$ respectively. Substituting (2.21) in (2.19) it can be shown that

$$x(k) = x(k-1) + \Delta t \times f(x(k-1)\Delta t, u(k-1)\Delta t, w(k-1)\Delta t) \tag{2.22}$$

In subsequent sections the time instants is shown as subscripts.

$$x_k = x_{k-1} + \Delta t \times f(x_{k-1}, u_{k-1}, w_{k-1}) \tag{2.23}$$

where f is n-dimensional state equation, x_k and x_{k-1} are state vectors of system $x_k \epsilon \mathbb{R}^n$, u_k is known input vector with $u_k \epsilon \mathbb{R}^p$, w_k is either n-dimensional process uncertainty or modelling uncertainties in system model with $w_k \epsilon \mathbb{R}^n$. Similarly discretizing output equation

$$y_k = h(x_k, u_k, v_k) \tag{2.24}$$

where h is m-dimensional output equation, y_k is m-dimensional measured output $y_k \epsilon \mathbb{R}^m$, v_k is measurement noise $y_k \epsilon \mathbb{R}^m$. The noise vectors w_k and v_k are assumed to be Gaussian, white, and mutually independent with zero mean and covariance matrices S_k and R_k respectively which are positive definite. EKF technique executes in a two-stage recursive process of prediction and update and standard equations and derivation can be found in [83, 84].

In order to circumnavigate the problem of the unreliability of the communication network, EKF formulation is modified based on [85]. The arrival of PMU data at centralized location at k_{th} time instant is considered a binary random variable γ_k. Successful data transmission is indicated by $\gamma_k = 1$ while if unsuccessful then $\gamma_k = 0$. while the probability of successful transmission is represented by $p_{\gamma_k}(1)$ and unsuccessful transmission by $p_{\gamma_k}(0)$. The probability distribution at the k^{th} instant is $p_{\gamma_k}(1) = \lambda_k$, and independent of the probability distribution at any other n^{th} time instant λ_n i.e. $k \neq n$. Based on this, the output noise v_k from standard KF is redefined as:

$$p(v_k/\gamma_k) = \begin{array}{ll} N(0,R) & if \quad \gamma_k = 1 \\ N(0,\sigma^2 I) & if \quad \gamma_k = 0 \end{array} \tag{2.25}$$

This implies observation variance at time k is R when $\gamma_k = 1$ and $\sigma^2 I$ otherwise. The approach taken is to rederive EKF equations using a "dummy" observation with a given variance when the actual data does not arrive and limiting solution as $\sigma \to \infty$. The intuition behind that is that when the data arrives from PMU to PDC ($\gamma_k = 1$), then

the standard Kalman filter operation holds and R is equal to the measurement covariance value. When the data does not arrive ($\gamma_k = 0$) then the value of R is obtained from a gaussian distribution with variance. With this the standard EKF equations becomes

Prediction Step :

$$\hat{x}_k^- = f\left(\hat{x}_{k-1}^+, u_{k-1}, 0\right) \tag{2.26}$$

$$C_k^- = F_{k-1} C_{k-1}^+ F_{k-1}^T + L_{k-1} S_{k-1} L_{k-1}^T \tag{2.27}$$

Update Step :

$$K_k = C_k^- H_k^T \left(H_k C_k^- H_k^T + \gamma_k M_k R M_k^T + (1-\gamma_k)\sigma^2 I\right)^{-1} \tag{2.28}$$

$$\hat{x}_k^+ = \hat{x}_k^- + K_k \left[y_k + h_k\left(\hat{x}_k^-, 0\right)\right] \tag{2.29}$$

$$C_k^+ = \left(I - K_k H_k\right) C_k^- \tag{2.30}$$

The important difference in this formulation compared to standard one is that state vector $\hat{x}_k^+$ and aposterior covariance matrix C_k^+ are random variables being a function of γ_k.

2.3.2 Communication Delay Consideration

As specified in [86], the primary cause of communication delay is because of wireline latency i.e. communication line length. For a 100 km line length, the delay incurred should be 500 μs and varies in direct proportion to distance. However practical experience has shown that the delay per 100 km is 3 ms with maximum regional latency of 45 ms within North America [87] As generators in a power system network have wide spatial distribution hence there will be delays of the order of 10 ms. This implies that the PMU data of generator located close to centralized state estimator will incur minimum delay compared to one located far away. State estimation performed with PMU data without synchronization will lead to out of sequence measurement problem [88]. Thanks to time stamping of PMU data, it is possible to synchronize the state estimate measurements i.e. delay is known.

Apart from communication channel delays will be introduced by network switches, PDC and PMUs. Depending on the manufacturer and model, network switch delays will range from maximum of 250 μsec [89] to as low as 4 nsec [90].Based on the results presented in [91], it can be noted that a Class M PMU has latency of 100 msec while that of Class P PMU is 30 msec. PDC functionalities include data handling, processing, and storage and

forwarding it to next higher level operational centre. Information about PDC definition, function, latencies are outlined [92]. In the paper [93], simulations emulating a PDC with the latest functionalities and considering network delays with different PMU streams and different network condition is performed to have an estimate of PDC delays. It has been shown that PDC delays are typical of the order of 70 msec considering the normal operating condition of the communication network.

It is to be noted that the state estimation formulation for each generator can be executed separately as soon as the PMU data arrives. However to obtain full network state information, it is required that the state estimators for all the generators of the network have been executed. Thus the centralized state estimator will have latency equal to the maximum time delay incurred by each of the communication channels from generators to centralized estimator or PDC and the device latencies involved. A conceptual diagram describing the same with four PMUs is shown in Fig.2.7.

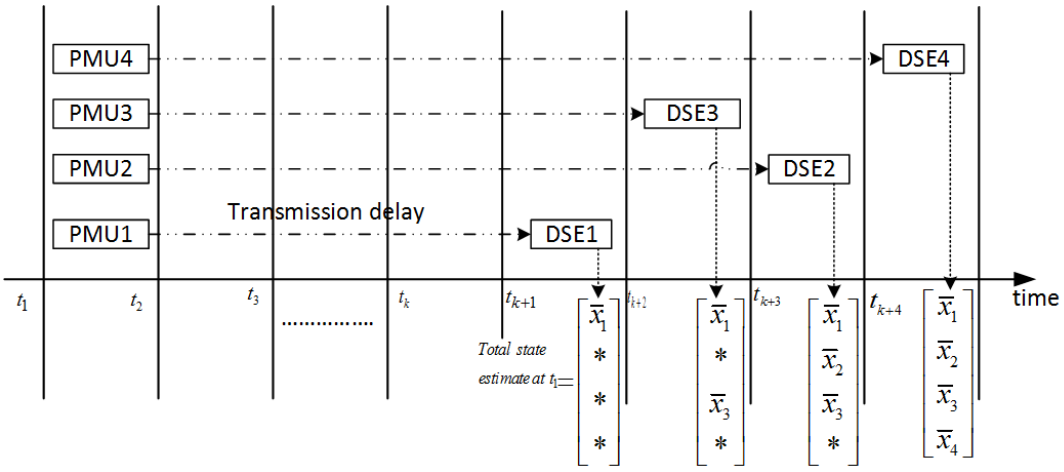

Fig. 2.7 Conceptual diagram for state estimate fusion considering communication channel delay

Although all four PMUs measure and transmit data at the same time, because of delay which is proportional to the length of the communication line, each of the state estimators in a centralized state estimator operates at different time instants. Aggregated state estimate for the entire network is obtained when PMU data is received and the state estimator executed. This simplified methodology of dealing with communication delay does not add any additional computational overhead and will cause a maximum delay of 45 ms for a generator located anywhere in North America from centralized state estimator.

Acceptability of this delay depends on the applications which will utilize the state estimates. For illustration, a 50-ms bound is considered a safe delay limit in most emergency WACS applications [50].

2.4 Simulation Results

The proposed Dynamic State Estimator (DSE) has been implemented using embedded function block in Simulink. DSE receives its signals from Simulink-based PMU models as shown in [94, 95]. PMUs are of type class-M and have internal frequency estimator. They provide DSE with input signal V_t and measured output signals $P_t(y_1), Q_t(y_2), f_r(y_3)$, and $I_t(y_4)$ at discrete time samples. Both the PMU and DSE is running at 64 points / cycle while the model runs at 256 points/cycle. The test system considered is the IEEE 39 bus system benchmark Fig. 2.8 with parameters specified in [51] and also listed in appendix C.

All the synchronous generator models are full 8^{th} order electromechanical model with saturation, stator transients, and rotor transient and sub transient dynamics. Exciter model is of 3^{rd} order with the first order transfer function for regulator and exciter and involves derivative feedback thus corresponding to the IEEET1 type model. The Governor model is of second order while the steam turbine is represented by four stage model for different stages of pressure variation. On the contrary, the DSE is rendered using a 6^{th} order model with mechanical torque and excitation voltage estimated as states. Two other signals that the generator requires are P_{ref} and V_{ref} which are available both locally and at the control center. The internal rotor angle (δ_i) is not estimated as a state unlike [63] but from the states using algebraic relation.

Initial values for states is $x_0 = [\delta_0; 0; 0; 0; 0; 0]$ in which δ_0 is the initial value for rotor angle of each machine which can be obtained from load flow. Covariance matrix S_0 is initialized as $10 \times I_{6\times6}$ and state and output noise matrix initialized as $w_k \sim N(0, Q_k) = N(0, 10^{-3} \times I_{6\times6})$ and $v_k \sim N(0, R_k) = N(0, 10^{-3} \times I_{4\times4})$.

The Simulink model is run with fixed step time $T_s = 1/(256 \times 60) = 6.51 \times 1e-5$ sec. This ensures that the sampling time of PMU is an integral multiple of network simulation time and any errors related to sampling interface error is avoided. Class-M PMUs are assumed to be connected to the low voltage terminal of generators or if connected to the high-voltage terminal, transformer and line reactance needs to be included in DSE as external reactance. The probability of successful data transmission is being set at $\lambda_k = 0.9$

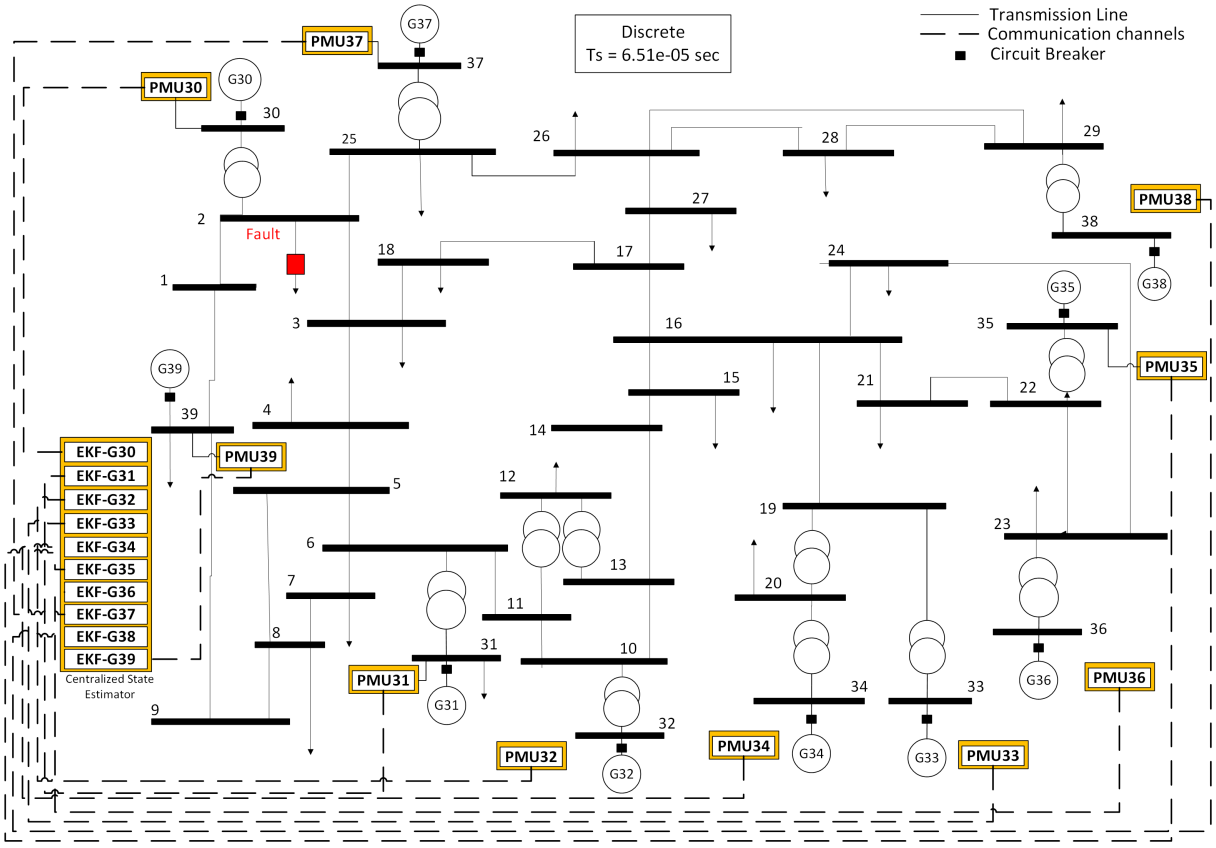

Fig. 2.8 IEEE 39-bus system with PMU and EKF-UI blocks on all generators and Centralized State Estimator located near generator G39

(90 % reception) unless specified otherwise which is more than reasonable consideration based on data in [87].

The Centralized State Estimator is assumed to be located near generator G39 and the communication delay of PMU of each generator is assumed to be proportional to the least length of the transmission line to G39. As the least transmission line length of G34 to G39 is 700 km so the delay in PMU signal received at CSE is considered to be approximately 21ms based on the reasoning in Section 2.3.2. Delays for other generators have been set accordingly.

2.4.1 Close 3 Phase to Ground Fault

In this simulation, the fault is considered on Bus B2 initiating at t=2 s and terminating after 10 cycles at t=2.1667 s. Comparison of estimation results of states x_1 , E_{fd} (from

combined x_4 and x_5) , T_m (from x_6) with actual ones are shown in Fig. 2.9. As there is no access to internal transient stator voltages (e'_q e'_d) for SimScape Power System (SPS) model, so it is not possible to show a comparison of state estimates with actual signals. However estimates x_2 and x_3 show improvement in comparison to results in [63], marked as EKF-UI in Fig. 2.9. It can be readily observed that estimated rotor speed ($\Delta\omega$) and rotor angle (δ) obtained by integrating ($\Delta\omega$) readily follows the actual signal quite closely. The dynamics of estimated Excitation Voltage obtained form states (x_4 and x_5) and actual ones are quite similar. The resulting difference is because of the approximations made by considering a simplified model of exciter in estimator while the actual exciter model in simulation is of the third order.

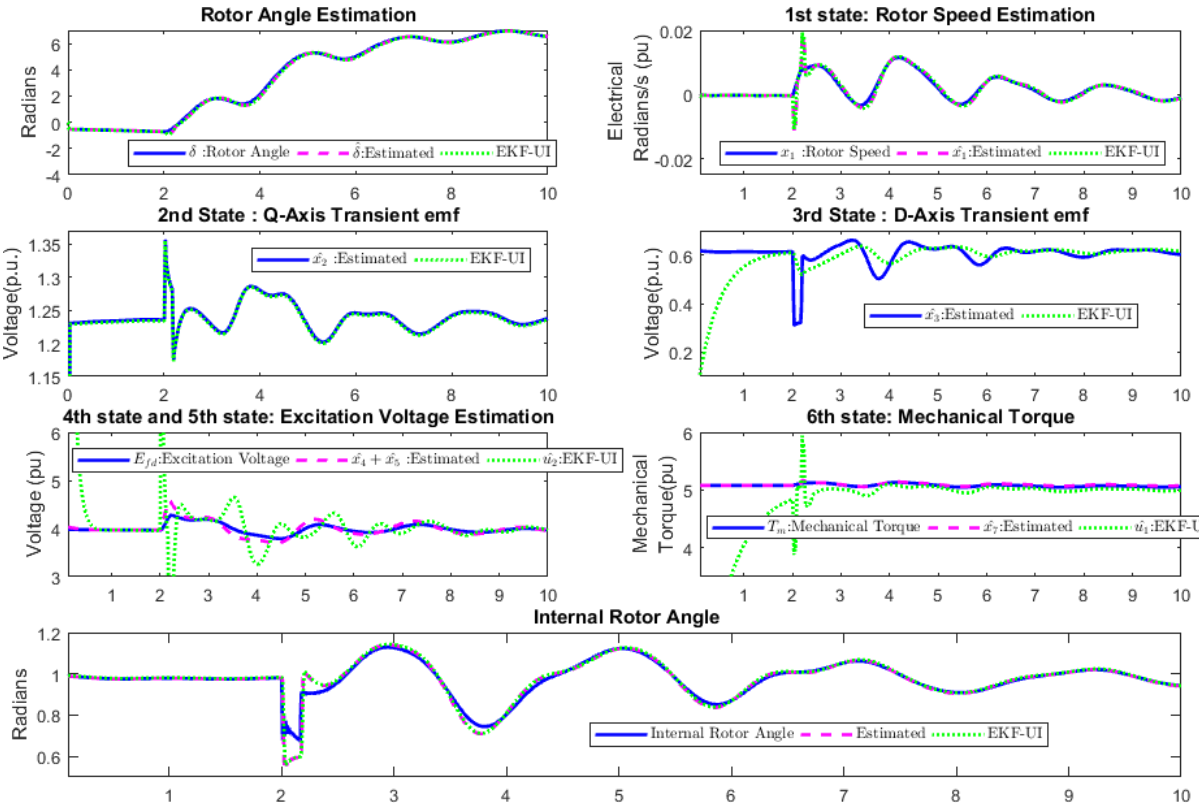

Fig. 2.9 Result of State Estimation for Generator G34 in the IEEE 39 bus system with a three phase to ground fault on bus B2 at t = 2sec for 10 cycles. Actual and Estimated States ($\delta, \Delta\omega, E_{fd}, T_m$, d and q-axis Transient emf from states x_2 and x_3 respectively and estimated internal rotor angle - δ_i)

The actual and estimated output comparison for Active Power (P_t), Reactive Power

(Q_t), frequency (f_r), and Current Magnitude (I_t) of generator G34 are shown in Fig. 2.10. The proposed estimated scheme is better than EKF-UI formulation in [63] as it is less oscillatory, does not produce spikes and jitters during initialization as well as during fault periods. Next, the estimated Torque (T_m) from the state tracks the actual one quite well despite considerable modeling order difference between the governor turbine model in estimator and Simulink. Once again in comparison with results from [63] it can be noticed that the new estimate is less oscillatory, has faster convergence to actual value after initialization, and result in less jittering signal responses to sudden disturbance.

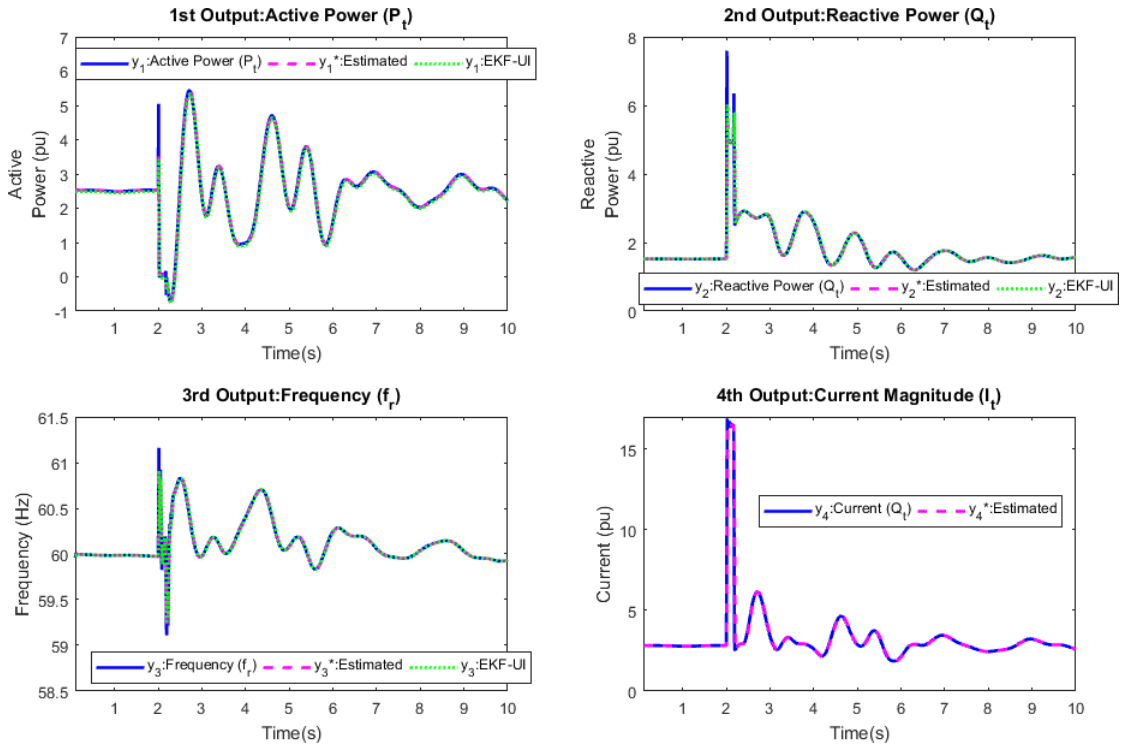

Fig. 2.10 Actual and Estimated Outputs (P¬t, Qt, fr and It) for a three phase to ground fault on bus B2 at t = 2sec for 10 cycles for Gen 34

Although internal rotor angle is not estimated as a state but computed algebraically using the equation in [63] still, the estimate is similar to the actual one as shown in Fig. 2.9. The d-Axis transient emf (e'_d) from state x_3 matches the estimate from EKF-UI. Because of a different formulation for i_q used in [63], the resulting estimate for state x_4 differs from the EKF-UI formulation. As a result of this consideration, state x_4 converges to actual value rapidly despite being initialized at zero value while the estimate in [63] takes nearly a

full second. Comparisons of estimated outputs versus actual outputs are presented in Fig. 2.10, where there is no discrepancy in all the four cases.

2.4.2 Remote 3-Phase to Ground fault

Based on reasoning provided in [63], validation with remote fault ensures that the estimator works properly when inter-area oscillations are dominant compared to local modes. Thus in the simulation fault on Bus B2 is considered while a state estimator located on generator G34 far away from fault is monitored. To demonstrate the performance of the state estimator for a remote fault, the DSE has been placed at Generator G34 while receiving electrical signals from PMU assumed to be located at bus B34. The disturbance is the same as mentioned in section A, three phase to ground fault on Bus B2 at t=2 sec and cleared after 10 cycles i.e. at t=2.1667 sec.

Comparisons of the state estimates with actual signals are shown in Fig. 2.11. It can be observed that even with the dominance of inter-area modes the estimator response readily trails the actual signals. The estimated controller signals of the exciter and prime mover i.e. E_{fd} and T_m tracks actual ones with a reasonable degree of accuracy. Also in comparison to estimates for E_{fd} and T_m from EKF-UI, it can be noticed that the estimates have improved as they are less oscillatory, with no spike during disturbance and have faster convergence to actual values.

A closer inspection in Fig. 2.12 reveals that despite the signal interruption in the output signal (10% of time for λ_k =0.9), the estimated output computed from state estimates can recover these missing values accurately, even during a fault condition. This demonstrates the robustness of the proposed estimator if used with low cost communication channels where data disruption occurs frequently. Hence it can be concluded that the proposed estimation scheme can track the actual signals despite the fact there is a significant modeling gap in the simulation model and state estimator as well as with delays and probabilistic data dropouts.

2.5 Sensitivity to Noise

The simulation results in previous sections have been performed with the assumption that measurement and input signals are devoid of any noise. A study of the impact of the noisy signal on the proposed state estimator has been performed in this section. An overview of

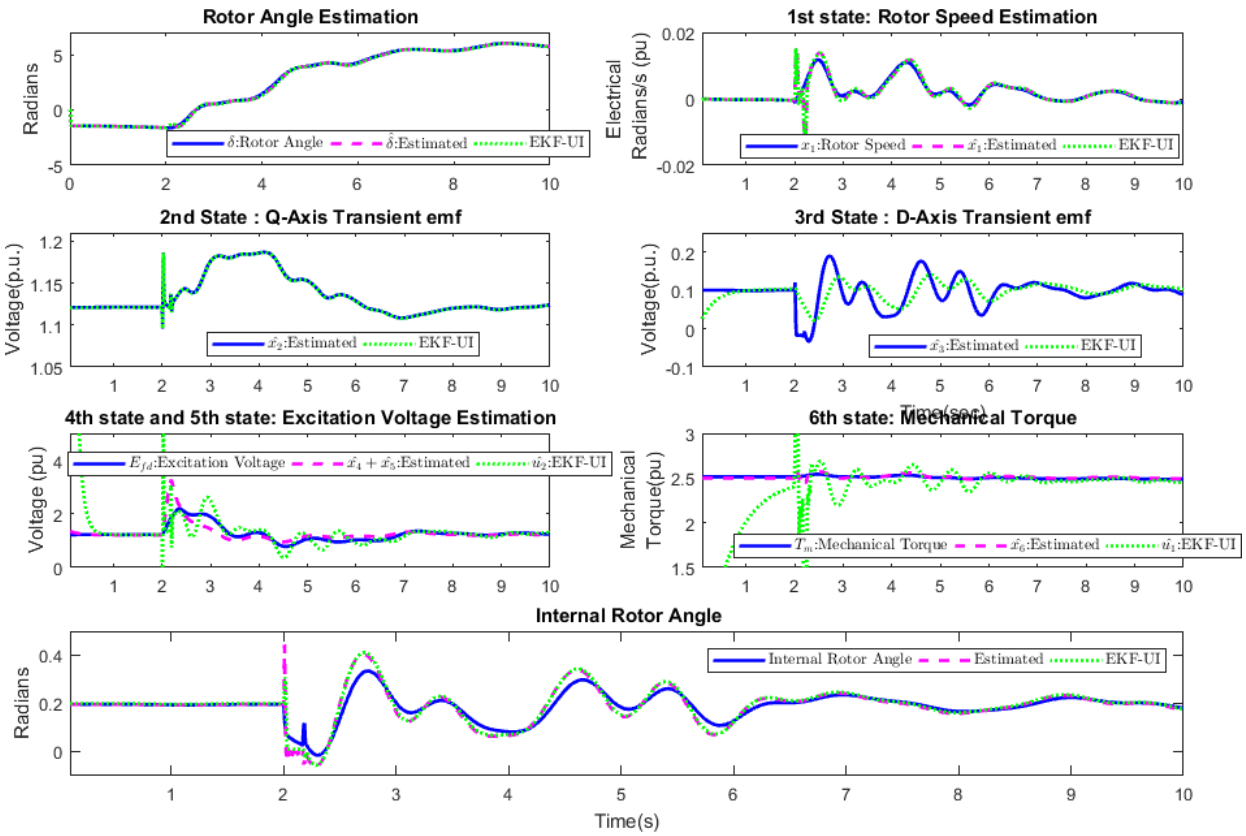

Fig. 2.11 Result of State Estimation for Generator G30 in the IEEE 39 bus system with a three phase to ground fault on bus B2 at t=2sec for 10 cycles. Actual and Estimated States ($\delta, \Delta\omega, E_{fd}, T_m$, d and q-axis Transient emf from states x_2 and x_3 respectively and estimated internal rotor angle - δ_i)

the extent of variation expected in measurements resulting from instrument transformers and PMUs are provided in [70]. The time synchronization accuracy is 0.2 μs according to IEEE Standard C37.118.1-2011 and C37.118.1a- 2014. This corresponds to a phase measurement error of $\pm$0.08 mrad for 60 Hz system and a frequency error of 0.005 Hz. Also, the current and voltage magnitude measurements are constrained by the accuracy of instrument transformers and IEEE Standard C57.13-2008 specifies the instrument transformers' accuracy within a range of 0.1 and 0.3 %. Based on these values and making the assumption of the presence of high level measurement noise, all the measurement signals are assumed to have a standard deviation of 10^{-3}. The noise simulation is performed by adding an "Additive White Gaussian" block in Simulink to the three phase voltage and current signals which means that PMU filtering characteristics are accounted for. No noise

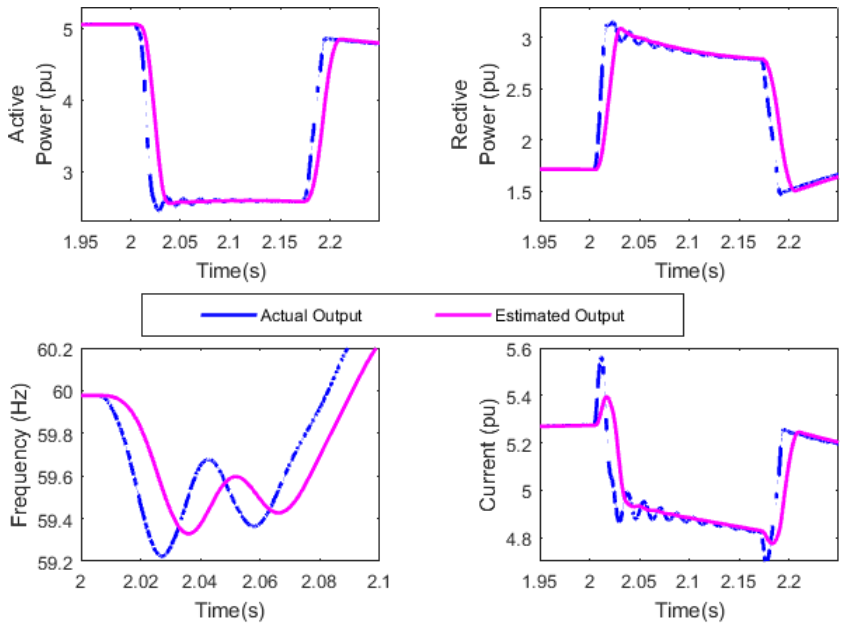

Fig. 2.12 Actual and Estimated Outputs (P_t, Q_t, f_r and I_t) for a three phase to ground fault on bus B9 at t=2 s for 10 cycles for Gen G30 considering communication delay and data transmission probability of λ_k =0.9

has been considered in the reference signals. As the internal states of the Simulink model are not accessible it was not possible to add process noise (modeling discrepancies between EKF and simulation amounts to process noise, although it is hard to characterize). Innovation vector (i.e. difference between predicted and actual output) of generator G34 for the same contingency as specified in section 2.4 is shown in Fig. 2.13.

The estimated output can track the actual output in the presence of expected noise and communication interruption and delay with a reasonable degree of accuracy. To take into consideration randomness of noise while testing the performance of the state estimator, simulation is repeated through multiple Monte-Carlo trials. Estimation accuracy is evaluated using the following metric [74].

$$MSE(\hat{x_k}) = \frac{1}{M}\sum_{m=1}^{M}(\hat{x}_{k,m} - x_{k,True})^2 \tag{2.31}$$

where M corresponds to M^{th} trial, k to k^{th} time step and $x_{k,True}$ is actual state estimated without any noise in the simulation model. Based on the results in [74] , M=50 has been considered to be a sufficient number of trials.

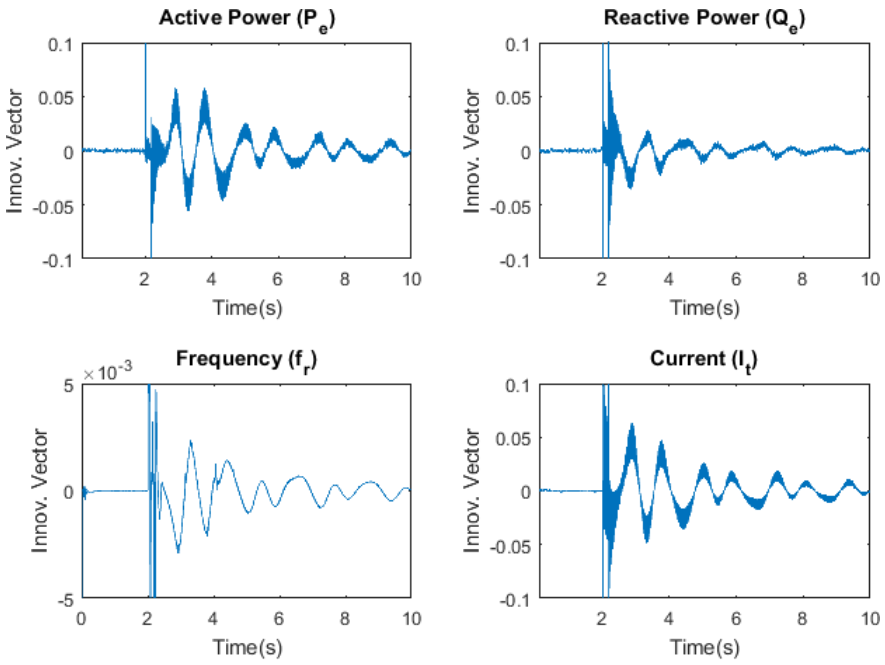

Fig. 2.13 Innovation vector of Gen G34 with noise standard deviation of 10^{-3} in input and measured output signals and data reception probability of $\lambda_k = 0.9$

To further study the effect of noise with higher variance, simulations are also performed with measurement noise standard deviation set at 0.01 and 0.1 which are 10 and 100 times the standard noise values expected in the dynamic state estimator. In order to observe the performance of the estimator across this broad range of noise variation, the above mentioned metric is computed in dB using $10log_{10}(MSE)$. Evaluation of the metric is performed on IEEE 39 bus with the same disturbance as considered in Section 2.4 . A comparison of the metrics for the three noise cases for generator G34 is shown in Fig. 2.14. Although the metrics are plotted for only one generator in the interconnected network, the results remain consistent for other generators as well as with disturbance variations.

2.6 Effect of increasing communication interruption

The effect on the performance of the state estimator with increasing probability of the disruption of communication channel has been studied in this section by decreasing the probability of data reception λ_k . The norm of innovation vector has been used as a figure

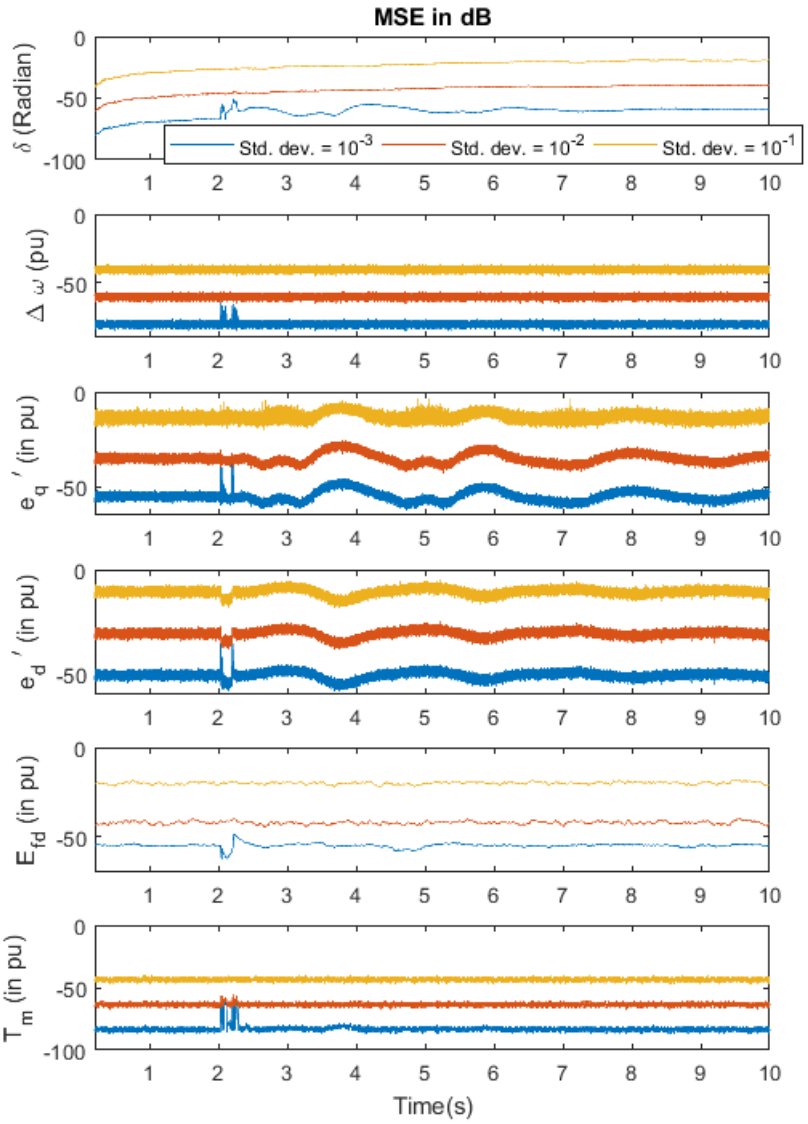

Fig. 2.14 Comparison of MSE for 50 sets of Monte Carlo simulation under varying noise levels of Gen 34

of metric for comparison and λ_k values of 0.9, 0.8 and 0.7 has been considered. Results have been demonstrated for Generator G30 with the same contingency as considered in Section 2.4. From Fig. 2.15, it can be observed that the norm value increases as the probability of data reception at centralized state estimator decreases. This implies that for

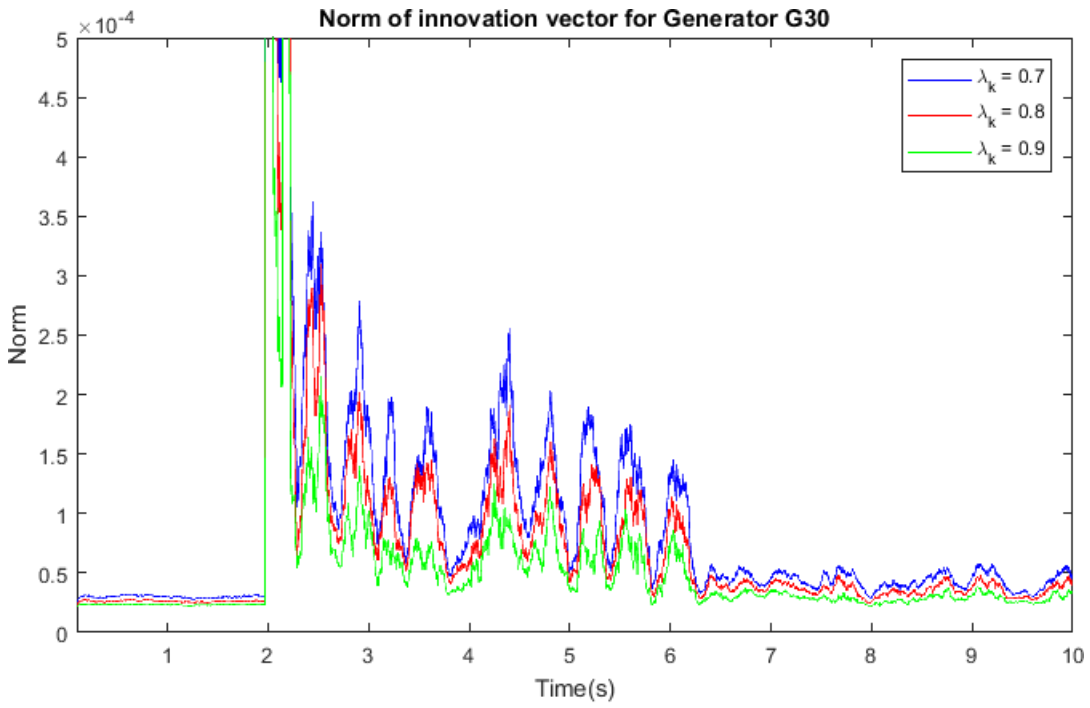

Fig. 2.15 Variation of norm of innovation vector with a variation of data reception probability λ_k at centralized state estimator

the proposed scheme, the performance of state estimates will deteriorate with decreasing capability of successful transmission of data. However, it highlights the robustness of the proposed estimator if used with cheap communication channels subject to frequent PMU data disruption.

2.7 Computation Times

The DSE blocks receive data at 24 points/cycle from PMU. Hence the computation time of whole centralized state estimator completion should be completed before the reception of data instant i.e. execution time for 60 Hz system should be less than 0.6944 ms. The system specification on which the study has been conducted is Intel Core i7 CPU @ 3.4 GHz (4 core), 8GB Ram, and 64 bit Operating System. The average computational time for each iteration is shown in Table 2.1. The average computational time of individual DSE is 0.4102 ms per iteration. This makes it feasible to operate it in real time. In order to evaluate the cumulative computational performance of the state estimator, using parallel

pool feature of Matlab it was attempted to distribute the state estimator computation among the 4 cores of the processor. However, since the test network consists of 10 DSE so each processor will have to perform the computation of $2 \sim 3$ DSE. Thus testing was done by considering 4 DSE together and the average time required for each iteration is 0.5954 ms. This once again reaffirms the feasibility of implementation of the proposed scheme in real-time provided each DSE is executed on an individual processor. Execution of all the ten DSE on four cores requires 1.63 ms which implies that the sampling rate at which DSE receives data have to be reduced to 10 points/cycle. It has been observed that the estimation performance is only affected to a minor extent as a result of sampling rate reduction.

Table 2.1 Computational Times

Methodology	Average Computational time for one iteration (in ms)
Single DSE single core	0.4102
Four DSE four core	0.5954
Ten DSE four core	1.6338

2.8 Conclusion

This chapter proposed an improved methodology for dynamic state estimation and its performance evaluated by considering probabilistic communication interruption and delays. Convergence to actual states occurs within a few cycles after zero state initialization. Also despite the modeling differences between the state estimator and simulation model, the performance of the estimator against actual signals has been validated to a reasonable degree of accuracy. Minimizing the overall order of estimator resulted in a shorter computational time of individual state estimator. Furthermore, satisfactory results have been attained in te presence of reasonably high noisy signals the overall DSE performance was further validated successfully on an interconnected network based on a real power system model.

The benefits of this state estimator are summarized below

1. The input to state estimator is Power Reference (P_{ref}) and Voltage reference (V_{ref}) which are decided by system operators and easily available with a time scale of 5 min to a full season, depending on operation practices.

2. Exciter output signal (E_{fd}) and Governor output torque (T_m) estimation are improved significantly compared to the results shown in [63].

3. No assumption has been made about the model of exciter and governor in simulation, making the DSE generic.

4. The overall order of estimator has been kept to a minimum even though the actual simulation models for generator, exciter, and governor have higher order.

Chapter 3

Parameter Validation of Dynamic State Estimator

3.1 Introduction

Chapter 2 established a robust mechanism for dynamic state estimation that can track the states of the generator as well as of governor and exciter accurately despite communication interruption. The system model parameters need to be known with a reasonable degree of precision to estimate the states properly. The last chapter assumes that the parameters of the model in dynamic state estimation block are the same as that of the actual model. However, there is a possibility of mismatch of values and it would be interesting to note the effect of parametric variability on dynamic states of synchronous generators.

In this chapter, the impact of individual parametric variation on the states has been studied through Monte Carlo Simulations. Furthermore, the effect of the choice of the type of Kalman filter with parametric variability has been investigated as well by considering an Unscented Kalman filter along with the Extended Kalman filter. A conference publication (C) has been made based on the findings in this chapter.

3.2 Methodology

A block diagram representation of the simulation process is shown in Fig. 3.1. The synchronous generator corresponds to any one of the 10 generators in the IEEE 39 bus network with PMUs located on the bus terminals. The phasor values are passed to the state esti-

mator blocks which operate using the reduced order model elucidated in the last chapter. Two state estimator blocks have been considered, one operates using Extended Kalman Filter and the other using Unscented Kalman Filter formulation. The parameter values provided to the state estimator blocks are varied based on Monte Carlo (MC) method [96]. By setting a different parameter value in DSE, a simulation is executed involving a contingency and the state deviation is observed. Therefore each of the simulations is executed by setting a different parameter value in DSE than the one in a generator which is considered as true value and so the state estimates of DSE are expected to deviate from the actual ones.

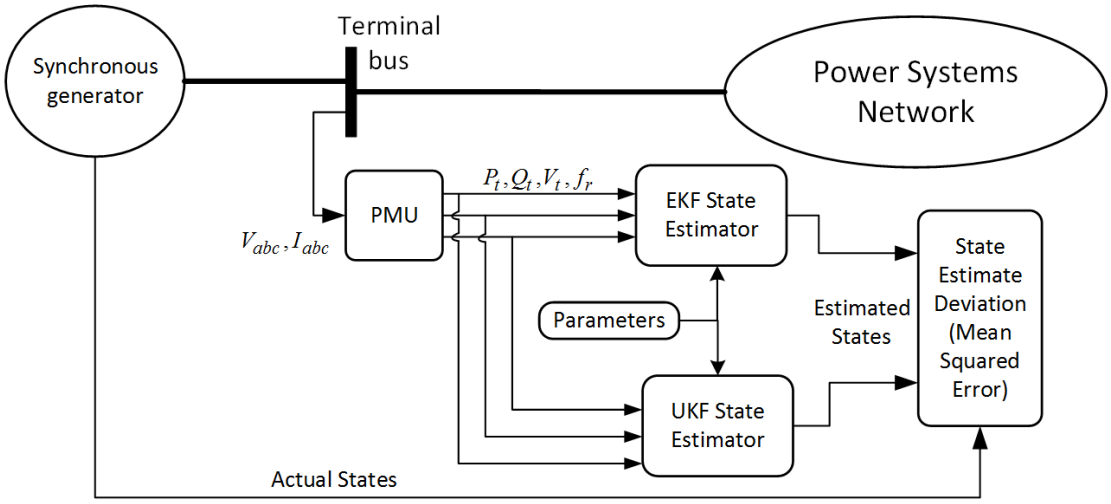

Fig. 3.1 Block diagram representation of parameter validation of simulation model setup

The mathematical model considered in each DSE block is as mentioned in Section 2.2.3. In a concise format, the equations can be represented as

$$\dot{x} = f(x, u, \alpha) \tag{3.1}$$

$$y = g(x, \alpha) \tag{3.2}$$

where $\alpha = \left[x_d\ x_q\ x'_q\ x'_d\ T'_{d0}\ T'_{q0}\ J\ K_a\ T_a\ R_p\ T_g\right]$. Each of these 11 parameters is sampled from a Gaussian distribution which involved creating a normal distribution with a standard deviation of 30 % and then multiplying the distribution by the actual parameter value. During sampling, very few of the parameter values assumed a negative value, and since this is not practically possible so a greater number of sample values than what was required have

been considered and the cases with negative values have been discarded. The deviations of each state estimate from actual ones are evaluated for several parameter values sampled from multivariate Gaussian distributions. To quantify the deviation of state estimates, mean squared error is computed as

$$MSE\left(\hat{x}_k\right) = \frac{1}{M}\sum_{n=1}^{M}\left(\hat{x}_{k,n} - x_{k,True}\right)^2 \tag{3.3}$$

where M corresponds to the number of Monte Carlo simulations performed, $\hat{x}_{k,n}$ is the state estimate from DSE at k^{th} time instant of n^{th} Monte Carlo simulations performed and $x_{k,True}$ is the true state at k^{th} time instant from synchronous generators. For computing, overall estimation errors following metric are used

$$MMSE\left(\hat{x}\right) = \frac{1}{K}\sum_{k=1}^{K} MSE\left(\hat{x}_k\right) \tag{3.4}$$

where K is the number of Monte Carlo trials. The above figures of metrics are based on formulation in [96]. The model considered in DSE is of lower order compared to that used in the actual model. Because of the modeling difference between state estimator and simulation model, there is a possibility of deviation between $\hat{x}_{k,n}$, and $x_{k,True}$ even if the parameters values used in DSE and the simulation models are the same. This can be evaluated through $e_k = \hat{x}_{k,True} - x_{k,True}$ where $\hat{x}_{k,True}$ is the state estimate with actual parameters in DSE. However, since we are interested in only studying the effect of the effect of parametric variation so the resulting difference arising from estimation accuracy needs to be isolated. This is done by modifying equation (3.3) to

$$MSE\left(\hat{x}_k\right) = \frac{1}{M}\sum_{n=1}^{M}\left(\hat{x}_{k,n} - \hat{x}_{k,True}\right)^2 \tag{3.5}$$

The metrics in equations (3.4) and (3.5) are computed both for EKF DSE and UKF DSE to compare and observe the effect on the type of Kalman filter considered.

3.3 Simulation

The simulation model considered in the IEEE 39 bus network with the simulation time step and model order as specified in section 2.4. A 3 phase line to ground fault is considered at

t=2 sec on bus B19 for a duration of 10 cycles and then removed. The effect of parametric variation on the dynamic states of Generator G34 which is located close to the fault location is first considered. It is to be noted that noise has been considered in these models.

The parameters of the generators as specified in α are varied one at a time and the simulation is repeated to observe the difference in the state estimates as a result of the variation. Each parameter is sampled from the Gaussian distribution for 100 times and a 10 sec simulation is executed for each of them with the rest of the parameters being at their actual ones. The state deviation metric MSE for the individual parameter at each time instant k is plotted in Fig. 3.2 and 3.3.

It can be noted that the variation of the d-axis steady state reactance x_d affects the steady state value of state corresponding to field exciter voltage E_{fd} significantly although the transient behaviour is not affected. This is because the steady state component is determined by the state variable x_5 and it appears in equation (2.10) which contains the parameter x_d. Similarly, the variation of the q-axis steady state reactance (x_q) affects the d axis transient emf (e'_d) because it occurs in equation (2.11). Based on relation in [63] internal rotor angle δ_i is affected by x_q variation. It is also interesting to note that the field exciter voltage E_{fd} is affected by this variation although there are no algebraic or dynamical relation indicating dependency on x_q. However, it can be argued that since δ_i appears in equations (2.3) and (2.18) and because of its dependency on x_q, E_{fd} is affected.

Variation of d axis transient reactance x'_d affects the q-axis emf e'_q while that of q axis transient reactance x'_q affects the d-axis emf e'_d as shown in the third and fourth plots of Fig. 3.2 which can be explained through equations (2.11) and (2.12) respectively. Negligible state estimate deviation occurs due to variations of the d and q axis time constants T'_{d0} and T'_{q0}.

The first plot in Fig. 3.3 shows that the effect of the inertia parameter on the state estimate deviation is negligible. The exciter gain K_a and the time constant T_a affects the transient behaviour of exciter field voltage E_{fd} because of the dynamical equation (2.12). Changes in droop constant parameter R_p affect the estimation of governor torque because of equation (2.13) during transient condition while T_g variation does not affect any of the states.

The effect of parametric variation on the states also can be noted from the MMSE plots in Fig. 3.4 which shows the overall effect rather than depicting individual variations at different time instants. Table 3.1 shows in detail the state deviation of individual parametric

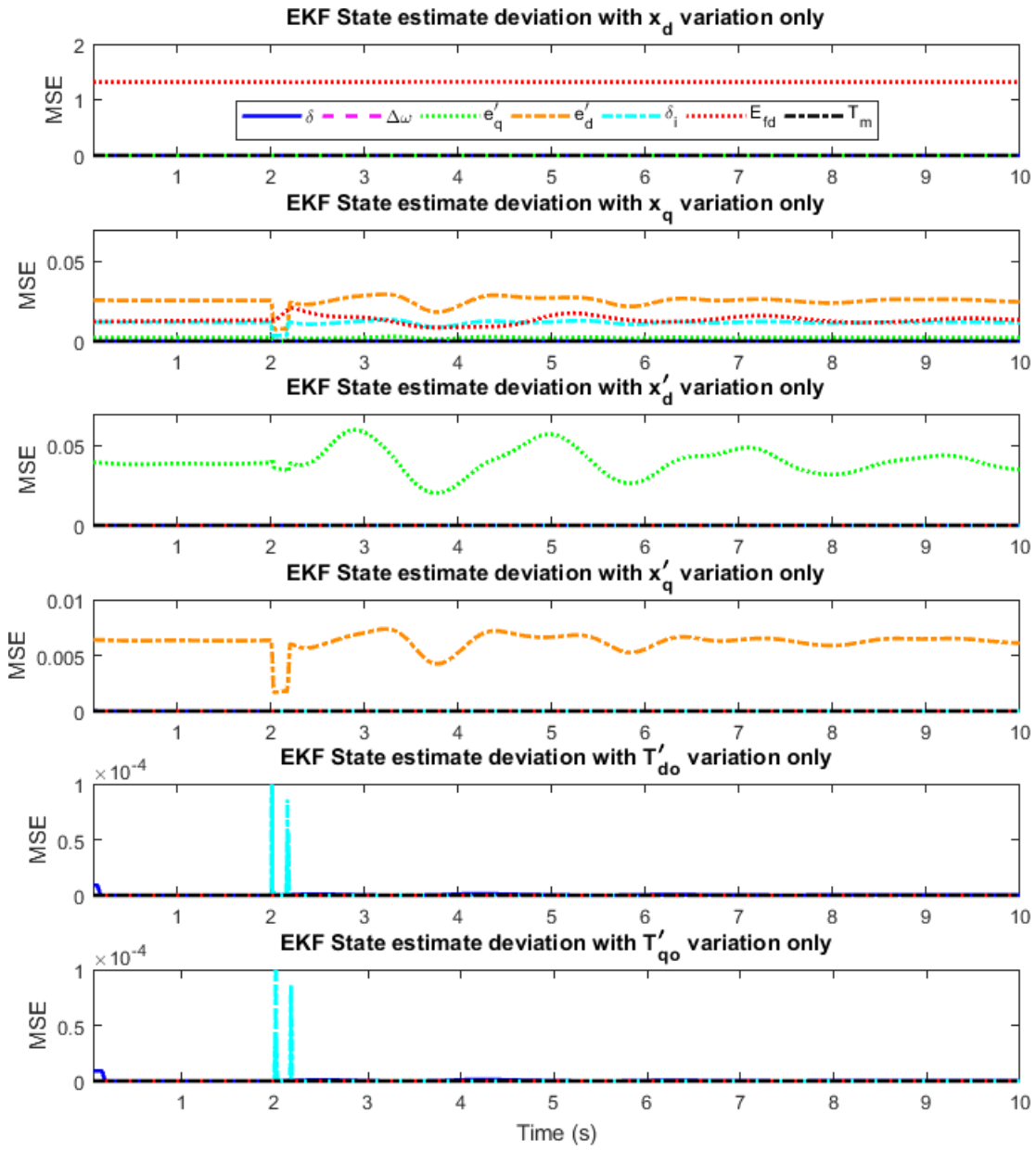

Fig. 3.2 Comparison of mean squared error (MSE) of generator (G34) states with individual parametric variation of x_d x_q x'_d x'_q T'_{d0} T'_{q0} computed form 100 Monte Carlo Simulation with an EKF based DSE

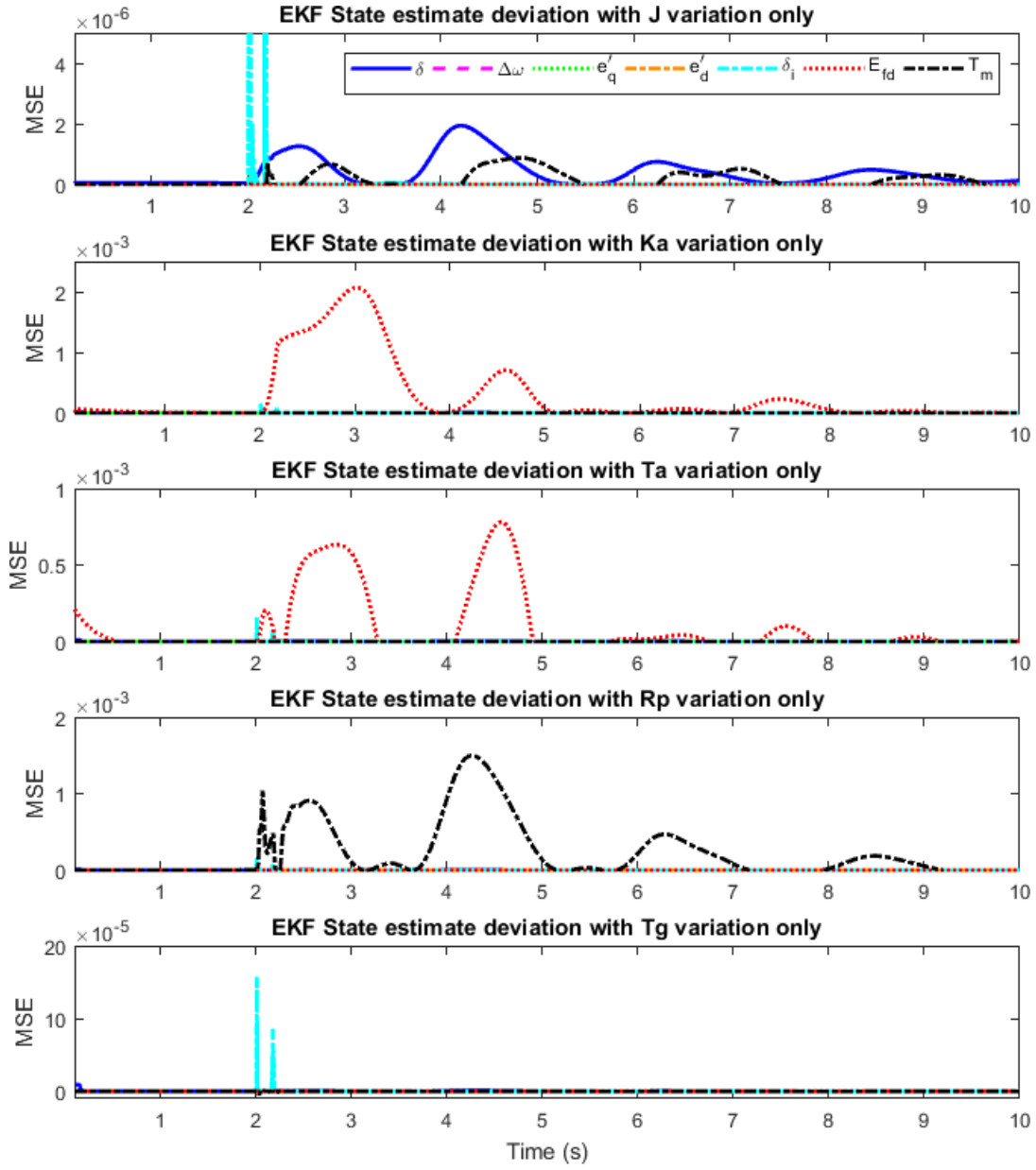

Fig. 3.3 Comparison of mean squared error (MSE) of generator (G34) states with an individual parametric variation of H K_a T_a R_p T_g computed form 100 Monte Carlo Simulation with an EKF based DSE

variation with different types of kalman type filter. In Fig 3.4, the effect of parametric variation on the significantly affected states is shown and some of them are scaled by a suitable factor for ease of visualization. From the top two plots of Fig 3.4, it can be noted that parameter x_d primarily affects the exciter field voltage E_{fd} while x_q variation affects e'_d mostly while also affecting δ_i and E_{fd} to a minor extent. Also, the bottom two plots show that state e'_q is only affected by x'_d variation while e'_d is affected by x'_q variation.

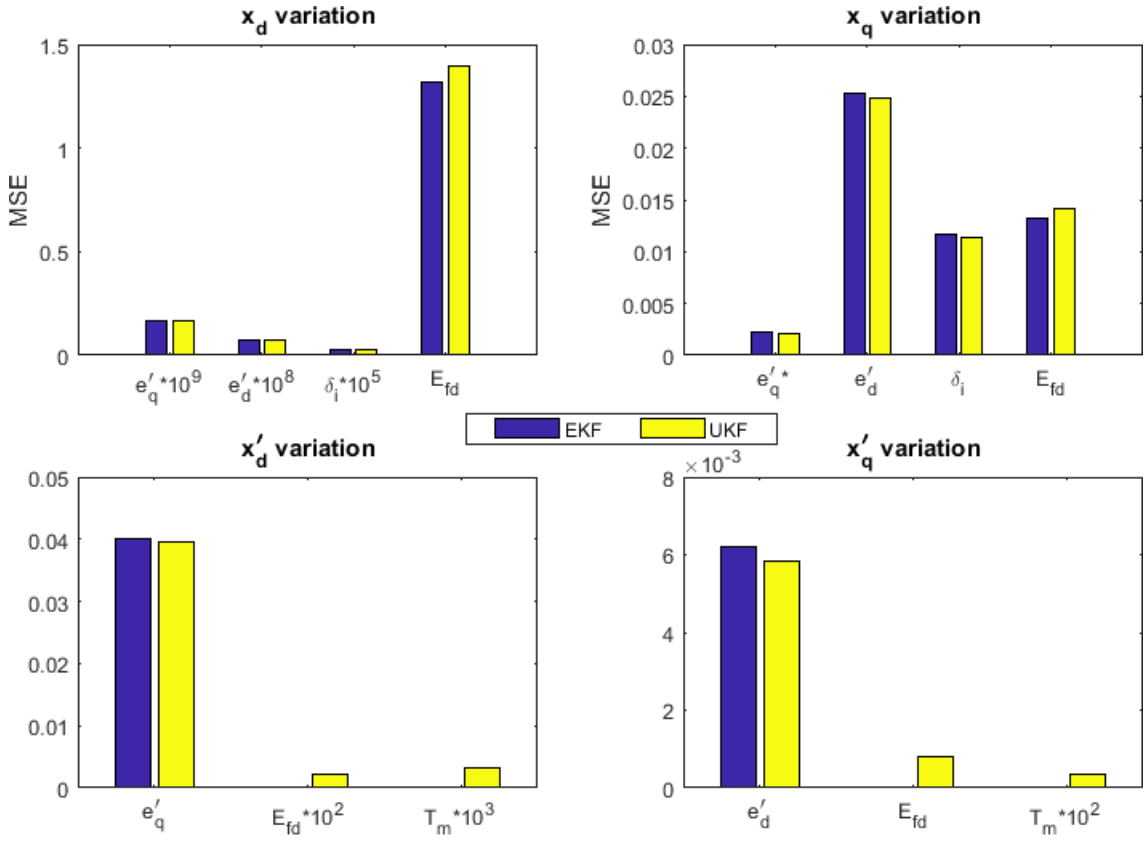

Fig. 3.4 Comparison of mMSE of dynamic states for individual parameter variations of x_d x_q x'_q x'_d with two dynamic state estimators (EKF and UKF)

It can be noted that the state estimate deviation for UKF and EKF are similar which corroborates the fact that impact on state estimate of parametric variation is independent of the choice of Kalman filter. However, there are a few cases where there is some difference observed. Effect on E_{fd} due to variation of x'_q and x'_d is considerably more for UKF (10^{-4}) compared to EKF (10^{-11}) but since the order of state deviation being small (10^{-4}), this can be ignored. Similar observation can be made about state deviation of E_{fd} during

variation of parameters T'_{q0} and T'_{d0}. Governor torque T_m state deviation is also less for EKF compared to UKF but the values being very small (order of 10^{-6}), the effect of Kalman filter choice is trivial.

Parameters	Filter type	δ	$\Delta\omega$	e'_q	e'_d	δ_i	E_{fd}	T_m
x_d	EKF	3.53E-07	5.61E-12	1.65E-10	7.54E-10	2.53E-08	1.317	1.01E-13
x_d	UKF	1.48E-07	7.84E-13	1.64E-10	7.51E-10	2.50E-08	1.399	3.32E-06
x_q	EKF	3.53E-07	5.61E-12	2.19E-03	2.523E-02	1.16E-02	1.33E-02	2.57E-13
x_q	UKF	1.48E-07	7.84E-13	2.13E-03	2.48E-02	1.14E-02	1.42E-02	3.32E-06
x'_d	EKF	3.53E-07	5.61E-12	4.01E-02	7.55E-10	2.53E-08	1.04E-10	1.00E-13
x'_d	UKF	1.48E-07	7.84E-13	3.97E-02	7.51E-10	2.50E-08	2.22E-05	3.32E-06
x'_q	EKF	3.53E-07	5.61E-12	1.65E-10	6.22E-03	2.53E-08	5.78E-11	5.29E-14
x'_q	UKF	1.48E-07	7.84E-13	1.64E-10	5.82E-03	2.50E-08	8.25E-04	3.32E-06
T'_{q0}	EKF	3.53E-07	5.61E-12	1.65E-10	7.55E-10	2.53E-08	4.00E-10	1.00E-13
T'_{q0}	UKF	1.48E-07	7.84E-13	1.64E-10	7.51E-10	2.50E-08	2.37E-05	3.32E-06
T'_{d0}	EKF	3.53E-07	5.61E-12	1.65E-10	7.55E-10	2.53E-08	4.16E-10	1.01E-13
T'_{d0}	UKF	1.48E-07	7.84E-13	1.64E-10	7.51E-10	2.50E-08	2.37E-05	3.32E-06
H	EKF	5.18E-07	5.61E-08	2.90E-09	1.23E-09	2.59E-08	4.75E-15	3.22E-07
H	UKF	2.07E-07	7.89E-13	1.23E-09	1.02E-09	2.51E-08	1.55E-10	5.13E-05
K_a	EKF	3.53E-07	5.61E-12	1.65E-10	7.55E-10	2.53E-08	2.80E-04	5.66E-17
K_a	UKF	1.49E-07	7.92E-13	1.66E-10	7.58E-10	2.53E-08	2.68E-04	8.43E-08
T_a	EKF	3.53E-07	5.61E-12	1.65E-10	7.55E-10	2.53E-08	1.81E-04	5.66E-17
T_a	UKF	1.49E-07	7.92E-13	1.66E-10	7.58E-10	2.53E-08	1.26E-04	9.88E-07
R_p	EKF	3.65E-07	5.62E-12	1.65E-10	7.55E-10	2.53E-08	1.19E-15	2.24E-04
R_p	UKF	1.49E-07	7.92E-13	1.66E-10	7.58E-10	2.53E-08	1.91E-10	2.23E-04
T_g	EKF	3.53E-07	5.61E-12	1.65E-10	7.55E-10	2.53E-08	1.18E-15	9.02E-08
T_g	UKF	1.49E-07	7.92E-13	1.66E-10	7.58E-10	2.53E-08	1.00E-15	1.00E-08

Table 3.1 MMSE values of each dynamic state for individual parametric variation with different Kalman filter type

The effect of parametric variation is studied on a separate generator G30 for the same contingency as mentioned in the last paragraph are shown in Fig. 3.5 and Fig. 3.6. It is found that the effect of variation of most of the parameters is consistent with the same observations for the previous case of generator G34. Although for parameter variation of x_d we find that there is no steady state deviation for the field exciter voltage E_{fd} as noted

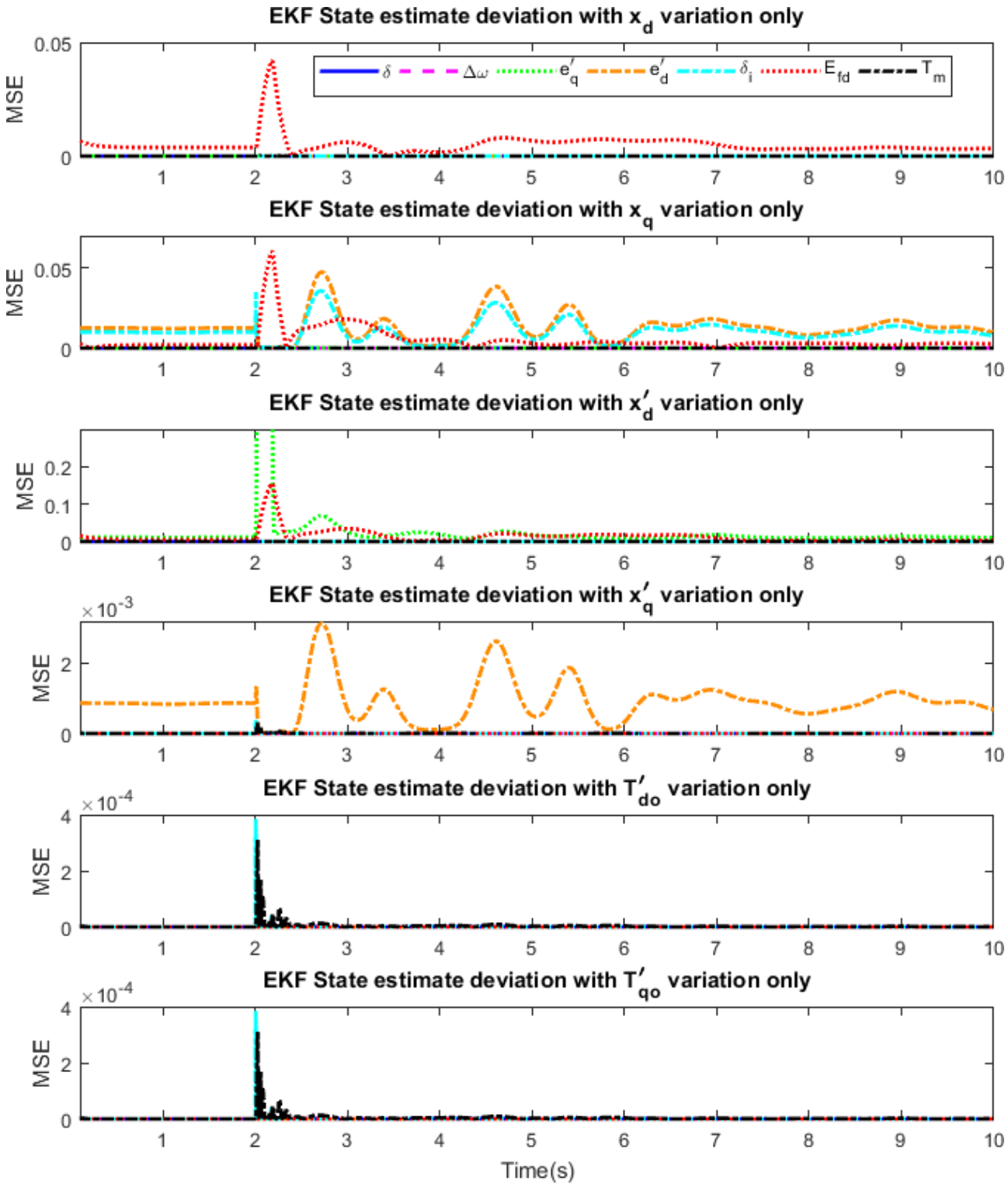

Fig. 3.5 Comparison of mean squared error (MSE) of generator (G30) states with an individual parametric variation of x_d x_q x'_d x'_q T'_{d0} T'_{q0} computed form 100 Monte Carlo Simulation with an EKF based DSE

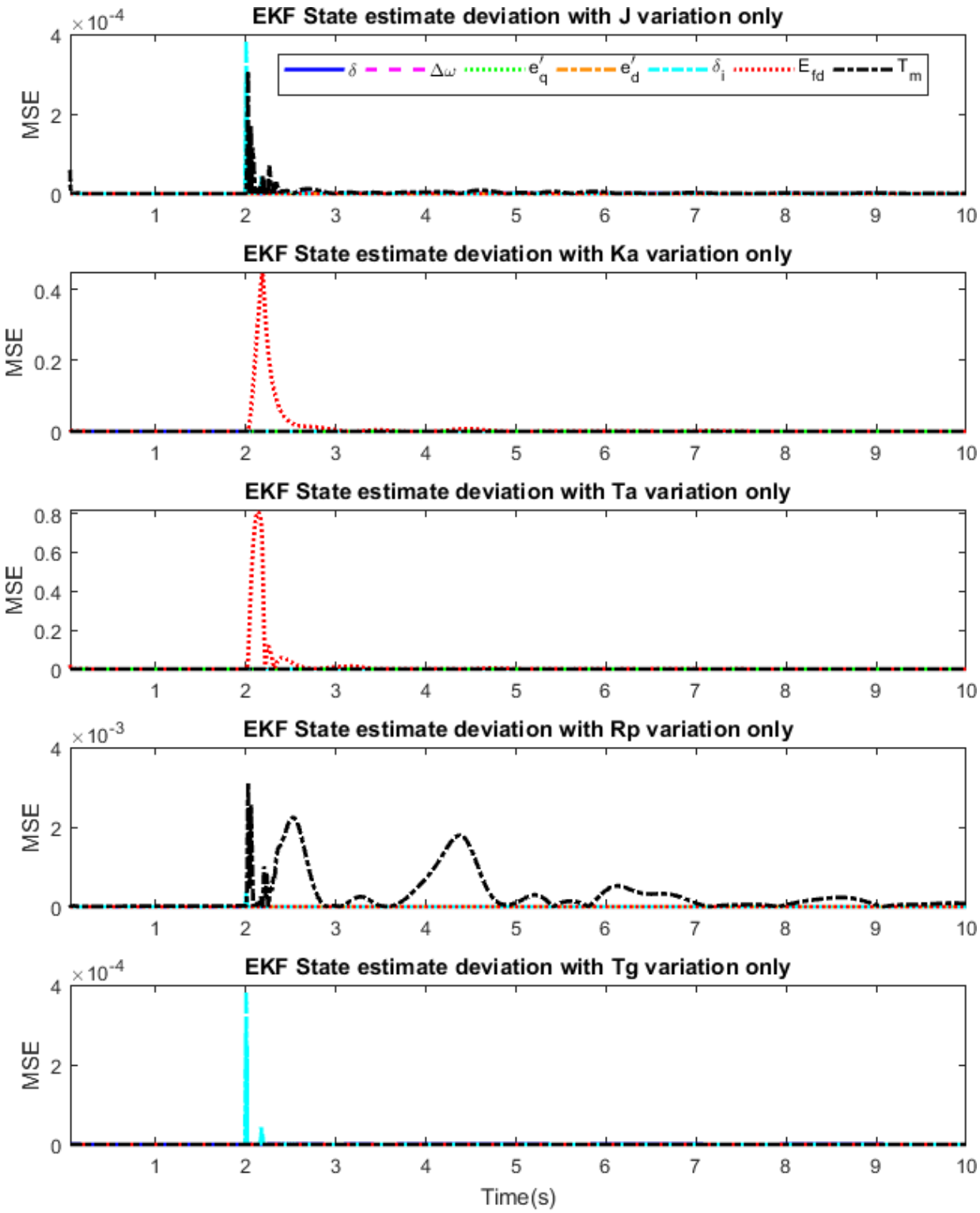

Fig. 3.6 Comparison of mean squared error (MSE) of generator (G30) states with an individual parametric variation of H K_a T_a R_p T_g computed form 100 Monte Carlo Simulation with an EKF based DSE

for generator G34 in the first plot of Fig. 3.2. This may be because the x_d value of G30 is relatively less compared to that of G34 and since the parameters have been sampled from the Gaussian distribution, so the variation of this parameter is relatively less and its effect on state deviation is also small. Variation of x_q affects e'_d, δ_i and E_{fd} while x'_d and x'_q variation affects e'_q and e'_d respectively. Change in values of time constants T'_{d0} , T'_{q0} , inertia J has negligible effect on the states. The parameters associated with the exciter equation i.e. K_a and T_a affect the exciter field voltage E_{fd}. However, variation of droop constant R_p affects the governor torque state to a minor extent while T_g does not have any significant effect on the other states. Generator G34 is closer to the source of disturbance while G30 is further away. Since the effect of parametric variation on the state estimates are similar so it can be inferred that the disturbance location does not have any impact on the analysis.

3.4 Conclusion

This chapter studies how the variation of parameter values, choice of kalman filter affects the state estimate of the 6th order dynamic state estimator model considered. The results of the study assists in understanding which parameter affects which of the states primarily and the crucial parameters whose values should be determined accurately so that the state estimates are computed with a reasonable degree of precision to actual ones. The findings of this chapter are summarized below:

1. The choice of the type of Kalman filter did not have any significant effect on parametric variation.
2. The type of disturbance considered did not affect how parametric variations affected state estimates.
3. Variation of d axis reactance x_d primarily affected E_{fd}.
4. Variation of q axis reactance x_q primarily affected. e'_d, δ_i, E_{fd}.
5. Variation of transient d axis reactance x'_d primarily affected e'_q.
6. Variation of transient q axis reactance x'_q mostly affected e'_d.

7. Negligible effect on state estimates due to variation of time constants (T'_{d0} , T'_{q0}, T_a, T_g) and inertia J.

8. Variation of exciter gain K_a affected E_{fd} only during disturbance duration.

9. Variation of governor droop (R_p) affected T_m

Chapter 4

Instability Detector

4.1 Introduction

The first step towards establishing an automated remedial action scheme is to have a robust mechanism to detect network instability. To achieve this objective there should be an instability predictor that predicts the impending instability based on network variables or some indices which are a combination of the same. With the advent of Phasor Measurement Units in the early '90s there have been numerous attempts at using bus angles and frequency as indices for instability detector. Dynamics state estimators enable to compute the generator internal states from terminal PMU data and can be potentially used for instability detection.

The established centralized dynamic state estimator in Chapter 2 enables us to observe the d-q axis internal emfs of all the generators in the network as well as improved estimation of the rotor and frequency dynamics compared to generator terminal angle and frequency measurements. Instability detector trained on a subset of indices derived from dynamic states is expected to make an accurate and robust assessment of network stability.

This chapter demonstrates the intricate nature of the problem of identifying network instability from established indices and also discusses classifier selection and a comparative analysis of two different types of classifiers.

4.2 Instability Predictor

Initial attempts for transient stability prediction in real-time using terminal Phasor Measurement signals only can be found in [15]. An immediate application for an established Centralized State estimator would be to compute transient stability prediction indices. There are numerous publications on instability detection using decision trees and other machine learning techniques [17–21, 97, 98]. Most of them either involve using the data from Phasor Measurement Units (PMUs) [15] or considering idealized generator angle, speed, rate of change of speed, [16], and indices combining the same [18, 20] and thereby applying decision tree for instability detection. Based on a recent paper [20], instability indices γ_{COP}, κ_{COP} can be computed from state estimates rather than terminal PMU measurements by approximating rotor angle and speed with bus angle and frequency:

$$\gamma_{COP} = \sum_{i=1}^{N_G} \delta_i \left(\omega_i - \omega_{COP}\right) \tag{4.1}$$

$$\kappa_{COP} = \sum_{i=1}^{N_G} \omega_i \left(\delta_i - \delta_{COP}\right) \tag{4.2}$$

where $\omega_{COP} = \sum_{k=1}^{N_G} \omega_k P_{ek} / \sum_{k=1}^{N_G} P_{ek}$ and $\delta_{COP} = \sum_{k=1}^{N_G} \delta_k P_{ek} / \sum_{k=1}^{N_G} P_{ek}$. It is to be noted that in [50] a study has been performed that shows terminal bus angle and frequency do not effectively capture the dynamics of the generator and is not a good approximation. Also Section 4.2.1 shows the impact on these two indices when making this approximation. The new indices are based on centre of power (COP) formulation rather than centre of inertia (COI) ones which offers the advantage that it takes into consideration relative power generation of various generators and the inertia values are not required. In addition if a generator with large inertia contributes to relatively small power in the network then COI unnecessarily provides significant weightage to the speed and angle variation of that generator. This is because it is unlikely that a system will become unstable if a generator with considerable generation but small power injection fall out of synchronism with the network. Hence it is more reliable to take into consideration generator power while computing γ_{COP}, κ_{COP} as a measure of instability.

It has been demonstrated in [50] that the frequency signal of PMU connected at terminal

bus is not able to capture the oscillations effectively. Thus γ_{COP}, κ_{COP} computed from internal state estimates will have more pronounced variations and crisp features that should improve instability prediction.In addition time derivative of the energy function, W_{di} [99] is also an important index for instability detection.

$$W_d^{total} = \sum_{i=1}^{N_G} \frac{dW_i}{dt} = -\sum_{i=1}^{N_G} \left[\frac{T'_{doi}}{(x_d - x'_d)} \left(\frac{de'_{qi}}{dt} \right)^2 + \frac{T'_{qoi}}{\left(x_q - x'_q\right)} \left(\frac{de'_{di}}{dt} \right)^2 \right] \tag{4.3}$$

where N_G is the total number of generators in the network. Other variables are defined in nomenclature. Furthermore, the above equation needs time derivative of q and d axis information of internal emf of generator, which is readily provided by centralized estimator. Individual generator energy derivative index is give by

$$W_{di} = \frac{T'_{doi}}{(x_d - x'_d)} \left(\frac{de'_{qi}}{dt} \right)^2 + \frac{T'_{qoi}}{\left(x_q - x'_q\right)} \left(\frac{de'_{di}}{dt} \right)^2 \tag{4.4}$$

W_{di} index is computed from emf values while gamma and kappa are based on speed and power signals. It is to be noted that although equations (4.1),(4.2),(4.4) are written in continuous form, they operate based on discretized dynamic state estimate values. These three indices $\gamma_{COP}, \kappa_{COP}, W_{di}$ enabled by the centralized state estimator would result in a robust detection of instability.

4.2.1 Visualization of Indicators

The behavior of instability indices studied by considering three phase fault on buses B20 (close to the generator) and B18 (close to load) in the benchmark IEEE 39 bus network. For each of these cases, gamma and kappa indices as established in the previous section has been plotted for a disturbance with a fault duration corresponding to the critical clearing time of the mentioned bus. These indices have been computed from dynamic state estimates as well as terminal bus measurements (PMU). For the gamma index, it can be observed in Fig. 4.1 that the index computed from DSE (B18-DSE, B20-DSE) has more pronounced variation compared to that computed from PMU data only (B18-PMU , B20-PMU). This is because the state estimator can capture the true and magnified variation in generator speed following initiation of disturbance rather than approximating it with terminal frequency [50]. Improvement in kappa computed from DSE and PMU is not as

noticeable as gamma however the deviation from zero steady state value is large for index evaluated from DSE compared to PMU one. The third index W_{di} can only be computed using a centralized state as it needs time derivatives of e'_q, e'_d for all the generators in network.

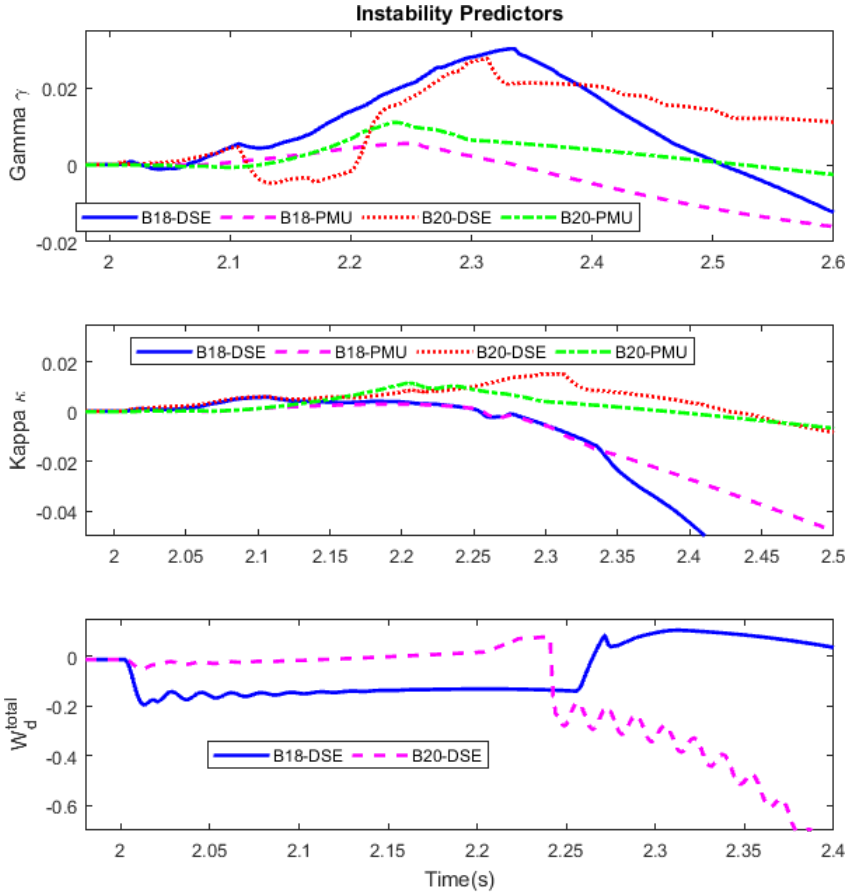

Fig. 4.1 Comparison of Instability Predictors computed from State Estimates (DSE) and Terminal Measurement (PMU) for fault initiating at t=2 sec on buses B18 (close to the generator) and B20 (close to load) in IEEE 39 bus system

In Fig. 4.2 a comparison of the instability indices for a stable and unstable fault is shown. Although there is a distinct difference between the stable and unstable cases for each of the index, however the nature of the variation of the indices are complex and it is difficult to classify between the cases. Therefore it is preferable to use a machine learning algorithm to perform complex classification of these indices. It can be noted that all the three indices follow the same trajectory until the instance of fault clearance. So

the evolution of the indices post-fault clearance will be of significance for the classification problem.

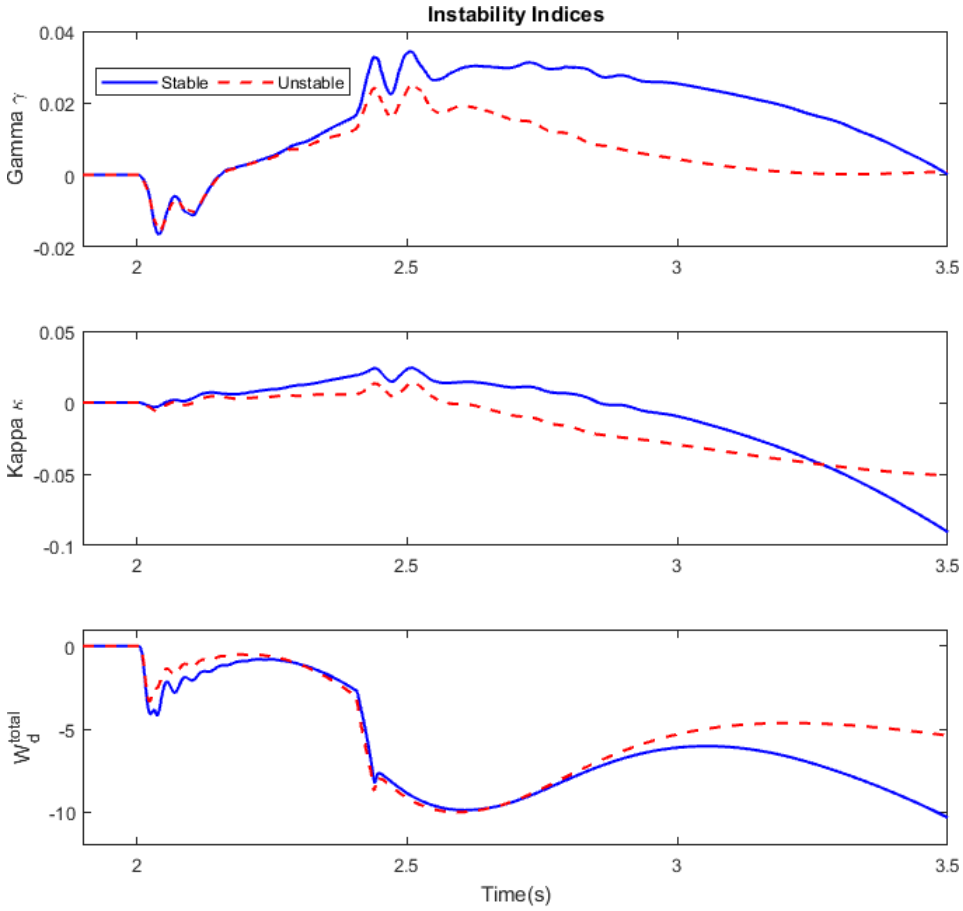

Fig. 4.2 Comparison of Instability Predictors for Stable and Unstable fault computed from State Estimates (DSE) for fault initiating at t=2 sec on the middle of line connecting buses B39 and B1 in IEEE 39 bus system

4.3 Classifier Design

4.3.1 Instability Detector

To perform instability prediction with the established indices, a classifier has to be trained on indices computed from scenarios with contingencies at different locations in the network and varying loading conditions. Hence in a network with a total of N_G number of generators, the total number of instability indices in the network would be N_G number

of W_{di} as well as gamma and kappa, resulting in a total of $N_G + 2$ number of instability indicators for each scenario. An interesting feature of the indices used in classifiers is that γ_{COP}, κ_{COP} are centralized while W_{di} indices for individual generators are decentralized which brings complementary features in the proposed predictor model. In addition, since the combination of instability predictors are from electrical as well as electro-mechanical quantities, it is expected to result in robust classification. Based on sample computed indices in Fig. 4.2 it can be noted that they are not easily separable in terms of stable and unstable scenarios and a complex classifier is needed for accurate prediction to attain the desired "3 nines" reliability [18]. A comparative assessment of two instability detectors has been made. One of them is the traditional ensemble decision tree classifier that operates on spectral features extracted from the indices and the other is based on a multi-variate long short term memory network that operates directly on the time series data.

4.3.2 Classifier Selection : Ensemble Decision Tree

Decision trees identify the critical attributes and corresponding thresholds from the feature set and establish a secure operating boundary for instability prediction [19]. It thus offers the advantage of being easily interpretable and performs well on a large dataset [100]. However a decision tree suffers from the limitations of not being robust to small changes in training data, often creates complex trees that lead to overfitting and uses greedy algorithms leading to locally optimized decisions [100]. To overcome the limitations of decision trees, a superposition of basic algorithmic operations are needed [101]. This leads to the notion of ensemble which includes boosting [102], bagging [103], Random Forest [104], Stochastic gradient boosting [105], random subspace method [106]. A comparative assessment shows that random forest and boosting algorithm attains better accuracy and performance relative to other ones [107], [101] in power systems dynamics applications. Nonetheless as specified in [108], with increasing complexity in the model structure, the comprehensibility offered by a simple decision tree is lost at the expense of increased accuracy. Therefore Adaptive Boosting (AdaBoost) has been selected as the ensemble learning algorithm for the individual ensemble decision tree. It creates a strong learner by iteratively adding weak learners (i.e. decision trees here) in each round of training. Moreover, it has the added advantage of being resistant to overfitting and has been regarded as one of the best out-of-box classifiers [109], although it is still susceptible to noisy data and outliers.

Structure

The classifier Structure is shown in Fig. 4.3

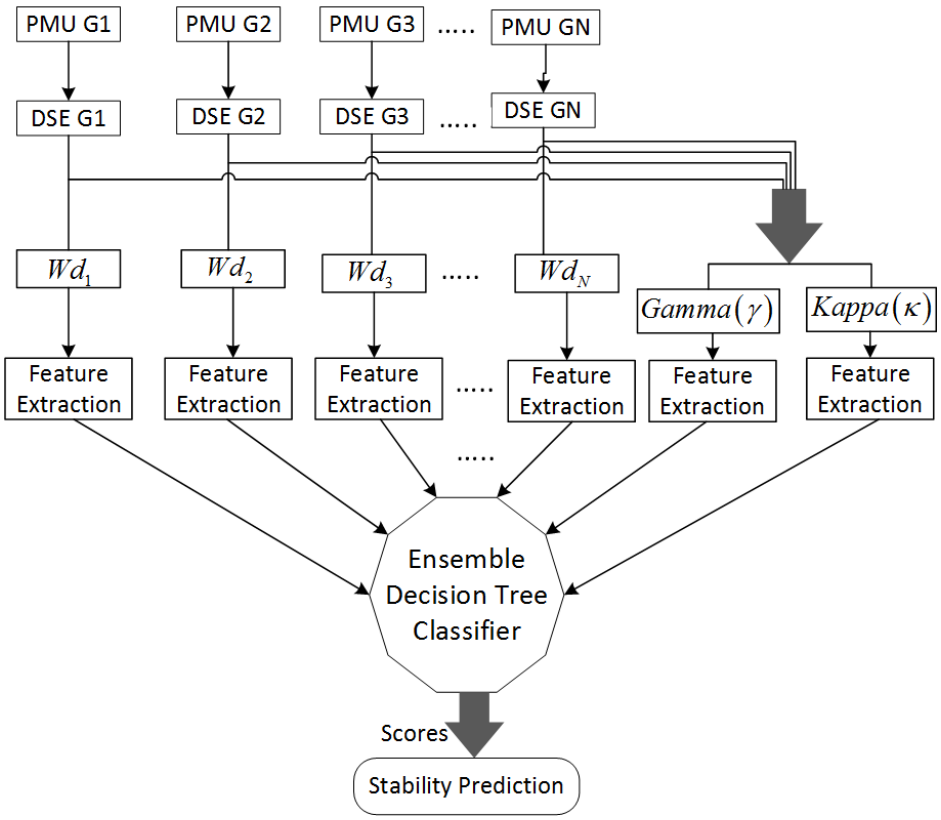

Fig. 4.3 Ensemble Decision Tree Classifier Structure

Here a spectral method based feature extraction technique is used to extract out the relevant features before training a classifier. The feature extraction process involves a fourier transformation of the computed indices over a fixed window size, typically for the duration of the disturbance under consideration. A detailed list of features alongwith a short description of each computed is mentioned in Appendix A. Few of the features being extracted consists of peak widths, number of peaks, power in the peaks, quantiles, moments, autocorrelation, power in specific frequency bands etc. Features are normalized before training a classifier. The formulation is based on the methodology specified in [110, 111].

When the data arrives from the PMU, the DSE module computes the dynamic states and the instability indicators are evaluated instantaneously. An example consisting of

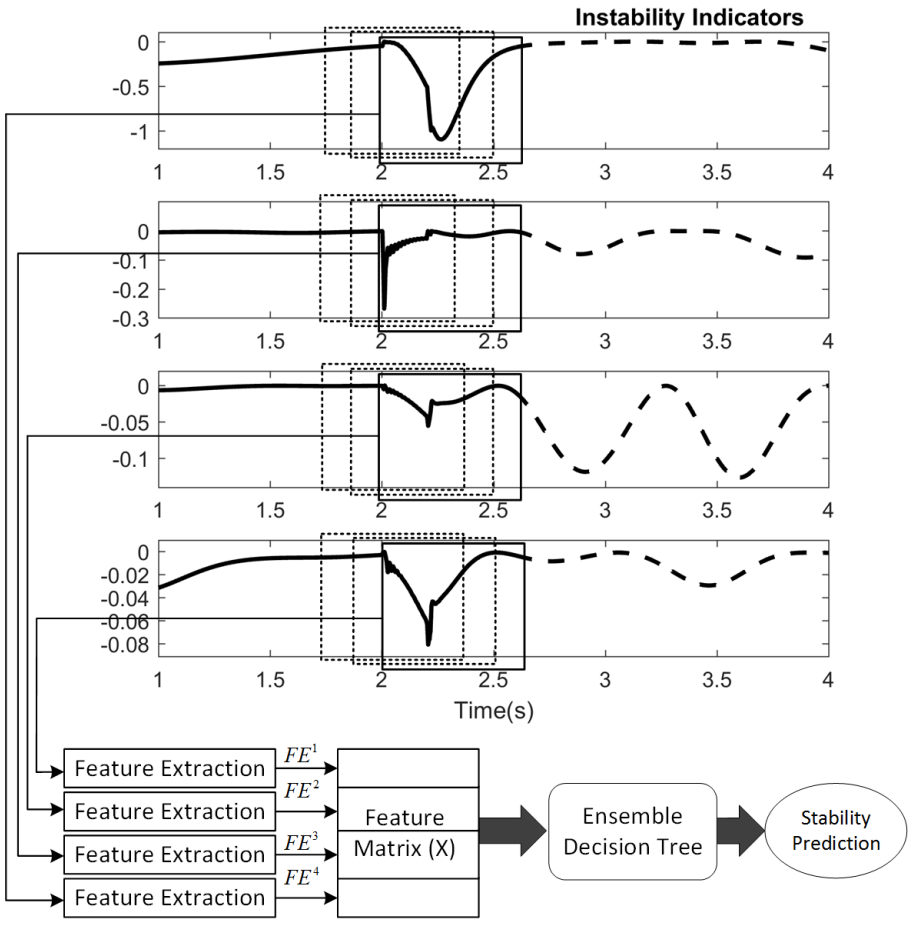

Fig. 4.4 Operation of Moving window classifier Ensemble Decision Tree

four instability indicators are shown in Fig. 4.4. An overlapping moving window data frame over the computed instability indices sends the data to feature extraction blocks which computes the feature vector FE^i , the superscript corresponding to the i^{th} instability indicator number. The feature vectors are concatenated into a larger feature matrix $FM = [FE^1\ FE^2\ FE^3\ FE^4]^T$ which is provided as input to the ensemble decision tree classifier. The output of the classifier consists of a prediction label and score that shows confidence in the prediction. The process repeats itself over subsequent time instants as shown in Fig. 4.4 and we obtain the final prediction of proposed instability predictor at discrete time intervals.

The function of the classifier block is to learn a mapping of the feature matrix FM to

a classification label $y \in \{S, U\}$ where 'S' corresponds to Stable and 'U' corresponds to Unstable cases. In addition to the classification label, the classifier also indicates confidence in the classifier performance.

4.3.3 Classifier Selection: Multivariate LSTM (MLSTM)

Although conventionally decision tree based classifiers have been used for instability detection, few recent works involved using artificial neural networks [112], energy based support vector machine features [113], and fuzzy knowledge based system [108]. In [22] using an ensemble of extreme learning machine early warning prediction of dynamic insecurity is demonstrated while a time adaptive Long Short Term Memory Network (LSTM) is used for real time instability detection in [24].

LSTM based classification model offers the following advantages compared to a decision tree or traditional classifiers:

1. Feature engineering is not required and feature extraction is difficult because intrinsic features of time series data are challenging to capture [114].
2. Considers temporal dependency within a channel and correlation across channels.
3. Generalizable on new data and incremental update possible i.e. no need to retrain the whole model.

An LSTM network can learn temporal dependencies without the problem of vanishing gradient as faced by a recurrent neural network [115]. Recently a paper has been published [116] that incorporates Convolution blocks and attention mechanisms in the LSTM network and has been shown to the outperform existing state of the art time series classification model. The advantages offered by [116] with regards to a conventional LSTM block are

1. Convolution Layer: One-dimensional filters which convolve over the input data to capture the evolution of the input signals over time
2. Attention Mechanism: Focuses on a targeted section of sequence that enables the network to learn long-term dependencies not captured by LSTM

3. Squeeze and Excite block: Squeeze operation exploits contextual information outside the local receptive field by using a global average pool to generate channel wise statistic. Excite block aggregates information from squeeze operation which captures channel wise dependencies.

The performance of LSTM classifier is investigated in the current instability prediction model and compared with that of the traditional model

Structure

An overview of the structure of the classifier is presented in Fig. 4.5. The difference in classifier structure in contrast to that in Fig.4.4 is that the MLSTM operates directly on the computed instability indices and does not need any feature extraction.

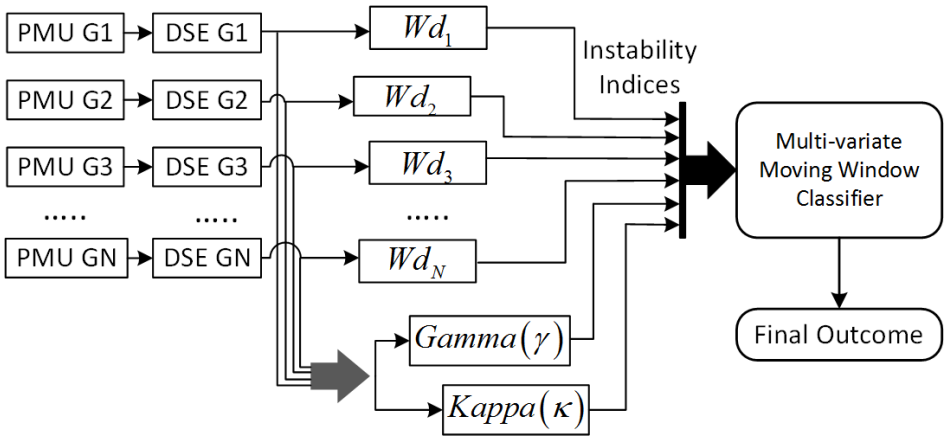

Fig. 4.5 Operation of Moving window classifier Ensemble Decision Tree

The operation is explained using Fig.4.6 by considering only four instability indices for simplicity. An overlapping moving window extracts the data frames from individual indices and concatenates them into a matrix on which the moving window classifier operates. Assuming a sliding window size of 'N_W' sample each of the instability indicators is concatenated into a matrix of $X = [\bar{x}(t_0) \quad \bar{x}(t_1) \quad \bar{x}(t_2) \quad \cdots \quad \bar{x}(t_{N_W})]$ where $\bar{x}(t_i) = [x_1(t_i) \quad x_2(t_i) \quad x_3(t_i) \quad \cdots \quad x_k(t_i)]$ and $x_k(t_i)$ represent k^{th} channel at i^{th} time instant.

Similar to the previous example, the MLSTM model provides us with a score that is synonymous with the probability of belonging to a particular class i.e. Stable or Unstable.

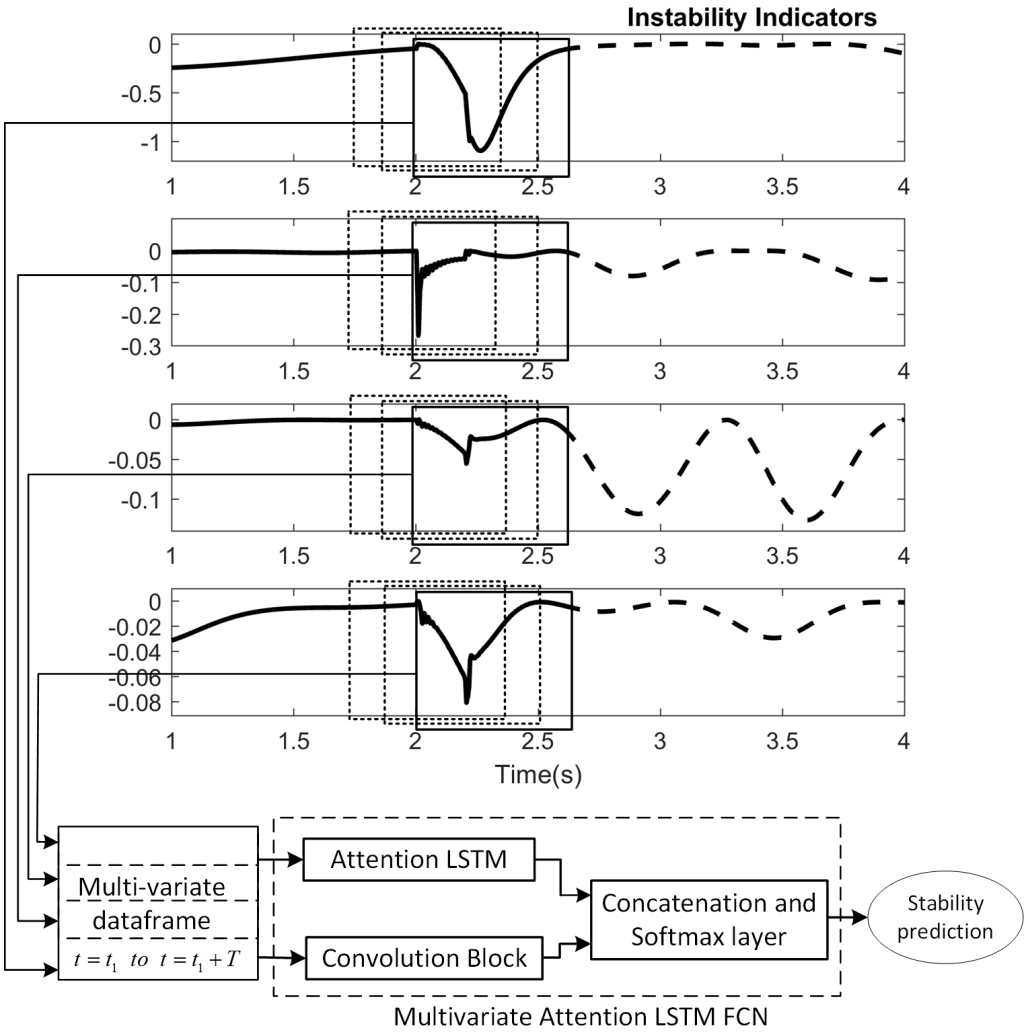

Fig. 4.6 Operation of Moving window classifier Ensemble Decision Tree

4.3.4 Training of model

Training of the prediction model involves performing some simulations by incorporating possible contingency scenarios in the network at varied loading profile conditions and expected generation schedules through the day-ahead forecast. Assuming there are N_{OP} number of operating points and K number of contingency scenarios for each of these operating points detailed time domain simulations are performed for individual contingencies resulting in a total of $N_{OP} \times K$ number of training cases. Each of the training cases is classified as "Stable" (S) or "Unstable" (U) based on pre-defined dynamic performance metrics

(eg. transient stability, angle/frequency deviation, out-of-step, numerical divergence etc.) As stated in [117] , mathematically this can be expressed as

$$y_t = \begin{array}{ll} 1(Stable) & if \quad \eta > 0 \\ 0(Unstable) & if \quad \eta \leq 0 \end{array} \tag{4.5}$$

where $\eta = (360 - \delta_{max})/(360 + \delta_{max})$ and δ_{max} is the maximum angle deviation of any two generators in degree. Each case is allocated a label based on the value of η at the end of the simulation. Contingency scenarios are indexed and represented by a vector $C_m = \{\bar{p_1}, \bar{p_2}, ...\bar{p}_{NG}, y_m\}$ where $\mathrm{C_m}$ correspond to $\mathrm{m^{th}}$ contingency scenario, $\bar{p_i}$ depicts the time domain data sent by $\mathrm{i^{th}}$ terminal generator PMU and $\mathrm{y_m}$ is the dynamic stability label of the $\mathrm{m^{th}}$ contingency scenario, $y_m \in \{S, U\}$ ascertained from stability criteria.

This method of generating training cases leads to an unbalanced dataset as there are mostly stable cases compared to unstable ones. With the loading increase, as the grid becomes more and more stressed, the probability of unstable cases increases but it does not exceed that of the stable cases. Hence the methodology of dataset balancing as specified in [18] is used. Based on the security criteria, contingency scenarios are limited to N-1 or N-2 cases, while the fault duration is varied between 6 and 12 cycles.The operating times of zone 1, zone 2 and zone 3 of distance protection relays are of the order of 0∼2 cycles, 18∼24 cycles, 0.8∼1 sec respectively [118, 119].

System instability is indicated by the value of η which is negative when angular divergence happens and positive in stable condition when all the generator angles are in synchronism. Typically dataframes are identified as Stable and Unstable cases based on the instantaneous values of η. However the value of η becomes negative only when the maximum angular divergence between two generators exceed 360 degrees and is positive before that happens even for an unstable case. Typically angular divergence happens a few seconds after an unstable fault has initiated. So if we label the data frames based on the instantaneous value of η then the data frames after fault initiation till angular divergence happens will be incorrectly labelled as Stable. To avoid this, dataframes are labelled based on the system state at end of simulation is determined based on the value of η. If at the end of simulation time $\eta > 0$, all the data windows extracted from a Stable case, has the label 'S' while for the Unstable case, the data windows before fault inception has label of 'S' and after has label of 'U' regardless of when the angular divergence happens or $\eta \leq 0$. This way of labelling the dataset and training a classifier helps identifying features or trends in

dataset before the actual instability occurs and thus creates an anticipatory behavior in the classifier. Therefore for a dataframe 'D' at time instant 't' the labelling is given by

$$y_t^D = \begin{matrix} 1(Stable) & if & \left(\eta_{t=t_f} > 0\right) || \left(\eta_{t=t_f} \leq 0 \ \& \ t \leq t_{ft\_st}\right) \\ 0(Unstable) & & if \quad \left(\eta_{t=t_f} \leq 0\right) \& \left(t > t_{ft\_st}\right) \end{matrix} \tag{4.6}$$

where t_f is the final simulation time instant and t_{ft_st} is the instant of fault start. Offline training of the model may not be enough to reflect actual system conditions because of variability resulting from proliferation of renewable and distributed generations. However as the operating horizon approaches, it is possible for the system operators to discern the actual imminent operating point more accurately and include contingency simulations at these new operating points into the training set. Hence the prediction model accuracy for decision tree based detector can be improved through retraining of the entire model or restructuring of the decision tree [19, 120]. The MLSTM model retraining would involve training the classifier on the new dataset while initializing from the last trained weights.

4.3.5 Performance Metrics

The data is randomly split into training and testing set and performance evaluation is made on the testing set. The following three metrics as specified in [18, 108, 121, 122] are used for assessment

1. Reliability : (Total number of unstable cases - Total number of cases converted to stable cases)/ Total number of unstable cases
2. Security : (Total number of stable cases – total number of cases converted to unstable cases)/ total number of stable cases
3. Accuracy : (Total number of cases – number of mis-classifications)/ Total number of cases

4.4 Results

4.4.1 Details of Classifier Model

The parameters of Ensemble Decision tree classifier has been optimized using the Statistics and Machine Learning Toolbox of matlab and it was found that with 'Gentle AdaBoost'

learning method was the optimal one with 479 Learning Cycles and 0.4158 as Learning Rate and Minimum Leaf Size of 1. The feature extraction block performs fourier transformation on a rectangular window with 288 datapoints over each indices and 92 features were extracted from each dataframe for W_{di} indices and 91 features from gamma and kappa. This implies that for each dataframe a total of 1114 features were extracted. The data has been normalized to zero mean and unit variance. The highly comparative timeseries analysis toolbox (HCTSA) [111] is used for feature extraction and the list of features used is specified in Appendix A.

The MLSTM model consists of 16 LSTM cells and the Convolution block consists of 3 blocks of 128-256-128 filters with initialization and weighing of the kernel as proposed in [116]. The dropout rate has been set at 80% to prevent overfitting and number of training epochs at 500 to prevent overfitting. For training of models, an Adam optimizer with initial and final learning rates of $1e^{-3}$ and $1e^{-4}$ is used. The data has been normalized to zero mean and unit variance. MLSTM model is implemented in python using Keras [123] library.

4.4.2 Initial Database Generation

The benchmark IEEE 39 bus network is considered for comparing and evaluating the classifier performance. The network consists of 10 generators and 34 lines and this results in 12 instability indices. A three-phase to ground fault is simulated on all the lines for a period of 12 cycles and the lines are tripped after 12 cycles by the opening of circuit breakers on either end of the line. This is carried out for different loading scenarios ranging from 80% to 130% in intervals of 5%. Faults are considered at 25%, 50%, and 75% of the length of the line. This resulted in a total of 1014 cases and around 95,000 data frames after database equalization [18]. The data is split into 80% testing and 20% training case through random selection from the total dataset for initial evaluation. Details of dataframe are shown in Table 4.1

The critical clearing time of each line was determined to be around 12 cycles at nominal loading. Stable scenarios were generated by performing simulation at the critical clearing time for each line which was around 12 cycles at nominal loading for most of them while for unstable ones it was by increasing the fault duration by 1 cycle. A classifier trained on time-series data set from these simulations will be able to fit a separating hyperplane or demarcating surface based on a scenario that is most difficult to distinguish. Any other

Classifier Details	Values (Testing Set)	Values (Robustness set)
Total no. of simulation data frames	94962	N/A
No. of training data frames	75970	N/A
No. of test data frames	18992	5260

Table 4.1 Classifier dataset details

scenario with lesser fault clearing time duration eg. 4 to 5 cycle is easily distinguished by the classifier. With increasing loading on the network, the critical fault clearing time reduces which is determined at different loading levels and scenarios are generated accordingly for classifier training. In practical scenario 4 to 5 cycle would be a reasonable duration and the 12-cycle setting is only relevant because this is a test system, which allows to develop and demonstrate an effective algorithm for separating between stable and unstable cases in the general sense.

4.4.3 Robustness Assessment Test Set

A robustness assessment of the established instability detector is performed by generating an operating condition different from that used in classification by varying the loads in the network randomly. In the network under consideration generator G39 and load on bus 39 represents the equivalent external system of the New England area [124]. The generation capacity of G39 is reduced by 20% to reflect the change in the operating condition of the external system. The remaining loads in the network are varied randomly in the range of 80% to 120% of their values in the nominal condition. Contingencies involved 3 phase fault on each of the lines followed by tripping of the line. The fault location has been set to vary randomly between 25% to 75% of the transmission line. The proposed Instability detector has been used to determine stability and the 34 cases resulted in about 5260 data frames with 3860 stable and 1400 unstable ones.

4.4.4 Classifier Performance Comparison

The second column in Table 4.2 compares the performance of the ensemble decision tree and MLSTM on the testing set, with the latter achieving higher accuracy than the decision tree.

	Testing Set Accuracy		Robustness Set Accuracy	
Metrics	MLSTM	Ensemble DT	MLSTM	Ensemble DT
Accuracy	99.86 %	99.59%	98.15%	97.60%
Reliability	99.99 %	99.86 %	99.69 %	99.14 %
Security	99.87%	99.73%	98.47 %	98.45%

Table 4.2 Classifier Performance details

Also, it was able to achieve the three nines of reliability i.e. it can detect an unstable case with near perfect certainty. Additionally, it should be noted that the classifiers can attain good accuracy even though it has been trained on a considerably smaller dataset compared to results in [18, 24]. As evident from the third column in Table , MLSTM was able to attain an accuracy of 98.15% accuracy compared to 97.6 % for decision tree. This implies that MLSTM can capture the variance in data more effectively. Inclusion of the remaining incorrect cases in training of DT classifier as mentioned in [19] will make it more robust while the MLSTM training involves running a few iterations over incorrectly classified sets and initializing with last trained weights.

The cross validation reported in Table 4.2 demonstrates that the recurrent neural network has a good generalization capability given that the security and reliability rates are 98.5% and 99.7% on the robustness set and test set respectively even though the machine learning is limited to the trained space only. The robustness set and test set are not involved in training and the test set is correlated but not part of the training set.

4.4.5 Training and Testing time

Training of the MLSTM was done on a GTX 1060 GPU and took 16 hrs to complete while the decision tree with feature extraction was done on Intel i7 processor (4 cores) and took approximately 3 hrs. The prediction time for MLSTM is around 0.6 msec only as it is executed on GPU while that of Decision Tree is around 150 msec with feature extraction requiring around 110 msec. Although parallel processing toolbox of Matlab has been used for feature extraction and prediction, however since we have 12 indices in our network so each processor had to work on 3 of them. Increasing the number of cores will reduce the computation time of feature extraction.

4.5 Conclusion

In conclusion, it can be stated that both the classifiers can attain a reasonable degree of accuracy with MLSTM exhibiting slightly better reliability on testing as well as on a new dataset. One of the reasons for the good performance of the two classifiers is because of the inclusion of W_{di}. The new instability indices are complementary to the conventional ones (γ_{COP},κ_{COP}), the former is based on electrical signals only and distributed while the latter includes electromechanical signal and centralized. Also, together they provide more spatio-temporal information to the decision tree and LSTM model. Although, it might be argued that since a moving window classifier with over lap has been used, this might have also added to the accuracy improvement of the testing set. But the performance of robustness set which does not include any dataframes from training and testing set shows that it is not the case.

The decision tree classifier is based on Fourier operation and quite a large number of spectral features (104) have been extracted for training the decision tree attributing to enhanced classification results. It is to be noted that the parameters of the decision tree have been optimized to reach maximal accuracy as indicated in section 4.4.1. Although no parameter optimization has been done on the LSTM network the model has been designed and tested with tuned parameters on a wide range of classification problems with very different nature of time series data [116]. This might explain why the LSTM worked well in this network stability detection without requiring further tuning.

The MLSTM requires greater training time and hardware resources for its execution compared to the decision tree. However it has a smaller prediction time as it does not require any spectral feature extraction from the indices. The computational time increases as the number of indices in the network increases. Updating the MLSTM model is easier compared to the restructuring of the decision tree as the latter involves developing an optimal test for each node that would check the classification for each node and substitute it with a new one if incorrect.

Chapter 5

Automated Remedial Action Scheme

5.1 Introduction

In this chapter, the problem of conventional remedial action scheme as stated in chapter 1 is addressed through an energy function based remedial action scheme that operates on dynamic state information of the network. A methodology for online remedial action scheme is presented and it demonstrates the benefit of the proposed scheme over the existing remedial action scheme on benchmark network.

The first part of the chapter focuses on establishing a method for identifying the critical generators in real time and the subsequent sections focus on taking corrective action in incremental steps and monitor the system for further actions if necessary to stabilize the system. No offline simulation training is required for the operation of the Remedial Action Scheme.

5.2 Critical Generator identification

The proposed online Remedial Action Scheme involves identifying critical generators from the rate of transient energy change indices (W_{di}) as well as the transient energy components that are dominant during the fault duration. Equations involved in individual generator transient energy function as presented in [99] are

$$W_i^T = W_i^{KE} + W_i^{PE} \tag{5.1}$$

$$= \frac{1}{2}M\left(\frac{d\delta}{dt}\right)^2 + W_i^{21} + W_i^{24} + W_i^{25} + W_i^{26} \tag{5.2}$$

$$W_i^{21} = -P_m\left(\delta - \delta_0\right) \tag{5.3}$$

$$W_i^{24} = \frac{1}{2}\left[(i_d^2 - i_{d0}^2)x'_d + (i_q^2 - i_{q0}^2)x'_q\right] \tag{5.4}$$

$$W_i^{25} = \int_{E'_{q0}}^{E'_q} i_d dE'_q \tag{5.5}$$

$$W_i^{26} = \int_{E'_{d0}}^{E'_d} i_q dE'_d \tag{5.6}$$

where W_i^{KE} and W_i^{PE} corresponds to i^{th} generator Kinetic and Potential Energy and the subscript '0' correspond to values at the instant of disturbance inception. W_i^{21} indicates energy change associated with the governor and prime movers, W_i^{24} is energy stored in all series connected reactances including transient reactances, W_i^{25} accounts for the effect of the field coil and AVR and W_i^{26} explains energy variation of damper winding on q-axis of individual generator. In addition, there are two potential energy terms corresponding to load buses expressed as

$$W^{22} = \sum_{i=1}^{N_L}\int_{t_0}^{t} P_{Li}\left(\frac{d\delta_i}{dt}\right)dt \tag{5.7}$$

$$W^{23} = \sum_{i=1}^{N_L}\int_{V_0}^{V}\left(\frac{Q_{Li}(V_i)}{V_i}\right)dV_i \tag{5.8}$$

where N_L corresponds to the number of load buses in the network. Variation of W_i^{21} term is slow as it is associated with generator inertia and also true for W^{22} as load bus angle does not change rapidly. It has been demonstrated in [99] that $W^{21} = \sum_{i=1}^{N_G} W_i^{21} = W^{22}$ and W_{23} variation is negligible. Also during fault duration, it has been found that variations of W_{21} ,W_{22} is small and the dominant component in W_i^{PE} is W_i^{24}. Thus using eqn (5.2)

we can obtain an accurate estimate of individual machine potential energy terms based on the dynamic states information without having to evaluate the energy over load buses. However the assumption has been seen to be valid only within a certain time after fault initiation, preferably till fault clearance and subsequent instances would require network wide TEF computation.

In Fig. 5.1 the W_{di} indices and the individual machine energy W_i^T and generator angles are plotted for a three phase fault on one of the lines of the IEEE 39 bus network, cleared after 12 cycles by opening the line. It can be noted that generator G32 attains the highest values of W_{di} immediately after fault occurrence (t=2 s) and also have the highest total energy at fault clearance (t=2.2 s).

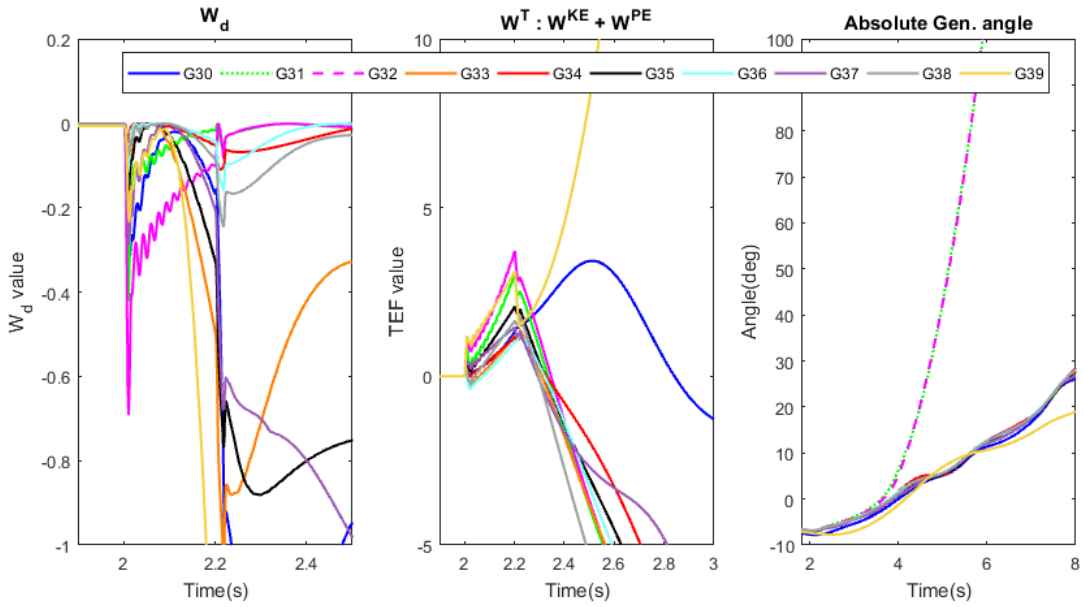

Fig. 5.1 Comparison of Instability Index (W_{di}), Transient Energy Function (W_i^T) and Rotor angle δ_i of individual generator following a 3phase fault on Line5B3B4

Although G31 had the second highest value of W_{di}, W_i^T value ends up being less than G39, which represents the equivalent generator of an external network, and attains the second highest energy in the network at the instant of fault clearance. Following the disturbance, as the external network starts oscillating against the network under consideration, the angle difference and speed deviation increases resulting in a rapid increase of W_i^{KE} and W_i^{21} components of G39 compared to other generators.

Index	Time(s)	G32	G39	G31
W_i^T	2.2	3.967	2.989	2.203
$\|W_{di}\|$	2	0.692	0.234	0.421

Table 5.1 Critical Generator Ranking for a fault on Line5B3B4

This is evident from the G39 transient energy function plot which starts increasing monotonically after the disturbance. In addition from the rotor angle plots it can be observed that generators G31 and G32 separate out from the rest of the network at t=3.5 s when no action is taken. Because the energy change of transmission lines and loads are not included, the total TEF value of the network after fault clearance does not remain constant.

This pattern based on sound TEF principles has been observed for all of the simulations in IEEE 39 bus leading to instability and thus offers a method of automatically identifying the critical generators in the network well before the actual instability sets in. Algorithm for critical generator identification methodology can be formulated as :

1. Rank generators based on W_{di} at fault initiation : R_{di}
2. Rank generators based on Transient Energy Function (W_i^T) at fault exit : R_i^T
3. If $R_i^T(1) = R_{di}$, mark i_{th} generator as critical
4. Represent the top three generators in ranked lists R_{di} R_i^T through sets $P(S_1)$, $P(S_2)$
5. Find $B \in P(S_1) \cap (S_2)$ such that $B \neq \{\Phi\}$ and order B as R_i^T then B provides critical generator set
6. If $B = \{\Phi\}$ critical generator not identified, then compute and monitor coherency matrix

5.3 Response based Remedial Action Scheme

A high value of W_{di} implies that the corresponding generators will gain a significant amount of transient energy and is validated by the W_i^T indices at the end of the disturbance. Following a contingency, based on the computed instability indices W_{di} and Transient Energy Function W_i^T , the generators are ranked in order of decreasing absolute values of

W_{di} and W_i^T . The ranking is based on W_i^T values in the event of non-conformity of the two lists. If the prediction model indicates imminent instability then the first generator on the ranked list is tripped to stabilize the network. The recursive formulation of the RMS-based coherency matrix [125] is used to determine the coherent generator groups based on the rotor angles from the dynamic state estimator:

$$\alpha_{nl}(t_k) = \alpha_{nl}(t_{k-1}) + \frac{\Delta t}{2}(X_{nl}^2(t_k) + X_{nl}^2(t_k + \Delta t)) \tag{5.9}$$

where $X_{nl}(t_i) = [(x_n(t_k) - x_{n0}) - (x_l(t_k) - x_{l0})]$, $\Delta t = t_k - t_{k-1}$ subscript n,l correspond to generators and '0' to values at fault inception. Since angle coherency is being evaluated $x_n(t_k)$ corresponds to n^{th} generator angle at time k^{th} time instant.

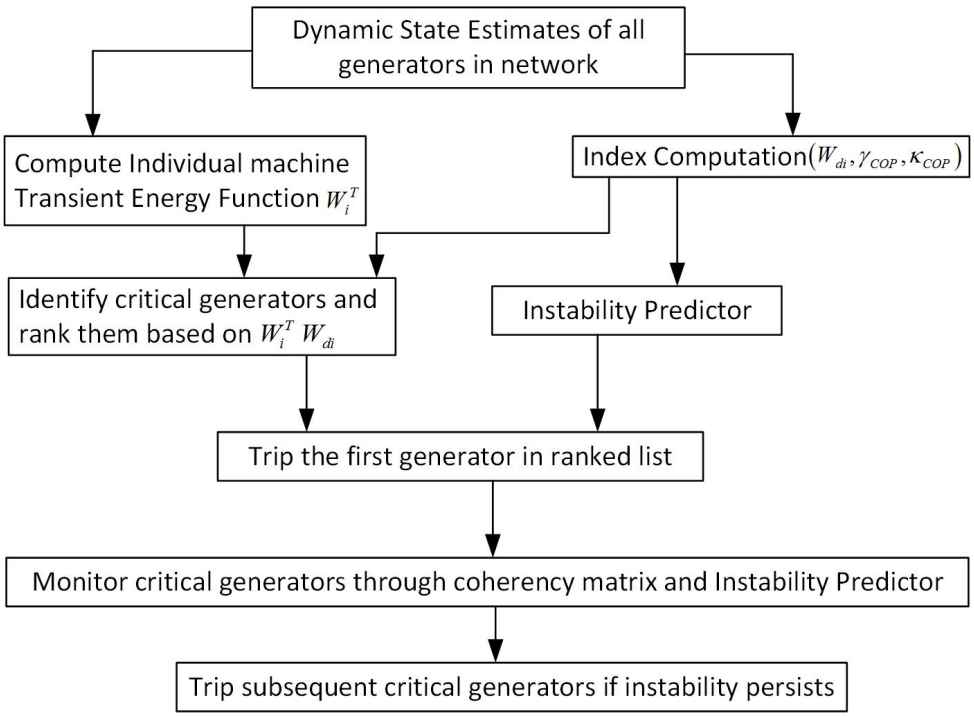

Fig. 5.2 Outline of proposed Response based Remedial Action Scheme

The identified remaining critical generators are monitored through the coherency matrix and if the coherent groups continue to separate, then the next generator in the list is tripped and monitoring is continued. The moving window classifier as described in the previous section would also be predicting the system stability during the monitoring stages after each

RAS action. This provides a new methodology for implementing a Remedial Action Scheme that identifies the runaway generator extemporaneously using dynamic state information and related disturbance severity indices. Block diagram of the proposed response based Remedial Action Scheme elucidating the concept described is shown in Fig. 5.2

5.4 Simulation Results

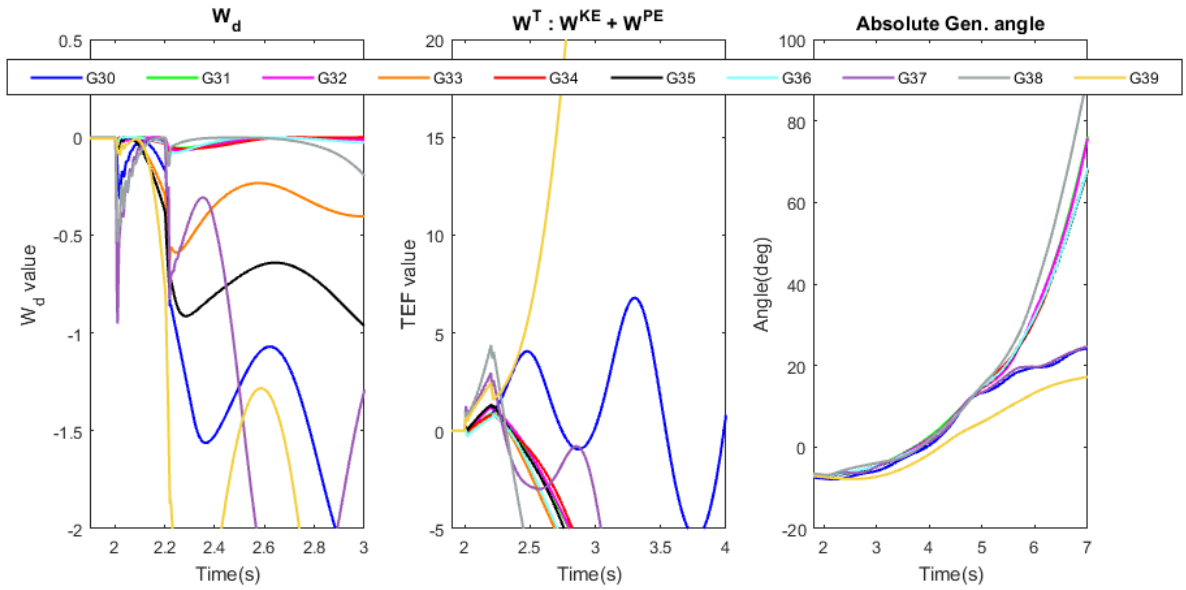

Fig. 5.3 Comparison of Instability Index (W_{di}), Transient Energy Function (W_i^T) and Rotor angle δ_i of individual generator following a 3phase fault on Line30B25B26

An example of the operation of critical generator identification in an IEEE 39 bus system is shown in Fig. 5.3. In the first two plots of figure the W_{di} indices and Transient Energy of individual generators W_i^T are shown for a three phase fault on Line30B25B26. It can be noted from Table 5.2 that the W_{di} indices for G37 and G38 are at their highest values at fault inception and W_i^T values for G38 is maximum at fault clearance, followed by G37 and G39. Thus the identified critical generators in the network for the contingency under consideration are G37, G38, G39. The absolute values of the generator angle are shown in the third plot of Fig 5.3 which depicts the system separating into two groups without any RAS action.

Index	Time(s)	G38	G37	G30
W_i^T	2.2	7.652	4.285	2.613
$\|W_{di}\|$	2	0.535	0.952	0.213

Table 5.2 Critical Generator Ranking for a fault on Line30B25B26

The Instability detector predicts an impending instability at t=2.25 s based on the computed indices ($\gamma_{COP}, \kappa_{COP}, W_{di}$) and according to the critical generator identification algorithm, Gen G38 is the critical generator and is tripped at t=2.3 s.The generator rotor angles relative to slack generator G39 before and after the application of RAS are shown in Fig. 5.4. Further separation of generators in the network is monitored through the coherency matrix and clustering of coherent groups through kmeans. The coherency matrices and the identified coherent groups computed at t=2.5, 3, 3.5 s are shown in Fig 5.4. Since the distance between the coherent cluster groups did not increase so no further action was taken. Thereby it can be noticed that the tripping of generator G38 stabilized the system. It is to be noted that the proposed method provides an innovative way of using the coherency matrix to not only identify the critical machine but also the action that needs to be taken to stabilize the system.

A multi shot example of the proposed RAS scheme is shown in Fig. 5.6 following a contingency on Line22B16B19 which would lead to instability in case no action is taken. Following a 3 phase fault on Line22B16B19, the energy indices values W_i^T and W_{di} of individual generators are plotted in the first two plots of 5.5 and generators G33 and G34 separate out from the rest of the network as can be noted from the third plot of Fig. 5.5.

It can be noted from the values in table 5.3 that generator G33 has the highest value of W_i^T at fault clearance and W_{di} at fault inception followed by G34. Generator G35 located in close electrical proximity to the fault location attained the third highest values for these indices. Based on this and the critical generator identification algorithm, G33 is first considered for tripping followed by G34 if required.

Index	Time(s)	G33	G34	G35
W_i^T	2.2	6.611	5.114	3.527
$\|W_{di}\|$	2	3.177	0.943	0.608

Table 5.3 Critical Generator Ranking for the fault on Line22B16B19

The Instability detector predicts an impending instability at t=2.4 s and identified

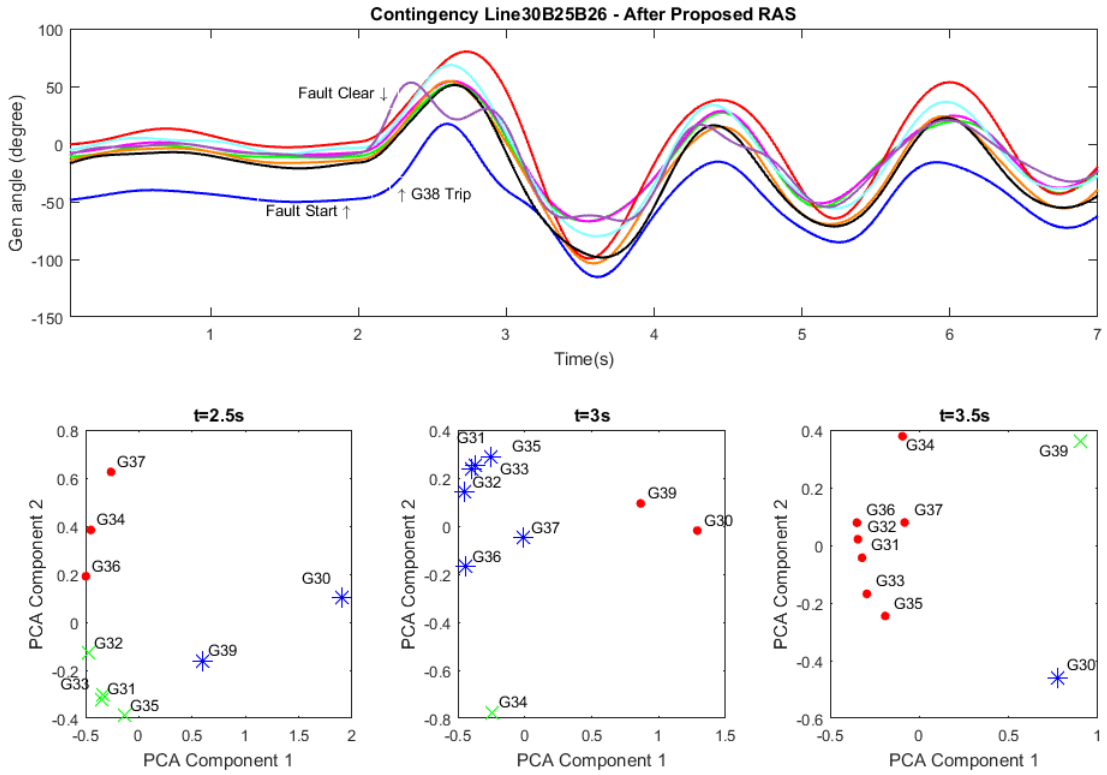

Fig. 5.4 Network stabilization through proposed RAS scheme following a 3 phase fault and subsequent clearing by tripping Line30B25B26 and coherent generator group monitoring after first critical generator tripping at t=2.5,3,3.5 s

critical generators are G33, G34. Generator G33 is tripped at this time and the generator group separation is monitored through the coherency matrix. It can be noticed from the coherency plots of Fig. 5.6 that the distance of G34 from the rest of the generators in the network at t=3s has increased compared to that at t=2.4s. and it is tripped subsequently. Further monitoring is continued through coherency matrices and since it does not indicate further separation as is evident from the coherency matrix at t=3.5s thus no more corrective actions are taken. The proposed methodology has been tested for other unstable cases and the proposed response based RAS is successfully able to detect instability and stabilize each of them.

Lastly, the performance of the proposed RAS action to stabilize the system following a fault on Line5B3B4 is shown in Fig 5.7 . Based on the indices plotted in Fig. 5.1 and

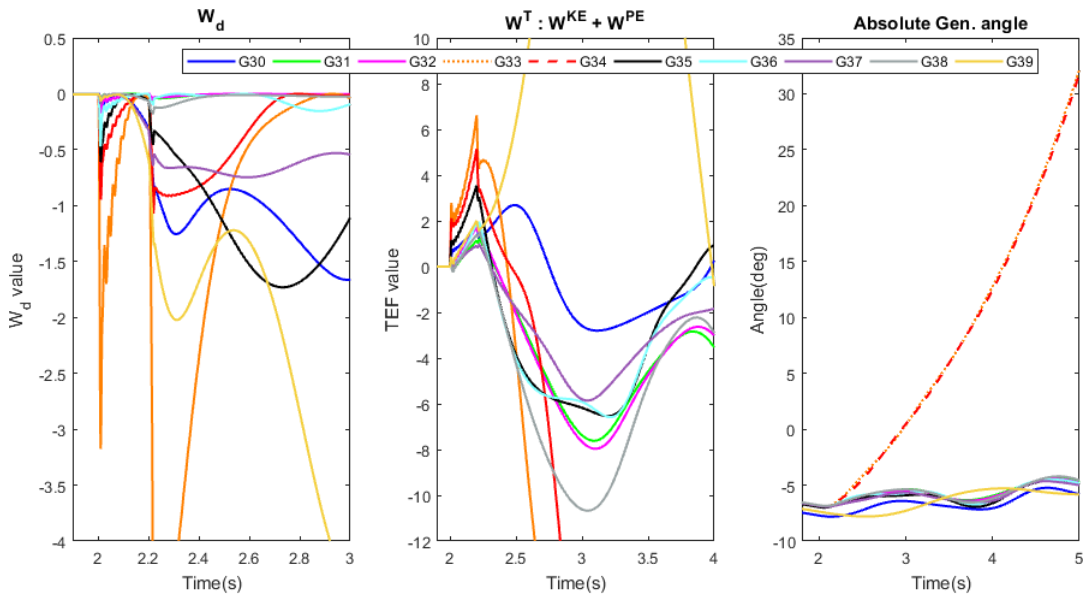

Fig. 5.5 Comparison of Instability Index (W_{di}), Transient Energy Function (W_i^T) and Rotor angle δ_i of individual generator following a 3phase fault on Line22B16B19

Table 5.1 it can be noted that G32 is the critical generator and is considered for tripping to ensure stability. The Instability Predictor detects impending stability at t=2.4 s and a generator trip signal is sent to G32. The coherency groups are monitored after sending the trip signal and since no further increase in separation occurs among the coherent generator group so no further action is taken.

5.5 Discussion

5.5.1 Type of instability mitigation and action

The proposed method only addresses the angular instability problem of the network as the instability detector scheme is trained on a database labeled based on an index dependent on maximum generator angular separation. It can deal with single or multi-swing instability, over a time frame up to 20s which is the standard simulation window used for classifying the cases. Control actions are limited to generator and load tripping only and do not consider other equipment's in the network such as reactive shunt devices.

Since the proposed framework is aimed at stabilizing a power system subjected to out-of-step of a critical machine or group of machines following a fault, fast reactive power

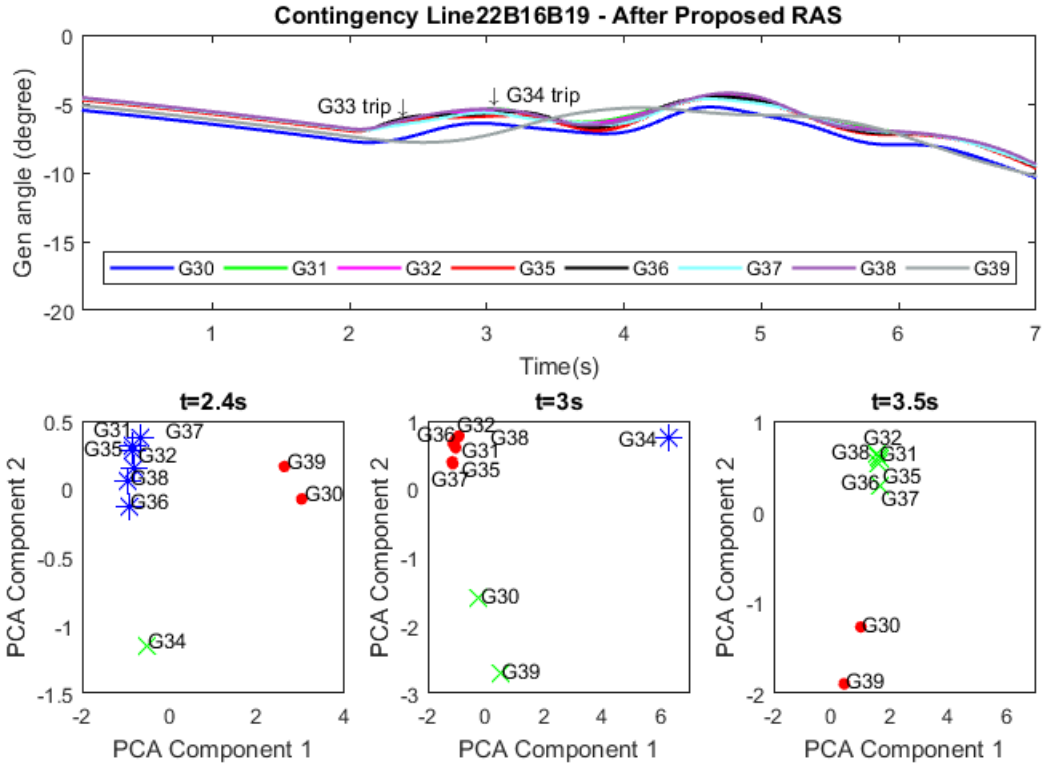

Fig. 5.6 Network stabilization through proposed RAS scheme following a 3 phase fault and subsequent clearing by tripping Line22B16B19 and coherent generator group monitoring after first critical generator tripping at t=2.5,3,3.5 s

switching can help but generator tripping based on excess energy variation is one of the most effective means [126] to deal with this situation without prior information on the network topology and generator size. In general, while it is possible to develop PMU based instability detectors which can address any type of instability over a given time frame [17], it is far more challenging to determine on-line the appropriate mitigation means (generator, loads, shunt capacitor, etc.) and even more challenging to determine the amount of corrective action for a given mean (i.e. MW or MVAR level of action).

5.5.2 Application Area

Mostly the existing RAS schemes are based on detecting network topology changes using substation breaker statuses and then shedding pre-planned amounts of generation and

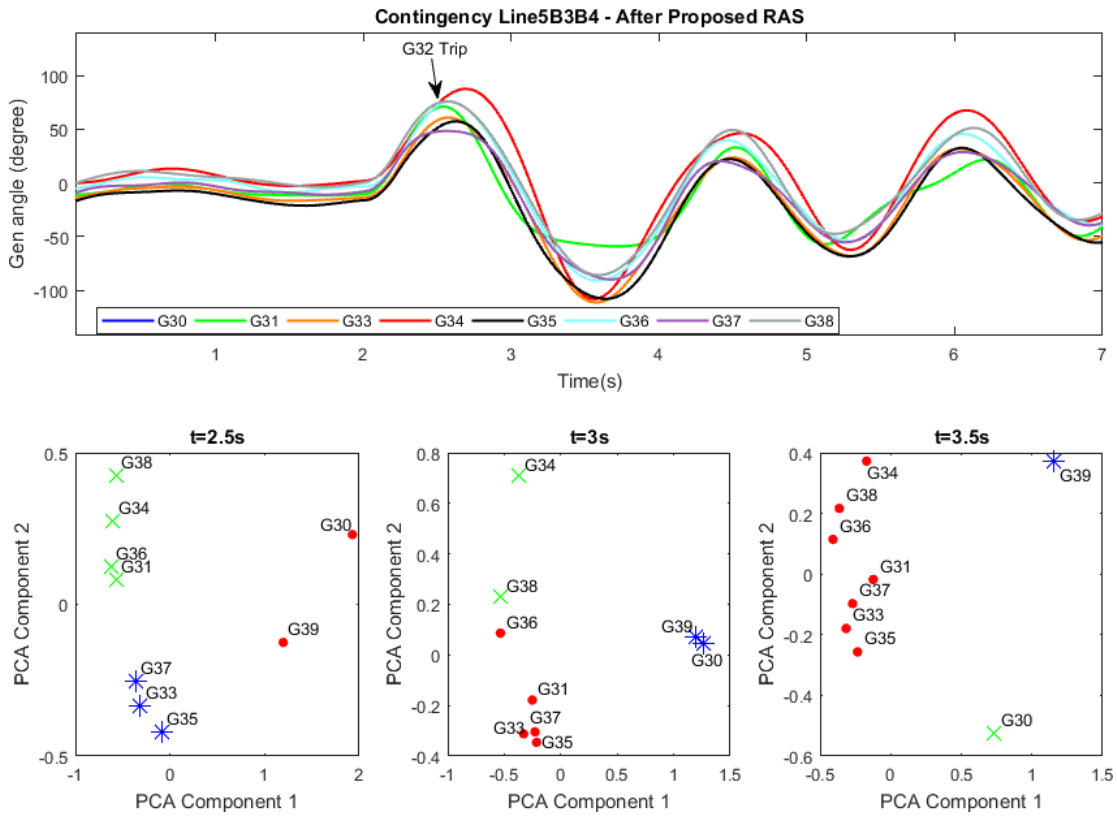

Fig. 5.7 Network stabilization through proposed RAS scheme following a 3 phase fault and subsequent clearing by tripping Line5B3B4 and coherent generator group monitoring after first critical generator tripping at t=2.5,3,3.5 s

loads at predetermined locations according to the contingency detected and prevalent pre-fault operating conditions. By contrast, the proposed scheme is aiming at two "ambitious" goals: blindly detecting instability occurrence without prior knowledge of breaker statuses and then automatically finding the best generator or load locations for shedding actions in a granular manner (i.e. one-generation unit or one load-shedding block at a time, these libraries of discretized atomic actions being the only required prior knowledge). Therefore, the concept is built assuming an implementation, intrinsically at the Balancing Authority (BA) level. This assumption alleviates the long distance information communication burden and avoids coordination requirements between entities not sharing a common interest, even though a grid code can (and should) force cooperation for the good of all. Furthermore, the method is computationally decentralized in such a way that it can be applied without change to a subset n_g of the N_g generators set in the system, in which case, the

pool of admissible generators will be limited to the n_g generators in the energy function summation.

5.5.3 RAS Protection system Interaction

The purpose of the RAS is to supplement the protection and control device operation to prevent violations of Reliability Standards such as TPL-001-4 [127] and will not be involved in the individual operation/mis-operation of protection relays that is not system critical. RAS operations may have overlap functionalities with protection devices and will require review to assess the situation in terms of the mis-operation of the device. The Remedial Action Scheme Reliability Subcommittee and North American Reliability Coordinator reviews these issues before a RAS is implemented [25]. Modern transmission system protection relays have a power swing block feature to prevent false operation that may occur if the power system locus passes through the operating zone of relays. However, if such a situation happens where the transmission line is tripped without fault but the generator remains stable then it is not a critical contingency that would result in system wide instability and the RAS execution will not happen. If the outage of the line is significant enough to create a variation in generator energy then it will be detected by the proposed methodology.

Additionally, it is to be noted that the proposed RAS is a response-based scheme that operates on generator angle information evaluated from individual generator DSE rather than generator out-of-step relays. Conventional RAS schemes are parameter and event based and they typically operate based on the operation status of circuit breaker and relays. In contrast, the proposed response scheme has not considered these signals but rather operates based on dynamic state information of generators evaluated from terminal phasor measurements.

5.6 Conclusion

Availability of dynamic state information and transient energy function (W_i^T) values computed from the same have made it possible to design the second stage of proposed RAS which involves the identification of critical generators on the fly following a disturbance. When the instability detector predicts an impending instability, the critical generator is identified extemporaneously from the ranking of the generator using individual machine

transient energy at the instant of fault clearance and tripping the corresponding one. Thereby network stability is monitored continuously through recursive coherency matrix and predictions of the moving window classifier. Further corrective actions are taken if required, according to the stability trajectory of the system. Successful demonstration of the proposed response-based multi-shot RAS has been made on an IEEE benchmark test system. The methodology provided is based on generator dynamic state rather than phasor measurements and demonstrates the utility and added benefit that a DSE provides in designing improved SIPS that minimizes disturbance impact while providing the same level of reliability, selectivity, and security.

Chapter 6

Summary and Conclusions

6.1 Summary

The main contribution of this thesis is the development of a viable technique that can identify an impending instability in the network following a contingency and maintain stability by determining and executing corrective action in real time.

Chapter 1 mentions the shortcomings of the existing Remedial Action Scheme which relies on offline simulation studies and executing preplanned contingency actions for avoiding system collapse. However, due to variability introduced through proliferating renewable energy resources, it is not possible to encompass all possible operating scenarios in simulation studies. In addition designing control actions for the unstable ones involves a computationally demanding process of investigating multiple scenarios for the post-contingency case. Thus it is clear that existing RAS architecture needs to be replaced or augmented through an approach that does not rely on simulation studies extensively but rather exploits the readily available network information provided by PMUs.

The subsequent chapter focuses on developing a centralized dynamic state estimator model which would be the foundation for the proposed online RAS scheme. The obvious advantage that the DSE provides is that it is able to estimate the internal emf dynamics of the generator as well as the exciter emf and governor torque from terminal phasor measurements only. Also, the network wide information is aggregated in a centralized location while addressing issues of communication interruption and delays.

The added information provided by DSE made it feasible to compute energy function based instability indices as well as conventional ones based on electromechanical angle and

frequency. These indices are used to design an instability detector. The performance and characteristics of two instability detectors that operate on two different operating principles have been compared and contrasted. One of the detectors uses a boosted decision tree that requires spectral features extracted from the indices while the other is based on a state of the art neural network model that operates directly on the indices.

The penultimate chapter establishes the proposed online RAS. It operates by identifying critical generators through individual generator energy formulation, implementing corrective actions in incremental steps, and observing the network through the coherency matrix. The identification and decision-making process are taken extemporaneously and thereby alleviates the computational burden and shortcomings of the existing RAS. A successful demonstration of the proposed algorithm has been shown on a benchmark interconnected system. Additionally, software in loop validation on a real time simulation platform (HyperSim) has been done in Appendix B.

An improved RAS scheme would result in improved network reliability which translates to profits for utility and improvement in customer satisfaction [49] as well as better utilization of renewable energy resources as it allows the grid to operate at reduced operating margins.

6.2 Conclusions

The main findings and contributions of this thesis are summarized in the following statements:

1. The operation of a federation of several dynamic state estimators each one of which is fully decentralized and correspond to one of the generators in the network is presented in the thesis. This is the first step required in making the RAS operational. Each of these DSE is able to tackle probabilistic missing data and transmission delay issues. Using analytical relation, the DSE estimates the field exciter voltage E_{fd} and governor torque T_m from the generator terminal PMU measurements. In general all the generator states are able to track the actual signals with less deviation and initialize rapidly compared to previously established estimator results. Also apart from, the PMU measurements, the only other input to each EKF state estimator is Power Reference (P_{ref}) and Voltage Reference (V_{ref}), which are reasonably known over time,

as a result of the 5-minute economic dispatch update by the control system operator and are almost constant or slowly varying quantities that are easy to acquire in a centralized setup.

2. Instability indices consist of individual generator energy derivative change W_{di} as well as γ_{COP} and κ_{COP} for instability prediction. W_{di} indices are computed from generator transient emfs e'_d and e'_q and show rapid variation in contrast to γ_{COP} and κ_{COP} computed from generator angle and speed which shows slow variation. In addition, another interesting feature of the indices is that γ_{COP} and κ_{COP} are centralized while W_{di} indices for individual generators are decentralized which brings complementary features in the proposed predictor model. Both the indices exhibit complex variation and is difficult to demarcate between stable and unstable scenario using a simple classifier. Thereby complex classification algorithms eg. decision trees and neural networks have been used for making predictions on model stability.

3. In contrast to existing RAS and SIPS schemes, most of which involve topology change detection and instability mitigation through pre-determined corrective actions, the proposed scheme presented in the thesis provides the advantage of using generator terminal measurement only. By utilizing the network wide generator state information provided by the federation of DSE, individual generator energy is computed instantaneously and by comparing multiple unstable scenarios a particular pattern has been observed. Based on this an algorithm has been devised that identifies the critical generators on the-fly and subsequently stabilizes the network through corrective actions consisting of tripping the identified critical (run-away) generators. Additionally, the proposed formulation is a multi-shot Remedial Action Scheme, and network stability is monitored continuously through recursive coherency matrix and predictions of the moving window classifier after each action. The successful operation of the proposed RAS has been demonstrated on the benchmark IEEE 39 bus system.

Apart from this a few other interesting findings reported in the thesis are

1. Parameter sensitivity analysis of the DSE has been performed which identifies the crucial parameters and also demonstrates how each of the states is affected by the variability of the parameters.

2. An interesting predictive property has been presented by comparing the W_{di} values, total energy value W^T, and the generator angle of individual generators. In a contingency resulting in instability, it is often the generators that have the highest rate of change of energy values W_{di} at the start of disturbance, and the highest total energy at end of disturbance are typically ones that separate from the rest of the network. Although the actual angular separation of generators often happens after a few seconds of disturbance clearance, however by noting the W^T and W_{di} values it is possible to determine the critical generators way before the actual instability occurs. This predictive property helps to identify the most disturbed generator and the actions to be taken in an expedited manner.

3. Lastly, the thesis provides a comparative evaluation of two different types of classifiers - the first one being a conventional decision tree classifier that operates on spectral features computed from the indices and the other one is a state of the art Multivariate Long Short Term Memory network. Each classifier offers a different set of advantages in terms of training time and prediction time although their accuracies are fairly similar.

6.3 Future Work

The established proposed RAS offers potential for further developments. A few of the areas where it can be applied would be

1. Making DSE more robust to data quality issues such as non-Gaussian Measurements, bad data, cyber attacks etc. Also hybrid state estimation approaches that leverages different theories would be more suitable for the power system model [128].

2. Extending the instability detector to predict other forms of instability eg. voltage and frequency instability by the inclusion of these scenarios in the training set. Also inclusion of forced oscillation events into the training space.

3. Extending the scope of possible action to other forms of mitigation action eg. generator run-back, shunt capacitor switching, etc and also determining the appropriate amount of corrective action for a given disturbance.

4. Evaluating the performance of the proposed scheme in a grid with an increasing amount of renewable energy penetration (wind, solar, and other distributed sources of energy). [128] suggests developing DSE for these asynchronous, intermittent, and interia-less sources at the point of common coupling which would allow to estimate the latent synthetic inertia and use it for rotor angle stability. The application of the proposed technique can also be extended to a grid with a significant amount of renewable energy based sources by modeling power electronics converters as Synchronous Generators through the concept of virtual inertia. A comparative evaluation of major virtual inertia topologies and possible future research direction for system level integration and modeling are presented in [129].

Appendix A

List of Spectral features

A complete list of the features used in the moving window ensemble decision tree classifier are shown in table below and a brief description of each of the features are provided.

Feature Names	**Brief Description**
SP-Summaries-fft.maxS	Maximum, and max peak width
SP-Summaries-fft.maxProm	Maximum prominence of any peak
SP-Summaries-fft.meanProm-2	Mean peak prominence of those with prominence of at least 2
SP-Summaries-fft.meanPeakWidth-prom2	Mean peak width of peaks with prominence of at least 2
SP-Summaries-fft.peakPower-2	Power in top 2 peaks
SP-Summaries-fft.peakPower-5	Power in top 5 peaks
SP-Summaries-fft.peakPower-prom2	Peak Power with prominence of at least 2
SP-Summaries-fft.w-weighted-peak-prom	Peak power weighted by prominence
SP-Summaries-fft.w-weighted-peak-height	Peak Power weighted by height
SP-Summaries-fft.peakpower1	Number of peaks required to get to 50% of power in peaks
SP-Summaries-fft.iqr	Inter Quartile Range

SP-Summaries-fft.fpolysat-a	Coefficient a after fitting polysat
SP-Summaries-fft.fpolysat-b	Coefficient b after fitting polysat
SP-Summaries-fft.fpolysat-r2	Polysat fitting parameter
SP-Summaries-fft.fpolysat-rmse	Polysat fitting root mean square error
SP-Summaries-fft.logiqr	Logarithm of Inter Quartile Range
SP-Summaries-fft.q25	25 % Quartile
SP-Summaries-fft.median	Median Quartile
SP-Summaries-fft.q75	75 % Quartile
SP-Summaries-fft.std	Standard Deviation of distribution
SP-Summaries-fft.stdlog	Standard Deviation of logarithm of distribution
SP-Summaries-fft.mean	Mean of distribution
SP-Summaries-fft.logmean	Mean of logarithm of distribution
SP-Summaries-fft.mom3	3rd order moment of distribution
SP-Summaries-fft.mom4	4th order moment of distribution
SP-Summaries-fft.mom5	5th order moment of distribution
SP-Summaries-fft.ac1	Auto-Correlation Coefficient 1
SP-Summaries-fft.ac2	Auto-Correlation Coefficient 2
SP-Summaries-fft.tau	Auto-Correlation Time Delay
SP-Summaries-fft.wmax-90	Frequency at which cumulative sum is a fraction of 90 % maximum
SP-Summaries-fft.wmax-95	Frequency at which cumulative sum is a fraction of 95 % maximum
SP-Summaries-fft.wmax-99	Frequency at which cumulative sum is a fraction of 99 % maximum
SP-Summaries-fft.w10_90	Width of measures from 10% to 90%
SP-Summaries-fft.w25_75	Width of measures from 25% to 75%
SP-Summaries-fft.fpoly2csS-p1	Polynomial fitted function coefficients 1
SP-Summaries-fft.fpoly2csS-p2	Polynomial fitted function coefficients 2

SP-Summaries-fft.fpoly2csS-p3	Polynomial fitted function coefficients 3
SP-Summaries-fft.fpoly2-sse	Polynomial fitted function parameters
SP-Summaries-fft.fpoly2-r2	Polynomial fitted function parameters
SP-Summaries-fft.fpoly2-rmse	Polynomial fitted function root mean square error
SP-Summaries-fft.spect-shann-ent	Shannon spectral entropy
SP-Summaries-fft.spect-shann-ent-norm	Norm of Shannon spectral entropy
SP-Summaries-fft.sfm	Spectral Flatness Measure
SP-Summaries-fft.areatopeak	Areas under power spectrum upto peak
SP-Summaries-fft.ylogareatopeak	Logarithm of area under power spectrum upto peak (semilog)
SP-Summaries-fft.linfitloglog-all-a1	Robust linear fit to log-log plot parameters
SP-Summaries-fft.linfitloglog-all-a2	Robust linear fit to log-log plot parameters
SP-Summaries-fft.linfitloglog-all-sigrat	Robust linear fit to log-log plot parameters
SP-Summaries-fft.linfitloglog-all-sigma	Robust linear fit to log-log plot parameters
SP-Summaries-fft.linfitloglog-all-sea1	Robust linear fit to log-log plot parameters
SP-Summaries-fft.linfitloglog-lf-a1	Robust linear fit to log-log plot parameters
SP-Summaries-fft.linfitloglog-lf-a2	Robust linear fit to log-log plot parameters
SP-Summaries-fft.linfitloglog-lf-sigrat	Robust linear fit to log-log plot parameters
SP-Summaries-fft.linfitloglog-lf-sigma	Robust linear fit to log-log plot parameters
SP-Summaries-fft.linfitloglog-lf-sea1	Robust linear fit to log-log plot parameters
SP-Summaries-fft.area-2_1	Area under power in specific frequency bands (2 bands)
SP-Summaries-fft.logarea-2_1	Area under logarithm of power in specific frequency bands (2 bands)

SP-Summaries-fft.area-2_2	Area under power in specific frequency bands (2 bands)
SP-Summaries-fft.logarea-2_2	Area under logarithm of power in specific frequency bands (2 bands)
SP-Summaries-fft.statav2-m	Ratio of mean and standard deviation in specific frequency bands (2 bands)
SP-Summaries-fft.statav2-s	Ratio of standard deviation in the splitted bands
SP-Summaries-fft.area-3_1	Area under power in specific frequency bands (3 bands)
SP-Summaries-fft.logarea-3_1	Area under logarithm of power in specific frequency bands (3 bands)
SP-Summaries-fft.area-3_2	Area under power in specific frequency bands (3 bands)
SP-Summaries-fft.logarea-3_2	Area under logarithm of power in specific frequency bands (3 bands)
SP-Summaries-fft.area-3_3	Area under power in specific frequency bands (3 bands)
SP-Summaries-fft.logarea-3_3	Area under logarithm of power in specific frequency bands (3 bands)
SP-Summaries-fft.statav3-m	Ratio of mean and standard deviation in specific frequency bands (3 bands)
SP-Summaries-fft.statav3-s	Ratio of standard deviation in the splitted bands
SP-Summaries-fft.area-4_1	Area under power in specific frequency bands (4 bands)
SP-Summaries-fft.logarea-4_1	Area under logarithm of power in specific frequency bands (4 bands)
SP-Summaries-fft.area-4_2	Area under power in specific frequency bands (4 bands)
SP-Summaries-fft.logarea-4_2	Area under logarithm of power in specific frequency bands (4 bands)
SP-Summaries-fft.area-4_3	Area under power in specific frequency bands (4 bands)

SP-Summaries-fft.logarea-4_3	Area under logarithm of power in specific frequency bands (4 bands)
SP-Summaries-fft.area-4_4	Area under power in specific frequency bands (4 bands)
SP-Summaries-fft.logarea-4_4	Area under logarithm of power in specific frequency bands (4 bands)
SP-Summaries-fft.statav4-m	Ratio of mean and standard deviation in specific frequency bands (4 bands)
SP-Summaries-fft.statav4-s	Ratio of standard deviation in the splitted bands
SP-Summaries-fft.area-5_1	Area under power in specific frequency bands (5 bands)
SP-Summaries-fft.logarea-5_1	Area under logarithm of power in specific frequency bands (5 bands)
SP-Summaries-fft.area-5_2	Area under power in specific frequency bands (5 bands)
SP-Summaries-fft.logarea-5_2	Area under logarithm of power in specific frequency bands (5 bands)
SP-Summaries-fft.area-5_3	Area under power in specific frequency bands (5 bands)
SP-Summaries-fft.logarea-5_3	Area under logarithm of power in specific frequency bands (5 bands)
SP-Summaries-fft.area-5_4	Area under power in specific frequency bands (5 bands)
SP-Summaries-fft.logarea-5_4	Area under logarithm of power in specific frequency bands (5 bands)
SP-Summaries-fft.area-5_5	Area under power in specific frequency bands (5 bands)
SP-Summaries-fft.logarea-5_5	Area under logarithm of power in specific frequency bands (5 bands)
SP-Summaries-fft.statav5-m	Ratio of mean and standard deviation in specific frequency bands (5 bands)
SP-Summaries-fft.statav5-s	Ratio of standard deviation in the splitted bands (5 bands)

Appendix B

Software in the Loop Simulation of Automated Remedial Action Scheme

B.1 Introduction

Real time simulation of a computer model implies that the simulation model executes at the same rate as an actual clock. Execution of complex power system models in real time is possible in target platforms called Real Time Simulators (RTS) offered by OPAL-RT and RTDS. This RTS provides a platform for cost effective and rapid testing of various control strategies. Besides, it is also an independent validation of the results in transient stability studies. The role, advantage, and applicability of using a Real Time Simulator are discussed in detail in [130]. This section is a "proof-of-concept" demonstration of the implementation of proposed Automated Remedial Action Scheme in a real time simulator software.

B.2 Simulation Setup

The proposed RAS implementation in Simulink is implemented in three separate blocks :

1. Dynamic State Estimator
2. Instability Detector
3. Critical Generator Identification

A block diagram overview of the Simulink model remedial action scheme is shown in Fig. B.1. Each of the individual blocks shown in the figure is either a Simulink Model or a user-defined function. The arrows indicate the flow of the signal. The bus terminal signals are provided to a Phasor Measurement Unit block which is an embedded function block as reported in [94]. Each of the individual PMU blocks is named 'PMU$_N$' where N represents the generator number it is connected to. The PMU blocks compute the phasor values and pass it on to the DSE Block which is a user-defined function that computes the generator dynamic states. This block however needs generator parameters to be specified within the user defined function as these values are not passed explicitly from the generator block to that of DSE block. The same naming convention as that of the PMUs is followed for DSE as well i.e. the dynamic state block for generator N is named as DSE$_N$.

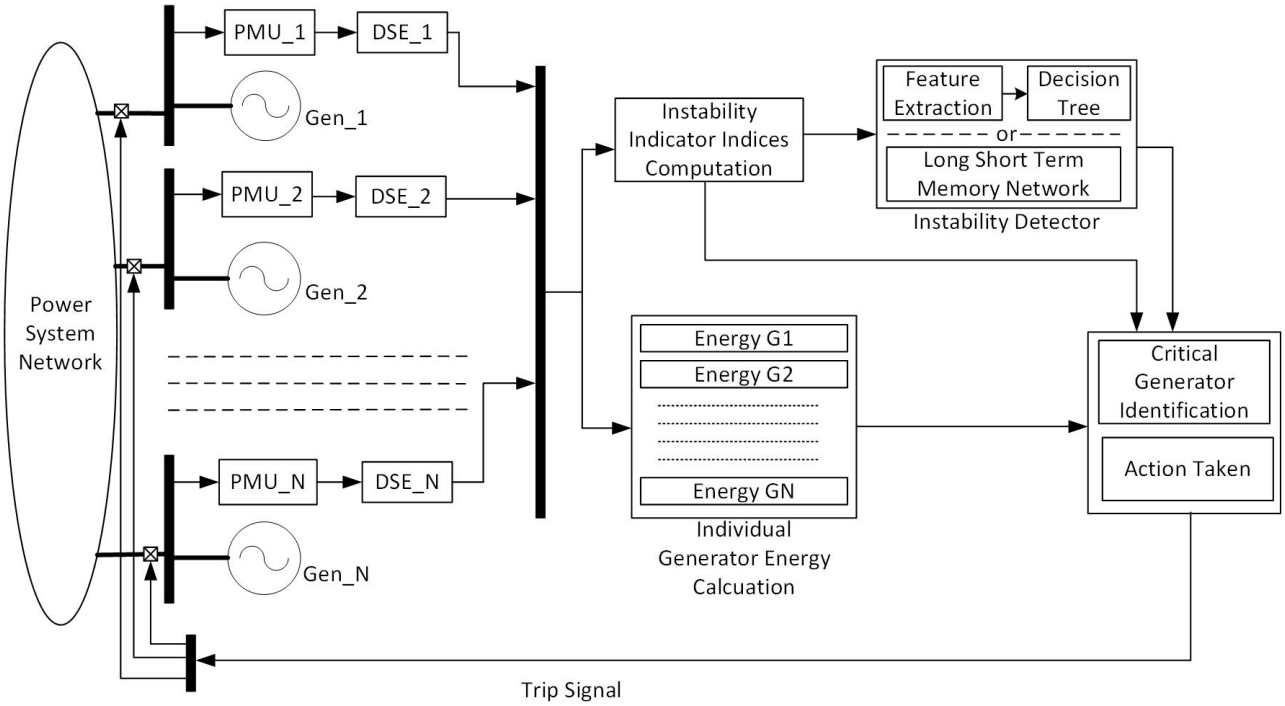

Fig. B.1 Overview of block diagram setup

Once the dynamic states have been computed they are aggregated together and passed on to the Instability Index Computation block and the Individual Generator Energy Calculation blocks, both of which are user defined function models. The former block computes the indices γ_{COP}, κ_{COP} as well as energy derivative change W_{di} index. All the indices are

computed based on instantaneous values received from the DSE block. These indices are passed on to the Instability detector block which either consists of a feature extraction module and decision tree or a Long Short Term Memory Network (LSTM) block. The feature extraction module operates on a particular window segment over the indices and then it passes the feature values to the trained decision tree classifier. Otherwise, the indices stored over the window segments are passed into the LSTM block. The prediction made by the instability detector as well as the computed instability index values are passed on to the critical generator identification block. Also using the dynamic state information individual generator energies are computed and transferred to the critical generator identification block which selects the generator for tripping and sends the signal to an individual circuit breaker. Each of the individual generator energy blocks also requires the generator parameter information which is explicitly specified within them. This critical generator identification block also computes the coherency matrix and monitors the network for further action if required.

Implementation details of each of these blocks are explained in detail in subsequent subsections.

B.2.1 Dynamic State Estimator Block

The Dynamic State Estimator for an individual generator is developed using user-defined function blocks. The states variable and other parameters (process and measurement noise) are defined using the 'persistent' command and initialized to zero value or predetermined values of the initial condition. The variables defined as persistent are local to the function yet their values are retained in memory between calls to the function. The differential equations corresponding to each state variable are solved using a simple method of Euler integration in the user defined function and do not call any Matlab solver. Also, the last received PMU values are stored using persistent variables until a new value is obtained to deal with communication interruption issues as discussed in Chapter 2. Each of the DSE blocks also computes the Energy derivative values W_{di} from the state variables and computation of γ_{COP} and κ_{COP} instability indices are done in a separate user defined function by combining the rotor angle and rotor speed state variables. The computed instability indices at each time step are passed on to both the Instability Detector and Critical Generator Identification blocks.

B.2.2 Instability Detector Block

Instability Detector operation requires the computation of spectral features over a time window of 250 ms with a 75% overlap. A separate Matlab user defined function is created for instability detection. The indices are stored in a matrix defined as a persistent variable and this block predicts discrete windows of 62.5 ms rather than at every simulation step. The computation of the spectral features requires the usage of several mathematical operations (eg. curve fitting) that are not directly available in Simulink as blocks. So these operations are executed using 'coder.extrinsic' command of Mtlab which uses the Matlab engine for these function call and bypasses code generation for the functions defined under extrinsic. It is to be noted that the output of an extrinsic function is a mxArray which is a C language opaque type. Therefore to use these variables as normal ones for an operation they need to be initialized before using it in a user defined function block. Also the operation of coder extrinsic is not fully compatible with all the functions (eg. fit) because the returned type is a C-object and the returned variable cannot be used for further operation. Hence an interfacing user-defined function has to be declared that converts the C-object into a structure suitable for subsequent further actions in Matlab code. The workaround has been proposed by Matlab support and the development team will address this issue in a future release of the product.

Once all the relevant features have been computed for individual indices, the features are concatenated, scaled, and normalized. The scaling and normalization values of each index are obtained while training the classifier with the initial database generation as explained in Chapter 4. The normalization is done using an outlier-robust sigmoid transformation and then scaled to the unit interval. The scaling values are loaded into the user defined function using the trained classifier prediction of system stability of the computed feature vector. However, Simulink currently does not support the loading of the trained classifier model into its workspace which is different from the Matlab base workspace. The workaround proposed was to transfer the computed feature vector from the Simulink workspace to the base workspace, make prediction and then transfer the prediction back to Simulink workspace. This is achieved by using the 'assignin' command of Matlab which allows the user to change the workspace of the corresponding variable. The predictions is made using the 'evalin' command which evaluates a particular expression and returns the result

in a specified format of output variables. The prediction results are transferred to the critical generator identification block for further operation. Principle components of the coherency matrix are computed and using the first two components kmeans clustering is done based on an automated optimized clustering policy. It is based on the elbow method that considers the percentage of variance explained as a function of the number of clusters and selects the cluster that does not lead to a relatively significant increase in explained variance. Computed coherency clusters are plotted at every time instant that provides a visualization of the generators' dynamics.

B.2.3 Critical Generator Identification Block

The Critical Generator Identification block consists of two subparts. The first one is a set of user defined function blocks for computing individual generator energy based on the equations mentioned in Section 5.2. The equations for computing the terms W_i^{KE}, W_i^{21} , W_i^{24} require knowledge of the variable values at the instant of the start of disturbance which is stored as persistent variables. Also since the evaluation of W_i^{25} and W_i^{26} requires variable from previous instants which are also stored in the same way. Parameters of individual generators are also defined inside each individual user defined function. The second part of the block consists of aggregating the individual generator energy as well as the energy derivative values and identifying the critical generator based on the algorithm stated in Section 5.2. Once the critical generator has been identified and an impending instability is predicted by an instability detector then a trip signal is sent to the corresponding generator model. Additional steps of connecting a load to the separated generator are taken to prevent numerical instability and ensuring that the simulation continues. Subsequent monitoring of instability after the first action is continued through the coherency matrix and further action through the generator trip signal is taken if required.

It is to be noted that a closed loop is formed starting from the generator terminal bus signals to PMU block, DSE block, Energy Computation block to Critical Generator Identification block which finally sends a trip signal to the circuit breaker. However, some errors resulting from multiple user defined function blocks and the 'goto' and 'from' blocks involved in the loop. The errors were caused as the solver faced problems when attempting to determine signal dimensions. This was addressed by specifying the output dimension

sizes of each of the MATLAB Function blocks.

B.2.4 Model Export : Simulink to HyperSim

Simulink allows the generation of standalone C/C++ code for Simulink models for deployment in a wide variety of applications. The C code for the current model can be imported into a Real Time Simulation software (RTS) and its performance can be validated. Hypersim, a RTS, offers the option of importing a user-defined model through its "Import UCM" feature from Simulink. The DSE model requires a phasor signal from the generator bus terminal to operate but HyperSim does not have a Phasor Measurement Block. So a PMU block developed in Simulink has been placed inside the Dynamic State Estimator block and C code generation has been performed on this combined model. This allows the possibility of connecting the Hypersim signals directly into the imported simulation block without requiring any pre-processing or needing to create a PMU model in Hypersim. Also, proper steps have been taken while making the model so that the required DSE parameters (generator and controller constants) can be modified by the user. This is because each of the 10 generators in the network have different generator and governor, exciter parameters which have to be individually set.

The DSE blocks provide the instability indicators and total energy of individual generators as output. These are connected to the imported Instability detector block and Critical generator identification block respectively. The output of the Instability detector which predicts network instability is connected to the critical generator identification block. The latter determines the unstable generator from the energy signals based on the algorithm stated in Section 5.3 and sends a trip signal to the corresponding generator.

Two other blocks that separately needed to be created and imported were a generator angle computation block and a model that behaves similarly to that of Simulink clock. Surprisingly in the current version of Hypersim software (R6.1.3.o698), there is no option of extracting the generator rotor angle directly and a custom model had to be used. The generator angle block consists simply of a discrete integrator and takes in generator speed signals in pu and provides a rotor angle as output in degrees. A provision for setting the

initial value of the rotor angle in the compiled model of angle calculator is kept and it is set to the nearest bus terminal voltage angle. Also, a user-defined script has been written to emulate the response shown by the 'clock' model in Simulink. The Point on wave (POW) synchronization block outputs a time signal but it occurs in discrete steps per second and at a random time. The newly defined block for clock requires the SyncOut signal of POW block and time step signal as input and continuous time signal in seconds as output. Also this overcomes the problem of a clock signal in Hypesim starting at different initial values rather than from zero.

B.2.5 Results

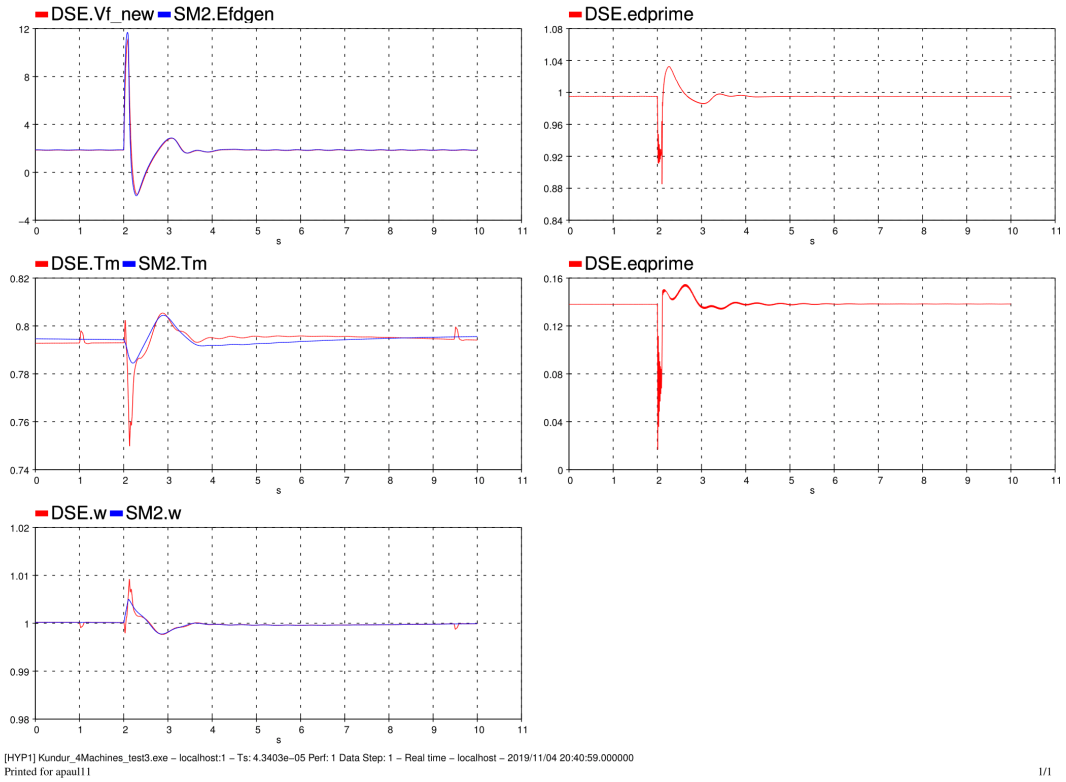

Fig. B.2 Comparison of Dynamic State Estimator signals with actual generator signals in HyperSim

An IEEE 39 bus network has been created in HyperSim based on the model used in

Simulink. However the model behavior is not exactly similar despite having exactly similar network parameters. In Fig. B.2 , the dynamic state estimator performance on one of the generators are compared with the actual generator signals. It can be observed that the dynamic state estimator can track the actual generator signals effectively. Since the internal model of the generator does not provide e'_q and e'_d signals it was not possible to compare the same with the generators.

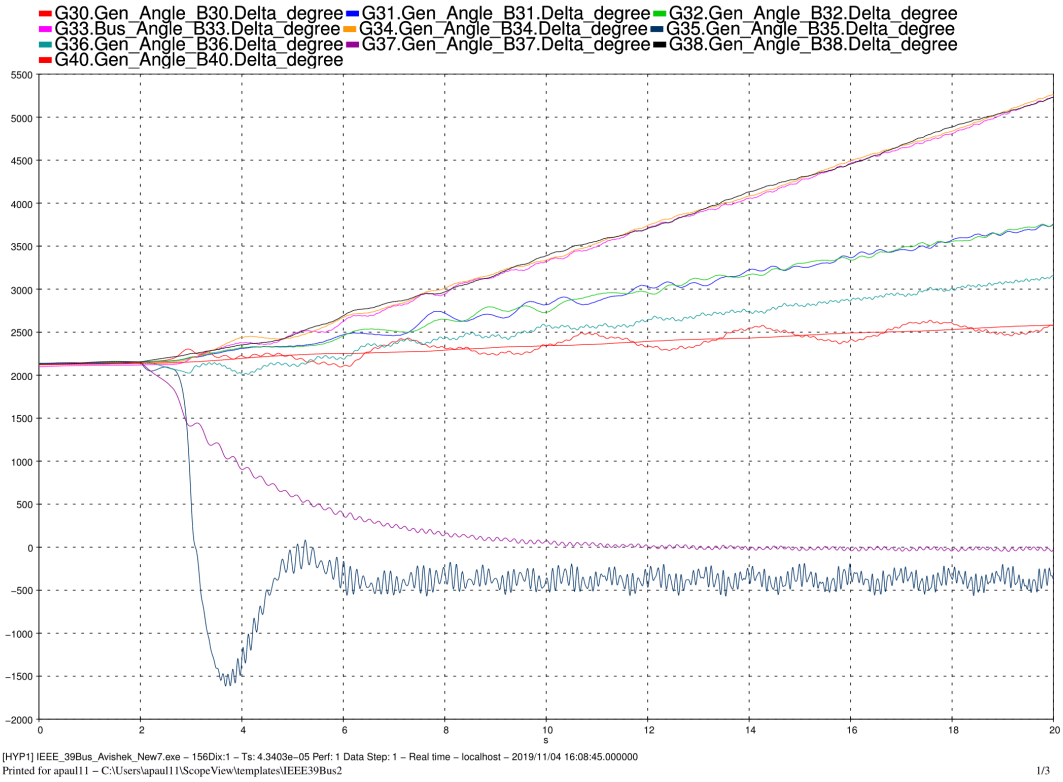

Fig. B.3 System Instability in IEEE 39 network in Hypersim due to a 3phase fault on Line30B25B26 at t = 2s and cleared at t = 2.2s without any RAS action taken

A 3 phase fault occurs in the middle of Line30B25B26 and it is subsequently cleared by tripping line B25B26 which results in an unstable scenario as shown in Fig. B.3. The performance of the proposed RAS algorithm is tested in this scenario in which Instability detector block successfully predicts an instability at t=2.4 sec and identifies G37 as the critical generator and trips it. It can be noted in Fig.0B.4 that the network is stable after

this and the generators behave coherently. It is to be noted that the generator angles in Fig. B.3 and Fig. B.4 are absolute generator angles. The identification of the critical generator is different from the simulation case of the same contingency when performed in Simulink as shown in Chapter 5. This demonstrates that although the proposed RAS does not guarantee a pre specified generator tripping for maintaining stability but adapts based on a variation of energy signals and takes different action leading to the same stabilizing action on the grid.

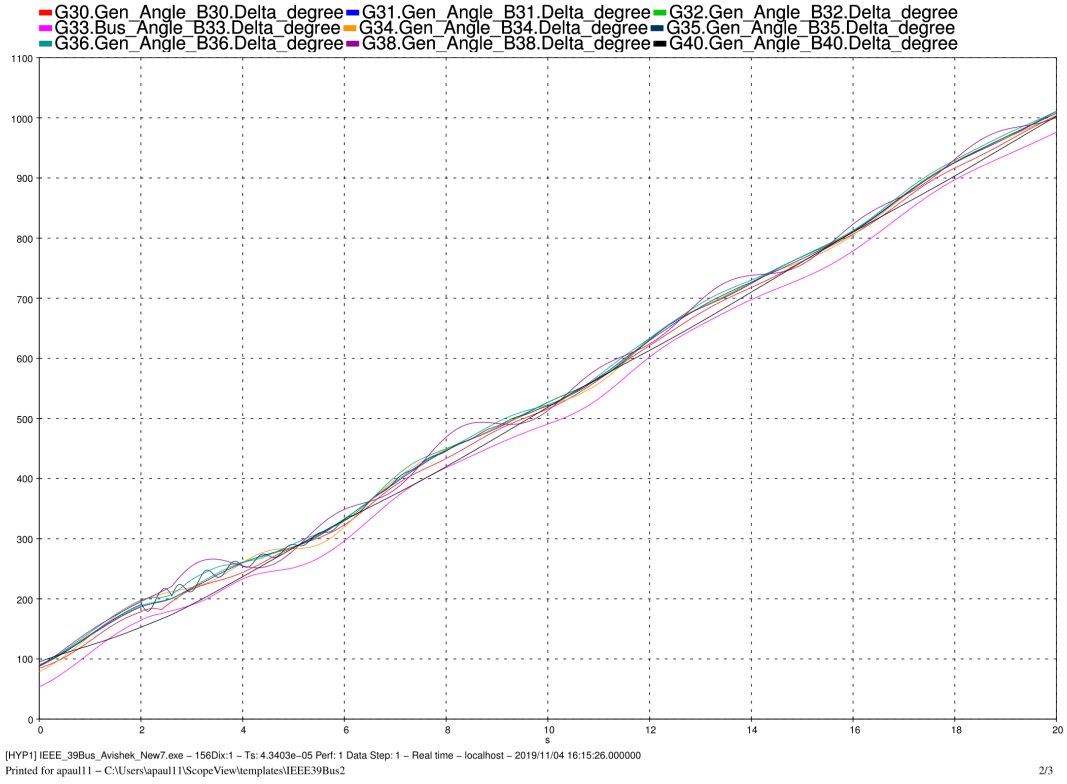

Fig. B.4 Demonstration of system stabilization after proposed RAS detects instability at t=2.4 s and trips identified critical generator G37 in IEEE 39 bus network in HyperSim

The performance of the implemented end to end simulation model has been validated on a separate software and it is operating satisfactorily. Using the imported models the same can be used on a real time simulator platform and a hardware validation of the proposed scheme can be done. The model is considerably large the real time simulator should have

sufficient computing capability (greater number of CPU cores) to avoid overruns which occurs when a target machine cannot compute the results for an individual time step in a simulation because of the processing tasks for the step overload the CPU in the target machine.

B.3 Conclusion

This section describes the technical details of the implementation of the proposed automatic remedial action scheme in an end to end Simulink model. Its performance has been validated and the possibility of code generation for standalone execution in other platforms has been confirmed as well. Although this ensures only a software validation of the proposed scheme, a hardware validation would simply involve importing the model into a real time simulator, setting up the test network, and evaluating the model.

Appendix C

Benchmark Data

The IEEE 39 Bus data used for simulation is provided below. All data are at 60Hz on 100 MVA base where applicable.

C.1 Generators

Parameters for two axis model of synchronous generators are shown in Table below with values on system base MVA

Gen. Num.	**H**	$\mathbf{R_a}$	$\mathbf{x'_d}$	$\mathbf{x'_q}$	$\mathbf{x_d}$	$\mathbf{x_q}$	$\mathbf{T'_{d0}}$	$\mathbf{T'_{q0}}$	$\mathbf{x_l}$
G39	500	0	0.006	0.008	0.02	0.019	7.0	0.7	0.003
G31	30.3	0	0.0697	0.170	0.295	0.282	6.56	1.5	0.035
G32	35.8	0	0.0531	0.0876	0.2495	0.237	5.7	1.5	0.0304
G33	28.6	0	0.0436	0.166	0.262	0.258	5.69	1.5	0.0295
G34	26.0	0	0.132	0.166	0.67	0.62	5.4	0.44	0.054
G35	34.8	0	0.05	0.01814	0.254	0.241	7.3	0.4	0.0224
G36	26.4	0	0.049	0.186	0.295	0.292	5.66	1.5	0.0322
G37	24.3	0	0.057	0.0911	0.290	0.280	6.7	0.41	0.028
G38	34.5	0	0.057	0.0587	0.2106	0.205	4.79	1.96	0.0298
G30	42.0	0	0.031	0.008	0.1	0.069	10.2	0	0.0125

C.2 Line/Transformers

Line and transformer data for the network as shown in tables below

Line Data

From Bus	To Bus	R(Ω)	X(Ω)	B(Ω)
1	2	0.0035	0.0411	0.6987
1	39	0.001	0.025	0.75
2	3	0.0013	0.0151	0.2572
2	25	0.0070	0.0086	0.1460
3	4	0.0013	0.0213	0.2214
3	18	0.0011	0.0133	0.2138
4	5	0.0008	0.0128	0.1342
4	14	0.0008	0.0129	0.1382
5	6	0.0002	0.0026	0.0434
5	8	0.0008	0.0112	0.1476
6	7	0.0006	0.0092	0.113
6	11	0.0007	0.0082	0.1389
7	8	0.0004	0.0046	0.0780
8	9	0.0023	0.0363	0.3804
9	39	0.0010	0.0250	1.200
10	11	0.0004	0.0043	0.0729
10	13	0.0004	0.0043	0.0729
13	14	0.0009	0.0101	0.1723
14	15	0.0018	0.0217	0.3660
15	16	0.0009	0.0094	0.1710
16	17	0.0007	0.0089	0.1342
16	19	0.0016	0.0195	0.3040
16	21	0.0008	0.0135	0.2548
16	24	0.0003	0.0059	0.0680
17	18	0.0007	0.0082	0.1319

From Bus	To Bus	R(Ω)	X(Ω)	B(Ω)
17	27	0.0013	0.173	0.3216
21	22	0.0008	0.0140	0.2565
22	23	0.0006	0.0096	0.1846
23	24	0.0022	0.0350	0.3610
25	26	0.0032	0.0323	0.5130
26	27	0.0014	0.0147	0.2396
26	28	0.0043	0.0474	0.7802
28	29	0.0014	0.0151	0.2490

Transformer Data

From Bus	To Bus	R(Ω)	X(Ω)	B(Ω)	Tap Magnitude	Tap Angle
12	11	0.0016	0.0435	0.0000	1.006	0.0
12	13	0.0016	0.0435	0.0000	1.006	0.0
6	31	0.0000	0.0250	0.0000	1.070	0.0
10	32	0.0000	0.0200	0.000	1.070	0.0
19	33	0.0007	0.0142	0.000	1.070	0.0
20	34	0.0009	0.0180	0.000	1.009	0.0
22	35	0.0000	0.0143	0.000	1.025	0.0
23	36	0.0005	0.0272	0.000	1.000	0.0
25	37	0.0006	0.0232	0.000	1.025	0.0
2	30	0.0000	0.0181	0.000	1.025	0.0
29	38	0.0008	0.0156	0.000	1.025	0.0
19	20	0.0138	0.000	1.06	0.0	

C.3 Load Bus

Load Bus Information of the network is shown in table below

Bus	**Type**	**MW**	**MVAR**
3	Static	322	2.4
4	Dynamic	500	184
7	Static	233.8	84.0
8	Dynamic	522	176
12	Dynamic	7.5	88
15	Static	320	153
16	Static	329	32.3
18	Static	158	30.0
20	Static	628	103
21	Dynamic	274	115
23	Static	247.5	84.6
24	Static	308.6	-92.0
25	Static	224.0	47.2
26	Static	139	17.0
27	Dynamic	281	75.5
28	Static	206	27.6
29	Static	283.5	26.9
39	Static	1104	250

Static loads exhibit constant impedance. Dynamic loads are modelled as shown in following equations with $n_p = 1.3$ and $n_q = 2$

$$P = P_0(\frac{V}{V_0})^{n_p} \tag{C.1}$$

$$Q = Q_0(\frac{V}{V_0})^{n_q} \tag{C.2}$$

C.4 Generator Bus

Bus	Gen. Num.	Volt[pu]	MW	MVAR
30	G30	1.0475	250	0
31	G31	0.9820	-9.2	-4.6
32	G32	0.9831	650	0.0
33	G33	0.9972	632	0.0
34	G34	1.0123	508	0.0
35	G35	1.0493	650	0.0
36	G36	1.0635	560	0.0
37	G37	1.0278	540	0.0
38	G38	1.0265	830	0.0
39	G39	1.03	1000	0.0

C.5 Exciter

All generators except G39 are equipped with an IEEE Type 1 exciter whose parameters are

Parameter Information	Values
Low Pass Filter Time Constant $T_r(s)$	20E-3
Regulator Gain K_a	5
Regulator Time Constant T_a	0.06
Exciter Gain K_e	1
Exciter Time Constant T_e	0.5
Damping Filter Gain K_f	0.08
Damping Filter Time Constant T_f	1
Maximum Regulator Output E_f^{max}	3.5
Minimum Regulator Output E_f^{min}	-3.0
Transient Gain Reduction T_b	0
Transient Gain Reduction T_c	0

C.6 Turbine and Governor

All generators except G39 are equipped with turbine and governor whose parameters are

Parameter Information	**Values**
Regulator Gain K_p	20
Regulator Droop R_p	0.05
Speed Relay Time Constant T_{sr}	0.001
Servo motor time Constant T_{sm}	0.15
Minimum rate of gate opening V_g^{min}	-0.1
Maximum rate of gate opening V_g^{max}	0.1
Minimum gate opening g_{min}	0
Maximum gate opening g_{max}	10
Steam Turbine constants [T_2 T_3 T_4 T_5]	[0.32 10 0.13 0.12]
Turbine torque fractions [F_2 F_3 F_4 F_5]	[0.5 0.5 0 0]

References

[1] NASPI, "PMUs and Synchrophasor data flows in north america," July 2017. [Online]. Available: https://naspi.org/node/749

[2] "An assessment of energy technologies and research opportunities," Department of Energy, Report, September 2015.

[3] "Caiso. iso generator interconnection queue." [Online]. Available: http://www.caiso.com/planning/

[4] M. Glavic and T. V. Cutsem, "Wide-area detection of voltage instability from synchronized phasor measurements. part ii: Simulation results," *IEEE Transactions on Power Systems*, vol. 24, no. 3, pp. 1417–1425, 2009.

[5] United States Department of Energy, "National electric transmission congestion study," Report, September 2015.

[6] U.S. Department of Energy, "Annual U.S. transmission review," March 2018.

[7] Y.N.Yu, "Electric power system dynamics," *Academic Press*, 1983.

[8] P. Kundur, *Power System Stability and Control*, 1994.

[9] C. W. Taylor, "Wacs-wide-area stability and voltage control system: R&d and online demonstration," in *IEEE Power Engineering Society General Meeting, 2004.*, Conference Proceedings, p. 4 Vol.1.

[10] "Final report on the august 14, 2003 blackout in the united states and canada: Causes and recommendations," Report, April 5 2004.

[11] "IEEE Standard for Synchrophasor Measurements for Power Systems – Amendment 1: Modification of Selected Performance Requirements," *IEEE Std C37.118.1a-2014 (Amendment to IEEE Std C37.118.1-2011)*, pp. 1–25, April 2014.

[12] M. G. Adamiak, A. P. Apostolov, M. M. Begovic, C. F. Henville, K. E. Martin, G. L. Michel, A. G. Phadke, and J. S. Thorp, "Wide area protection—technology and infrastructures," *IEEE Transactions on Power Delivery*, vol. 21, no. 2, pp. 601–609, April 2006.

[13] D. Ray, "Blackout of 2003: Description and responses," Power Engineering Research Center, Report, 2003.

[14] V. Rampurkar, P. Pentayya, H. A. Mangalvedekar, and F. Kazi, "Cascading failure analysis for indian power grid," *IEEE Transactions on Smart Grid*, vol. 7, no. 4, pp. 1951–1960, 2016.

[15] S. Rovnyak, S. Kretsinger, J. Thorp, and D. Brown, "Decision trees for real-time transient stability prediction," *IEEE Transactions on Power Systems*, vol. 9, no. 3, pp. 1417–1426, 1994.

[16] W. Liancheng and A. A. Girgis, "A new method for power system transient instability detection," *IEEE Transactions on Power Delivery*, vol. 12, no. 3, pp. 1082–1089, 1997.

[17] Y. Xu, Z. Y. Dong, J. H. Zhao, P. Zhang, and K. P. Wong, "A reliable intelligent system for real-time dynamic security assessment of power systems," *IEEE Transactions on Power Systems*, vol. 27, no. 3, pp. 1253–1263, 2012.

[18] I. Kamwa, S. R. Samantaray, and G. Joos, "Catastrophe predictors from ensemble decision-tree learning of wide-area severity indices," *IEEE Trans. on Smart Grid*, vol. 1, no. 2, pp. 144–158, 2010.

[19] M. He, J. Zhang, and V. Vittal, "Robust online dynamic security assessment using adaptive ensemble decision-tree learning," *IEEE Transactions on Power Systems*, vol. 28, no. 4, pp. 4089–4098, 2013.

[20] H. Supreme, A. D. l, I. Kamwa, and A. Heniche-Oussedik, "Development of new predictors based on the concept of center of power for transient and dynamic instability detection," *IEEE Transactions on Smart Grid*, vol. PP, no. 99, pp. 1–1, 2016.

[21] F. R. Gomez, A. D. Rajapakse, U. D. Annakkage, and I. T. Fernando, "Support vector machine-based algorithm for post-fault transient stability status prediction using synchronized measurements," *IEEE Transactions on Power Systems*, vol. 26, no. 3, pp. 1474–1483, 2011.

[22] Y. Zhang, Y. Xu, Z. Y. Dong, Z. Xu, and K. P. Wong, "Intelligent early warning of power system dynamic insecurity risk: Toward optimal accuracy-earliness tradeoff," *IEEE Transactions on Industrial Informatics*, vol. 13, no. 5, pp. 2544–2554, 2017.

[23] I. Kamwa, S. R. Samantaray, and G. Joos, "On the accuracy versus transparency trade-off of data-mining models for fast-response pmu-based catastrophe predictors," *IEEE Transactions on Smart Grid*, vol. 3, no. 1, pp. 152–161, March 2012.

[24] J. J. Q. Yu, D. J. Hill, A. Y. S. Lam, J. Gu, and V. O. K. Li, "Intelligent time-adaptive transient stability assessment system," *IEEE Transactions on Power Systems*, vol. 33, no. 1, pp. 1049–1058, 2018.

[25] N. A. E. R. Corporation, "Remedial action scheme definition development," Report, August 2014. [Online]. Available: https://www.nerc.com/pa/Stand/Prjct201005_2SpclPrtctnSstmPhs2/FAQ_RAS_Definition_0604_final.pdf

[26] A. P. S. Meliopoulos, R. R. Kovacs, N. D. Reppen, G. Contaxis, and N. Balu, "Power system remedial action methodology," *IEEE Transactions on Power Systems*, vol. 3, no. 2, pp. 500–509, 1988.

[27] M. M. Mahmoudi, S. Kincic, H. Zhang, and K. Tomsovic, "Implementation and testing of remedial action schemes for real-time transient stability studies," in *2017 IEEE Power & Energy Society General Meeting*, Conference Proceedings, pp. 1–5.

[28] Z. Yao, V. R. Vinnakota, Q. Zhu, C. Nichols, G. Dwernychuk, and T. Inga-Rojas, "Forewarned is forearmed: An automated system for remedial action schemes," *IEEE Power and Energy Magazine*, vol. 12, no. 3, pp. 77–86, 2014.

[29] H. Atighechi, H. Po, L. Jun, W. Guihua, and S. Ebrahimi, "A fast load shedding remedial action scheme using real-time data for bc hydro system," in *2016 IEEE Power and Energy Society General Meeting (PESGM)*, Conference Proceedings, pp. 1–5.

[30] R. Ramanathan, B. Tuck, and J. O. Brien, "Bpa's experience of implementing remedial action schemes in power flow for operation studies," in *2013 IEEE Power & Energy Society General Meeting*, Conference Proceedings, pp. 1–5.

[31] V. Madami, M. Adamiak, and M. Thakur, "Design and implementation of wide area special protection schemes," in *57th Annual Conference for Protective Relay Engineers, 2004*, Conference Proceedings, pp. 392–402.

[32] R. S. D. Miller and S. Manson, "PacifiCorp's Jim Bridger RAS: A dual triple modular redundant case study," March 2 2009. [Online]. Available: https://selinc.com/api/download/5207/

[33] V. Madani, D. Novosel, S. Horowitz, M. Adamiak, J. Amantegui, D. Karlsson, S. Imai, and A. Apostolov, "IEEE PSRC report on global industry experiences with system integrity protection schemes (SIPS)," *IEEE Transactions on Power Delivery*, vol. 25, no. 4, pp. 2143–2155, 2010.

[34] W. C. Flores, J. Barrionuevo, E. Atlas, and S. P. Torres, "An approach based on remedial action scheme to increase resiliency under failures in the central american power grid," in *2017 IEEE PES Innovative Smart Grid Technologies Conference - Latin America (ISGT Latin America)*, Conference Proceedings, pp. 1–6.

[35] D. S. Kumar and J. S. Savier, "Synchrophasor-based system integrity protection scheme for an ultra-mega-power project in india," *IET Generation, Transmission Distribution*, vol. 13, no. 8, pp. 1220–1228, April 2019.

[36] E. Ghahremani, A. Heniche-Oussedik, M. Perron, M. Racine, S. Landry, and H. Akremi, "A Detailed Presentation of an Innovative Local and Wide-Area Special Protection Scheme to Avoid Voltage Collapse: From Proof of Concept to Grid Implementation," *IEEE Transactions on Smart Grid*, vol. 10, no. 5, pp. 5196–5211, September 2019.

[37] C. Liao, Y. Hsu, Y. Wang, S. Lee, Y. Lin, and C. Chu, "Experiences on Remediation of Special Protection System for Kinmen Power System in Taiwan," *IEEE Transactions on Industry Applications*, pp. 1–1, March 2020.

[38] S. Hossain-McKenzie, M. Kazerooni, K. Davis, S. Etigowni, and S. Zonouz, "Analytic corrective control selection for online remedial action scheme design in a cyber adversarial environment," *IET Cyber-Physical Systems: Theory & Applications*, vol. 2, no. 4, pp. 188–197, 2017.

[39] A. Shrestha, V. Cecchi, and R. W. Cox, "Minimum-cost generation-shedding for dynamic remedial action scheme," in *2015 IEEE Power & Energy Society General Meeting*, Conference Proceedings, pp. 1–5.

[40] R. Liu, A. K. Srivastava, D. E. Bakken, A. Askerman, and P. Panciatici, "Decentralized state estimation and remedial control action for minimum wind curtailment using distributed computing platform," *IEEE Transactions on Industry Applications*, vol. 53, no. 6, pp. 5915–5926, 2017.

[41] M. Rostami and S. Lotfifard, "Optimal remedial actions in power systems considering wind farm grid codes and upfc," *IEEE Transactions on Industrial Informatics*, pp. 1–1, March 2019.

[42] L. A. Oquendo Class, K. M. Hopkinson, X. Wang, T. R. Andel, and R. W. Thomas, "A robust communication-based special protection system," *IEEE Transactions on Power Delivery*, vol. 25, no. 3, pp. 1314–1324, July 2010.

[43] Z. Li, G. Geng, and Q. Jiang, "Transient Stability Emergency Control Using Asynchronous Parallel Mixed-Integer Pattern Search," *IEEE Transactions on Smart Grid*, vol. 9, no. 4, pp. 2976–2985, July 2018.

[44] K. G. Ravikumar and A. K. Srivastava, "Designing centralised and distributed system integrity protection schemes for enhanced electric grid resiliency," *IET Generation, Transmission Distribution*, vol. 13, no. 8, pp. 1194–1203, April 2019.

[45] J. Lopez and C. Lu, "Adaptable system integrity protection scheme considering renewable energy sources output variations," *IEEE Transactions on Power Systems*, pp. 1–1, February 2020.

[46] J. Wen, W. H. E. Liu, P. L. Arons, and S. K. Pandey, "Evolution pathway towards wide area monitoring and protection: A real-world implementation of centralized ras system," *IEEE Trans. on Smart Grid*, vol. 5, no. 3, pp. 1506–1513, 2014.

[47] F. Valencia, R. Palma-Behnke, D. Ortiz-Villalba, A. De La Quintana, C. Rahmann, and R. Cifuentes, "Special Protection Systems: Challenges in the Chilean Market in the Face of the Massive Integration of Solar Energy," *IEEE Transactions on Power Delivery*, vol. 32, no. 1, pp. 575–584, 2017.

[48] T. Weckesser, H. Jóhannsson, and J. Østergaard, "Real-time remedial action against aperiodic small signal rotor angle instability," *IEEE Transactions on Power Systems*, vol. 31, no. 1, pp. 387–396, 2016.

[49] J. Mitra, M. Benidris, N. Nguyen, and S. Deb, "A visualization tool for real-time dynamic contingency screening and remedial actions," *IEEE Transactions on Industry Applications*, vol. 53, no. 4, pp. 3268–3278, 2017.

[50] I. Kamwa, L. Geoffroy, S. R.Samantraray, and A. Jain, "Synchrophasors data analytics framework for power grid control and dynamic stability monitoring," *IET Engineering and Technology Reference*, 2016.

[51] B. Pal and B. Chaudhuri, *Robust Control in Power Systems*, 1st ed. Springer US, 2005.

[52] L. Lima, R. Ramos, I. Hiskens, C. Cañizares, T. C. Fernandes, E. Jr, L. Gein-Lajoie, M. Gibbard, J. Kersulis, R. Kuiava, F. De Marco, N. Martins, B. Pal, A. Bohnen Piardi, J. Santos, D. Silva, A. K. Singh, B. Tamimi, and D. Vowles, "Benchmark Systems for Small-Signal Stability Analysis and Control," August 2015. [Online]. Available: https://resourcecenter.ieee-pes.org/technical-publications/technical-reports/PESTR18.html

[53] A. G. Phadke, "Synchronized phasor measurements-a historical overview," in *Transmission and Distribution Conference and Exhibition 2002: Asia Pacific. IEEE/PES*, vol. 1, Conference Proceedings, pp. 476–479 vol.1.

[54] P. Rousseaux, D. Mallieu, T. Van Cutsem, and M. Ribbens-Pavella, "Dynamic state prediction and hierarchical filtering for power system state estimation," *Automatica*, vol. 24, no. 5, pp. 595–618, 1988. [Online]. Available: http://www.sciencedirect.com/science/article/pii/0005109888901082

[55] N. G. Bretas, "An iterative dynamic state estimation and bad data processing," *International Journal of Electrical Power & Energy Systems*, vol. 11, no. 1, pp. 70–74, 1989. [Online]. Available: http://www.sciencedirect.com/science/article/pii/0142061589900100

[56] J. K. Mandal, A. K. Sinha, and L. Roy, "Incorporating nonlinearities of measurement function in power system dynamic state estimation," *IEE Proceedings - Generation, Transmission and Distribution*, vol. 142, no. 3, pp. 289–296, 1995.

[57] K. Nishiya, J. Hasegawa, and T. Koike, "Dynamic state estimation including anomaly detection and identification for power systems," *IEE Proceedings C - Generation, Transmission and Distribution*, vol. 129, no. 5, pp. 192–198, 1982.

[58] H. Zhenyu, K. Schneider, and J. Nieplocha, "Feasibility studies of applying kalman filter techniques to power system dynamic state estimation," in *2007 International Power Engineering Conference (IPEC 2007)*, Conference Proceedings, pp. 376–382.

[59] L. Lin, Linawati, J. Lie, and E. Ambikairajah, "A hybrid state estimation scheme for power systems," in *2002 Asia-Pacific Conference on Circuits and Systems*, vol. 1, Conference Proceedings, pp. 555–558 vol.1.

[60] E. Farantatos, G. K. Stefopoulos, G. J. Cokkinides, and A. P. Meliopoulos, "Pmu-based dynamic state estimation for electric power systems," in *2009 IEEE Power & Energy Society General Meeting*, Conference Proceedings, pp. 1–8.

[61] C. Jaewon, G. N. Taranto, and J. H. Chow, "Dynamic state estimation in power system using a gain-scheduled nonlinear observer," in *Control Applications, 1995., Proceedings of the 4th IEEE Conference on*, Conference Proceedings, pp. 221–226.

[62] H. Tebianian and B. Jeyasurya, "Dynamic state estimation in power systems: Modeling, and challenges," *Electric Power Systems Research*, vol. 121, pp. 109 – 114, 2015. [Online]. Available: http://www.sciencedirect.com/science/article/pii/S0378779614004441

[63] E. Ghahremani and I. Kamwa, "Local and wide-area pmu-based decentralized dynamic state estimation in multi-machine power systems," *IEEE Trans. on Power Sys.*, vol. 31, no. 1, pp. 547–562, 2016.

[64] E. Ghahremani and I. Kamwa, "Dynamic state estimation in power system by applying the extended kalman filter with unknown inputs to phasor measurements," *IEEE Transactions on Power Systems*, vol. 26, no. 4, pp. 2556–2566, 2011.

[65] S. J. Julier and J. K. Uhlmann, "Unscented filtering and nonlinear estimation," *Proceedings of the IEEE*, vol. 92, no. 3, pp. 401–422, 2004.

[66] G. Valverde and V. Terzija, "Unscented kalman filter for power system dynamic state estimation," *IET Generation, Transmission & Distribution*, vol. 5, no. 1, pp. 29–37, 2011.

[67] E. Ghahremani and I. Kamwa, "Online state estimation of a synchronous generator using unscented kalman filter from phasor measurements units," *IEEE Transactions on Energy Conversion*, vol. 26, no. 4, pp. 1099–1108, 2011.

[68] A. K. Singh and B. C. Pal, "Decentralized dynamic state estimation in power systems using unscented transformation," *IEEE Transactions on Power Systems*, vol. 29, no. 2, pp. 794–804, 2014.

[69] H. Tebianian and B. Jeyasurya, "Dynamic state estimation in power systems using kalman filters," pp. 1–5, Aug 2013.

[70] G. Anagnostou and B. C. Pal, "Derivative-free kalman filtering based approaches to dynamic state estimation for power systems with unknown inputs," *IEEE Trans. on Power Sys.*, vol. 33, no. 1, pp. 116–130, 2017.

[71] Y. Cui and R. Kavasseri, "A particle filter for dynamic state estimation in multimachine systems with detailed models," *IEEE Trans. on Power Systems*, vol. 30, no. 6, pp. 3377–3385, 2015.

[72] S. Kuang-Rong and H. Shyh-Jier, "Application of a robust algorithm for dynamic state estimation of a power system," *IEEE Transactions on Power Systems*, vol. 17, no. 1, pp. 141–147, 2002.

[73] V. Venkatasubramanian and R. G. Kavasseri, "Direct computation of generator internal dynamic states from terminal measurements," in *System Sciences, 2004. Proceedings of the 37th Annual Hawaii International Conference on*, Conference Proceedings, p. 6 pp.

[74] N. Zhou, D. Meng, Z. Huang, and G. Welch, "Dynamic state estimation of a synchronous machine using pmu data: A comparative study," *IEEE Trans. on Smart Grid*, vol. 6, no. 1, pp. 450–460, 2015.

[75] L. Fan and Y. Wehbe, "Extended kalman filtering based real-time dynamic state and parameter estimation using pmu data," *Electric Power Systems Research*, vol. 103, pp. 168–177, 2013. [Online]. Available: http://www.sciencedirect.com/science/article/pii/S0378779613001442

[76] P. Du, "Generator dynamic model validation and parameter calibration using phasor measurements at the point of connection," in *2014 IEEE PES General Meeting*, Conference Proceedings, pp. 1–1.

[77] T. D.Barfoot, *State Estimation for Robotics*. Cambridge University Press, 2017. [Online]. Available: http://asrl.utias.utoronto.ca/~tdb/bib/barfoot_ser15.pdf

[78] E. A. Wan and R. V. D. Merwe, "The unscented kalman filter for nonlinear estimation," in *Proceedings of the IEEE 2000 Adaptive Systems for Signal Processing, Communications, and Control Symposium (Cat. No.00EX373)*, Conference Proceedings, pp. 153–158.

[79] N. J. Gordon, D. J. Salmond, and A. F. M. Smith, "Novel approach to nonlinear/non-gaussian bayesian state estimation," *IEE Proceedings F - Radar and Signal Processing*, vol. 140, no. 2, pp. 107–113, 1993.

[80] Q. Yang, L. Chang, and W. Yu, "On false data injection attacks against kalman filtering in power system dynamic state estimation," *Security and Communication Networks*, vol. 9, no. 9, pp. 833–849, 2016. [Online]. Available: http://dx.doi.org/10.1002/sec.835

[81] L. M. Paz, J. D. TardÓs, and J. Neira, "Divide and conquer: EKF SLAM in O(n)," *IEEE Transactions on Robotics*, vol. 24, no. 5, pp. 1107–1120, 2008.

[82] J. N. Yang, S. Pan, and H. Huang, "An adaptive extended kalman filter for structural damage identifications ii: unknown inputs," *Structural Control and Health Monitoring*, vol. 14, no. 3, pp. 497–521, May 2007. [Online]. Available: https://onlinelibrary.wiley.com/doi/abs/10.1002/stc.171

[83] D.Simon, *Optimal State Estimation : Kalman, H-infinity, Non-linear approaches*. Hoboken,New Jersey, USA: Wiley-Interscience, June 2006.

[84] T. D. Barfoot, *State Estimation for Robotics*. Cambridge University Press, August 2017.

[85] B. Sinopoli, L. Schenato, M. Franceschetti, K. Poolla, M. I. Jordan, and S. S. Sastry, "Kalman filtering with intermittent observations," *IEEE Trans. on Automatic Control*, vol. 49, no. 9, pp. 1453–1464, 2004.

[86] Siemens, "Latency on a switched ethernet network," p. 9. [Online]. Available: https://cache.industry.siemens.com/dl/files/587/94772587/att_113195/v1/94772587_ruggedcom_latency_switched_network_en.pdf

[87] V.E.Solutions. [Online]. Available: https://enterprise.verizon.com/terms/latency/#latency

[88] N. Petra, C. G. Petra, Z. Zhang, E. M. Constantinescu, and M. Anitescu, "A bayesian approach for parameter estimation with uncertainty for dynamic power systems," *IEEE Transactions on Power Systems*, vol. 32, pp. 2735–2743, 2017. [Online]. Available: http://adsabs.harvard.edu/abs/2016arXiv160107448P

[89] N9500-32d data centre switch. [Online]. Available: https://img-en.fs.com/file/datasheet/n9500-32d-data-center-switch-datasheet.pdf

[90] Arista. 7130 connect series switches. [Online]. Available: https://www.arista.com/assets/data/pdf/Datasheets/7130-Layer-1-Quick-Look.pdf

[91] S. Blair, M. Syed, A. Roscoe, G. Burt, and J.-P. Braun, "Measurement and analysis of pmu reporting latency for smart grid protection and control applications," *IEEE Access*, vol. 7, pp. 1–1, March 2019.

[92] "IEEE Guide for Phasor Data Concentrator Requirements for Power System Protection, Control, and Monitoring," *IEEE Std C37.244-2013*, pp. 1–65, May 2013.

[93] P. Castello, C. Muscas, P. A. Pegoraro, and S. Sulis, "Active Phasor Data Concentrator performing adaptive management of latency," *Sustainable Energy, Grids and Networks*, vol. 16, pp. 270 – 277, 2018. [Online]. Available: http://www.sciencedirect.com/science/article/pii/S2352467717302503

[94] I. Kamwa, S. R. Samantaray, and G. Joos, "Wide frequency range adaptive phasor and frequency pmu algorithms," *IEEE Trans. on Smart Grid*, vol. 5, no. 2, pp. 569–579, 2014.

[95] I. Kamwa, S. R. Samantaray, and G. Joos, "Optimal integration of disparate C37.118 PMUs in wide-area pss with electromagnetic transients," *IEEE Trans. on Power Sys.*, vol. 28, no. 4, pp. 4760–4770, Nov 2013.

[96] S. Akhlaghi, N. Zhou, and Z. Huang, "A multi-step adaptive interpolation approach to mitigating the impact of nonlinearity on dynamic state estimation," *IEEE Transactions on Smart Grid*, vol. PP, no. 99, pp. 1–1, 2017.

[97] K. Sun, S. Likhate, V. Vittal, V. S. Kolluri, and S. Mandal, "An online dynamic security assessment scheme using phasor measurements and decision trees," *IEEE Transactions on Power Systems*, vol. 22, no. 4, pp. 1935–1943, 2007.

[98] Q. Gao and S. M. Rovnyak, "Decision trees using synchronized phasor measurements for wide-area response-based control," *IEEE Transactions on Power Systems*, vol. 26, no. 2, pp. 855–861, May 2011.

[99] K.R.Padiyar, *Structure Preserving Energy Functions in Power Systems: Theory and Applications*. CRC Press, 2013.

[100] T. Hastie, R. Tibshirani, and J. Friedman, *The Elements of Statistical Learning: Data Mining, Inference, and Prediction*, 2nd ed., ser. Springer Series in Statistics. New York, NY, USA: Springer-Verlag, 2008.

[101] A. Zhukov, N. Tomin, V. Kurbatsky, D. Sidorov, D. Panasetsky, and A. Foley, "Ensemble methods of classification for power systems security assessment," *Applied Computing and Informatics*, 2017. [Online]. Available: http://www.sciencedirect.com/science/article/pii/S2210832717300273

[102] R. Schapire, *The Boosting Approach to Machine Learning: An Overview*. New York: Springer, 2003.

[103] L. Breiman, "Random forests," *Machine Learning*, vol. 45, no. 1, pp. 5–32, 2001. [Online]. Available: https://doi.org/10.1023/A:1010933404324

[104] A. Saffari, C. Leistner, J. Santner, M. Godec, and H. Bischof, "On-line random forests," in *2009 IEEE 12th International Conference on Computer Vision Workshops, ICCV Workshops*, Conference Proceedings, pp. 1393–1400.

[105] J. H. Friedman, "Stochastic gradient boosting," *Computational Statistics & Data Analysis*, vol. 38, no. 4, pp. 367–378, 2002. [Online]. Available: http://www.sciencedirect.com/science/article/pii/S0167947301000652

[106] T. K. Ho, "The random subspace method for constructing decision forests," *IEEE Trans. Pattern Anal. Mach. Intell.*, vol. 20, no. 8, pp. 832–844, 1998.

[107] R. Banfield, L. Hall, K. Bowyer, and W. Kegelmeyer, "A comparison of decision tree ensemble creation techniques," *IEEE Trans Pattern Anal Mach Intell*, vol. 29, no. 1, pp. 173–180, 2007.

[108] I. Kamwa, S. R. Samantaray, and G. Joos, "On the accuracy versus transparency trade-off of data-mining models for fast-response pmu-based catastrophe predictors," *IEEE Transactions on Smart Grid*, vol. 3, no. 1, pp. 152–161, 2012.

[109] B. Kégl, "The return of AdaBoost.MH: multi-class Hamming trees," *eprint arXiv:1312.6086*, p. arXiv:1312.6086, 2013. [Online]. Available: https://ui.adsabs.harvard.edu/#abs/2013arXiv1312.6086K

[110] B. Fulcher, M. Little, and N. Jones, "Highly comparative time-series analysis: the empirical structure of time series and their methods," *J. Roy. Soc. Interface*, vol. 10, no. 83, 2013.

[111] B. Fulcher and N. Jones, "hctsa: A computational framework for automated time-series phenotyping using massive feature extraction," *Cell Systems*, vol. 5, p. 527, 2017.

[112] F. Hashiesh, H. E. Mostafa, A. Khatib, I. Helal, and M. M. Mansour, "An intelligent wide area synchrophasor based system for predicting and mitigating transient instabilities," *IEEE Transactions on Smart Grid*, vol. 3, no. 2, pp. 645–652, 2012.

[113] J. Geeganage, U. D. Annakkage, M. A. Weekes, and B. A. Archer, "Application of energy-based power system features for dynamic security assessment," in *2015 IEEE Power & Energy Society General Meeting*, Conference Proceedings, pp. 1–1.

[114] Z. Xing, J. Pei, and E. Keogh, "A brief survey on sequence classification," *SIGKDD Explor. Newsl.*, vol. 12, no. 1, pp. 40–48, 2010.

[115] S. Hochreiter, . 252, and r. Schmidhuber, "Long short-term memory," *Neural Comput.*, vol. 9, no. 8, pp. 1735–1780, 1997.

[116] F. Karim, S. Majumdar, H. Darabi, and S. Harford, "Multivariate LSTM-FCNs for Time Series Classification," *arXiv e-prints*, p. arXiv:1801.04503, Jan 2018.

[117] D. E. M. Pavella and D. Ruiz-Vega, "Transient stability of power systems : A unified approach to assessment and control," *Springer US*, vol. 1, no. 238, 2000.

[118] M. J. Thompson and D. L. Heidfeld, "Transmission line setting calculations - beyond the cookbook," pp. 850–865, 2015.

[119] y. . . u. . h. Power Research and Development Consultant Pvt. Ltd, title = Tutorial on Distance and Over Current Protection.

[120] P. E. Utgoff, N. C. Berkman, and J. A. Clouse, "Decision tree induction based on efficient tree restructuring," *Machine Learning*, vol. 29, no. 1, pp. 5–44, 1997. [Online]. Available: https://doi.org/10.1023/A:1007413323501

[121] I. Kamwa, R. Grondin, and L. Loud, "Time-varying contingency screening for dynamic security assessment using intelligent-systems techniques," *IEEE Trans. on Power Sys.*, vol. 16, no. 3, pp. 526–536, 2001.

[122] G. Ravikumar and S. A. Khaparde, "Taxonomy of pmu data based catastrophic indicators for power system stability assessment," *IEEE Systems Journal*, vol. 12, no. 1, pp. 452–464, 2018.

[123] A. M. L. d. Silva, M. B. D. C. Filho, and J. M. C. Cantera, "An efficient dynamic state estimation algorithm including bad data processing," *IEEE Transactions on Power Systems*, vol. 2, no. 4, pp. 1050–1058, 1987.

[124] P. W.Sauer and M.A.Pai, *Power System Dynamic Equilibrium, Power Flow, and Steady-State Stability*. Power Electronics and Power Systems: Springer International Publishing, 2014.

[125] I. Kamwa, A. K. Pradhan, G. Joos, and S. R. Samantaray, "Fuzzy partitioning of a real power system for dynamic vulnerability assessment," *IEEE Trans. on Power Sys.*, vol. 24, no. 3, pp. 1356–1365, 2009.

[126] G. Trudel, J. P. Gingras, and J. R. Pierre, "Designing a reliable power system: Hydro-quebec's integrated approach," *Proceedings of the IEEE*, vol. 93, no. 5, pp. 907–917, May 2005.

[127] NERC. (2015) Transmission operations (tpl-001-04). [Online]. Available: https://www.nerc.com/pa/Stand/Pages/AllReliabilityStandards.aspx?jurisdiction=United%20States

[128] J. Zhao, A. Gomez-Exposito, M. Netto, L. Mili, A. Abur, V. Terzija, I. Kamwa, B. C. Pal, A. K. Singh, J. Qi, Z. Huang, and A. P. S. Meliopoulos, "Power system dynamic state estimation: Motivations, definitions, methodologies and future work," *IEEE Transactions on Power Systems*, pp. 1–1, 2019.

[129] U. Tamrakar, D. Shrestha, M. Maharjan, B. Bhattarai, T. Hansen, and R. Tonkoski, "Virtual inertia: Current trends and future directions," *Applied Sciences*, vol. 7, no. 7, p. 654, Jun 2017. [Online]. Available: http://dx.doi.org/10.3390/app7070654

[130] P. V. Jean Bélanger and J.-N. Paquin, "The what, where, and why of real-time simulation," *Planet RT*, pp. 37–49, 2010.